

POLITECNICO DI TORINO

**Master's Degree Thesis in Biomedical Engineering**  
*Department of Mechanical and Aerospace Engineering*



**Multiplexed protein profiling of tumor-derived  
extracellular vesicles using an electrokinetic sensor**

**Supervisor:**

Prof. Danilo Demarchi

**External Supervisor:**

Sara Cavallaro,  
*Royal Institute of Technology,  
Applied Physics Department*

**Candidate:**

Lorenca Berisha

*Academic year 2019 – 2020*



# Abstract

Small extracellular vesicles (sEVs) that range in diameter between 30 and 200 nm are secreted from almost every cell type of the human body into the extracellular space surrounding the parental cell of origin. These nano-sized, cell-derived carriers, function as effective vehicles of intercellular communication, traveling in body fluids (blood, urine, pleural effusion, etc.) and transporting several active biomolecules and genetic information, such as RNAs and DNAs, between distant cells. This novel mechanism of intercellular communication has been nowadays acknowledged to have a significant role in the development of various diseases, such as cancer.

sEVs, often referred to as exosomes, are indeed secreted by tumor cells at an early stage and can act as suitable biomarkers, offering a promising option for non-invasive diagnostics, and therapy monitoring of different forms of cancer, including lung cancer. Most of the current biosensors for exosomal biomarkers detection that have been developed demonstrate good potential in cancer diagnostics. It is well known that in order to bring a device to clinical settings it is important to scan as many markers as possible, simultaneously, as this could lead to time and costs saving results. Moreover, the employment of the same device to scan different markers in parallel produces less chance of error.

In this thesis, a simple, low cost and label-free electrokinetic sensor for multiplexed extracellular vesicles' detection and profiling of their biomarkers' expression, investigated in commercially available silica capillaries, is presented. The method of detection investigated the streaming current variation which is recorded before and after the interaction between the sEVs' surface markers and the capture probes immobilized on the functionalized microcapillary's inner surface.

The detection was performed on sEVs originated from the non-small-cell lung cancer (NSCLC) H1975 cell line and from pleural effusions obtained from lung cancer patients, for a set of representative surface markers, such as CD63, CD9 and epidermal growth factor receptor (EGFR), the former two being common exosomal markers and the latter regarded as overexpressed in lung cancer.

The multiplexed platform was first validated with sEVs from the H1975 lung cancer cell line. Experiments were performed on control capillaries as well as on micro-capillaries functionalized with capture probes to test the stability of the signal. Repeated measurements on the capture probes functionalized micro-capillaries were conducted in order to investigate the reproducibility of their signals. Comparisons between control measurements and functionalized micro-capillaries interacting with H1975-derived EVs in order to examine the influence of non-specific binding and attempts of signal enhancement were carried out for both two-channels and four-channels measurements. The outcome resulted more problematic for the latter, stressing the need to further improve the multiplexed platform.

Moreover, the performance of the sensor with clinical samples, not investigated before, was tested with sEVs derived from pleural effusions of lung cancer patients. The experiments showed specific detection and promising results. As a future step, the sensor could be tested and integrated into a microfluidic platform.



# List of Abbreviations

sEVs	Small extracellular vesicles
NSCLC	Non small cell lung cancer
EGFR	Epidermal growth factor receptor
EVs	Extracellular vesicles
MV	Microvesicle
ISEV	International Society of Extracellular Vesicles
ILVs	Intraluminal vesicle
MVB	Multivesicular body
PS	Phosphatidylserine
MHC II	Major histocompatibility complex class II
ESCRT	Endosomal sorting complex required for transport
VAMP3	Vesicle associated membrane protein 3
PE	Phosphatidyl-ethanolamine
miRNA	Micro Ribonucleic acid
mRNA	Messenger Ribonucleic acid
tRNA	Transfer Ribonucleic acid
ssDNA	Single standed DNA
tRPS	Tunable resistive pulse sensing
DLS	Dynamic light scattering
NTA	Nanoparticle tracking analysis
TEM	Trasmission electron microscopy
SEM	Scanning electron microscopy
AFM	Atomic force microscopy
IB	Immunoblotting
EM	Electron microscopy

WB	Western Blotting
VEGF	Vascular endothelial growth factor
ELISA	Enzyme-linked immunosorbent assay
SPR	Surface plasmon resonance
NSB	Non-specific binding
EDL	Electrical double layer
PBS	Phosphate buffered saline
DIW	Deionized water
GA	Glutaraldehyde
PBS	Phosphate buffered saline
tri-ETHA	Triethanolamine

# Contents

<b>Abstract</b>	<b>2</b>
<b>1 Overview on Extracellular Vesicles</b>	<b>10</b>
1.1 Introduction . . . . .	10
1.2 History of extracellular vesicles . . . . .	11
1.3 Classification . . . . .	13
1.4 Biogenesis . . . . .	15
1.4.1 Exosomes . . . . .	15
1.4.2 Microvesicles . . . . .	15
1.4.3 Apoptotic bodies . . . . .	16
1.5 Methods of isolation . . . . .	17
1.6 Molecular composition . . . . .	18
1.6.1 Protein content . . . . .	18
1.6.2 Lipid content . . . . .	18
1.6.3 Nucleic acids content . . . . .	19
1.7 Characterization methods . . . . .	20
1.7.1 Physical analysis . . . . .	21
1.7.1.1 Electron microscopy . . . . .	21
1.7.1.2 Atomic force microscopy . . . . .	22
1.7.1.3 Tunable resistive pulse sensing . . . . .	23
1.7.1.4 Dynamic light scattering . . . . .	24
1.7.1.5 Nanoparticle tracking analysis . . . . .	25
1.7.1.6 Flow cytometry . . . . .	26
1.7.2 Biochemical analysis . . . . .	27
1.7.2.1 Immunoblotting . . . . .	27
1.8 Role of EVs in physiological and pathological conditions . . . . .	29
1.8.1 Lung cancer . . . . .	33
<b>2 State of the art</b>	<b>36</b>
2.1 Liquid biopsy detection methods . . . . .	36
2.1.1 Immunofluorescence-based detection . . . . .	36
2.1.2 Surface plasmon resonance-based detection . . . . .	38
2.1.3 Electrochemical-based detection . . . . .	39
2.2 Aim of the thesis . . . . .	39

<b>3</b>	<b>Experimental method</b>	<b>42</b>
3.1	Electrokinetic phenomena . . . . .	42
3.1.1	Zeta potential . . . . .	43
3.1.2	Streaming current . . . . .	45
3.2	Capillary surface functionalization . . . . .	46
3.2.1	Control functionalization . . . . .	48
3.3	Experimental setup . . . . .	49
3.4	Experiment conduction . . . . .	50
3.5	Data analysis . . . . .	53
3.6	EV characterization . . . . .	57
<b>4</b>	<b>Results and Discussion</b>	<b>61</b>
4.1	Preliminary characterization . . . . .	61
4.2	Capture probes' baseline characterization . . . . .	64
4.3	Two-Channels Measurements . . . . .	69
4.4	Four-Channels Measurements . . . . .	75
4.5	Clinical samples . . . . .	77
<b>5</b>	<b>Conclusions</b>	<b>82</b>
<b>6</b>	<b>Future perspectives</b>	<b>84</b>
	<b>Bibliography</b>	<b>94</b>
	<b>Appendix</b>	<b>96</b>



# Chapter 1

## Overview on Extracellular Vesicles

### 1.1 Introduction

Intercellular communication is an essential process in the development and preservation of homeostasis in living organisms, guaranteeing an efficient response to any alterations or risks that involve the environment surrounding cells. Such communication can be operated through cell-cell direct contact or the transfer of secreted soluble molecules, such as cytokines, metabolites, hormones and inflammatory mediators [1]. Cells derived from both prokaryotes and eukaryotes organisms modulate a diverse variety of biological processes through the transmission of biological signals between them. The dysregulation of this intercommunication process may lead to various diseases including cancer and immunological diseases [2].

In the last 20 years, another mechanism for intercellular communication has surfaced and it involves extracellular vesicles (EVs). The secretion of vesicles in the extracellular space is one of the strategies cells can use to communicate in a content that overcomes the signaling of soluble factors, considering that EVs are cell-derived carriers transporting several active biomolecules, genetic information, and surface receptors [3]. Such functional constituents change in accordance with the type of the parental cell as well as with the specific pathological or physiological circumstances existing at the moment of their encapsulation and secretion through the EVs [4]. The intercellular interaction occurs either by direct connection between the recipient membrane protein and the vesicle membrane protein or by incorporation of the vesicle content by the receiving cell [5]. Considering that it has been revealed that almost all cell types produce EVs [6], it seems incredible that EV signaling frequently possessed a smaller consideration as a means of regulation and crosstalk between cells. However, following the great progress that has been made in studying extracellular vesicles in the last decade, EVs are nowadays finally acknowledged as effective vehicles of intercellular communication, as nanocarriers from donor to recipient cells, as process mediators of immune responses and cell adhesion and as significant biomarkers in various illnesses from cancer to neurodegenerative diseases. As a matter of fact, EVs are found in high concentration in all biological fluids, therefore, liquid biopsies can be conducted with less critical and invasive approaches and this represents an important advantage for diagnosis and monitoring of such diseases.

Thus, understanding the role of EVs in intracellular communication can highlight how their manipulation in vivo or through specifically designed, clinical-grade EVs could result in effective diagnostic and therapeutic interventions in the coming years [1].

## 1.2 History of extracellular vesicles

Early evidence of such extracellular vesicles was provided for the first time in the 40s where it was discovered that a discrete quantity of coagulation elements found in platelet-free plasma could be sedimented [7]. Years later, in 1964 the term ‘platelet dust’ was used to describe these minor plasma elements that originate from platelets which are dragged down using high speed centrifugation and observed by electron microscopy [8]. In the following decades more evidence emerged of such particles found in other biological environments including rectal adenomas, tumor tissues, during bone calcification, in human semen, in bovine sera and human cell cultures [9].

The most relevant discovery came in 1983 when two groups of researchers would describe the generation and release of exosomes during studies on the transferrin recycling cycle. The conclusions drawn by the two groups revealed that when internalization of labelled transferrin occurred, they reallocated through endosomes into a multivesicular compartment and later released into the extracellular space by vesicles partially defining for the first time what would later be known as exosomes [10] [11].

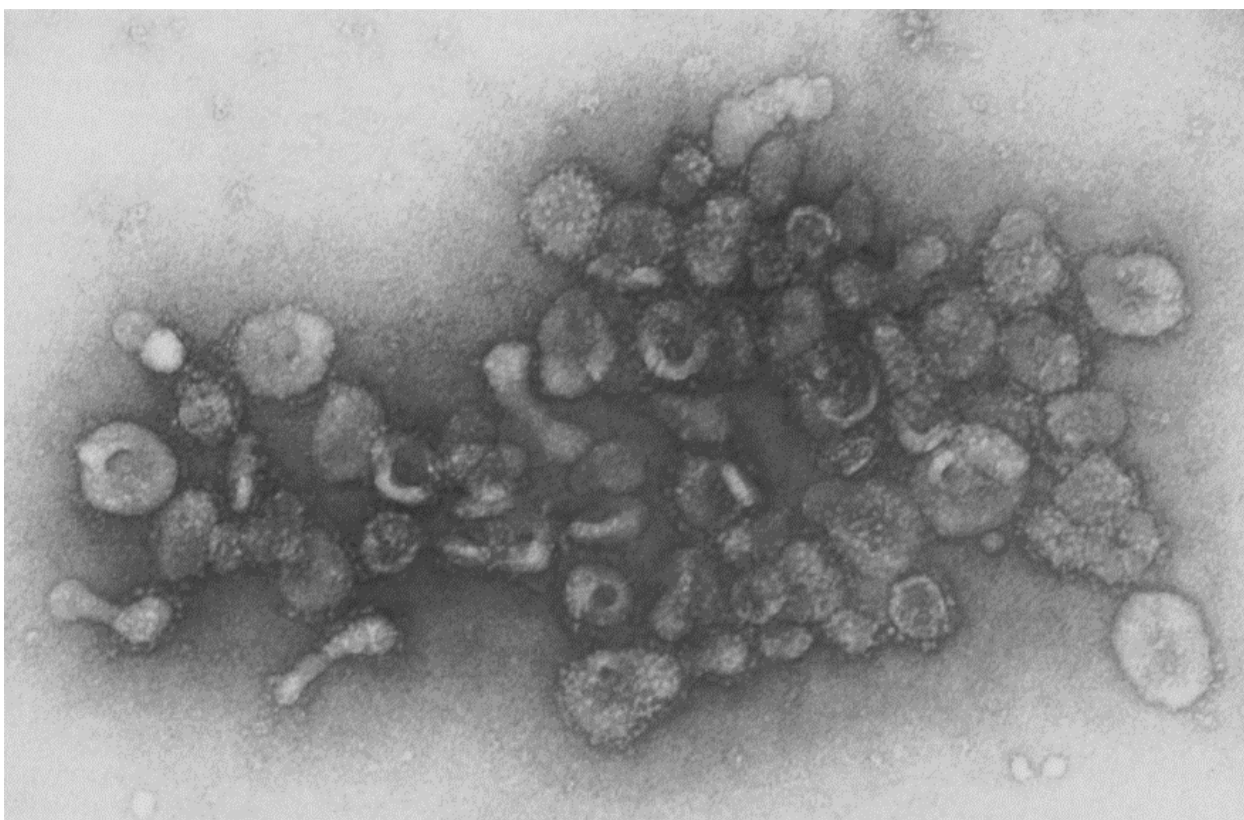


Figure 1.1: Electron microscope image of released vesicular material in the 1983 work of Pan and Johnstone [10]

Three years after the work of these two groups, for the first time, the term ‘exosomes’ was introduced to identify these vesicles [12].

Initially EVs were thought to serve just as disposal bins and to carry cellular waste in order to maintain a correct homeostasis. But this initial hypothesis was denied by Raposo et al. which submitted for the first-time proof that EVs possess further significant biological functions. In the 1996 article “B Lymphocytes Secrete Antigen-presenting Vesicles” it was shown that EVs which derive from B lymphocytes can produce an immunologic effect [13].

Another groundbreaking work came two years later when Zitvogel et al. published their work regarding the first procedure on murine tumors using EVs as a therapeutic means [14]. These findings were followed by two clinical trials conducted in 2005 which involved EVs derived from autologous dendritic cells which were employed in the treatment of metastatic melanoma and non-small cell lung cancer [15] [16].

In the last decades various studies have demonstrated the importance of extracellular vesicles. The work by Valadi et al. in 2007 was another breakthrough study in which was shown that EVs participate actively in the intercellular communication and that they can also release functional mRNA and miRNA into a receiving cell [17].

In 2011 Alvarez-Erviti et al. showed that the delivering of functional siRNA could be performed through engineered EVs as a targeting mean to the brain, highlighting how EVs possess a great ability to serve as natural delivery carriers for therapeutical purposes [18].

The number of scientific articles published over the last decades, as shown in *Fig. 1.2*, has grown exponentially in the EV research field, leading to a higher understanding of EVs’ biological role, their content as well as their biogenesis.

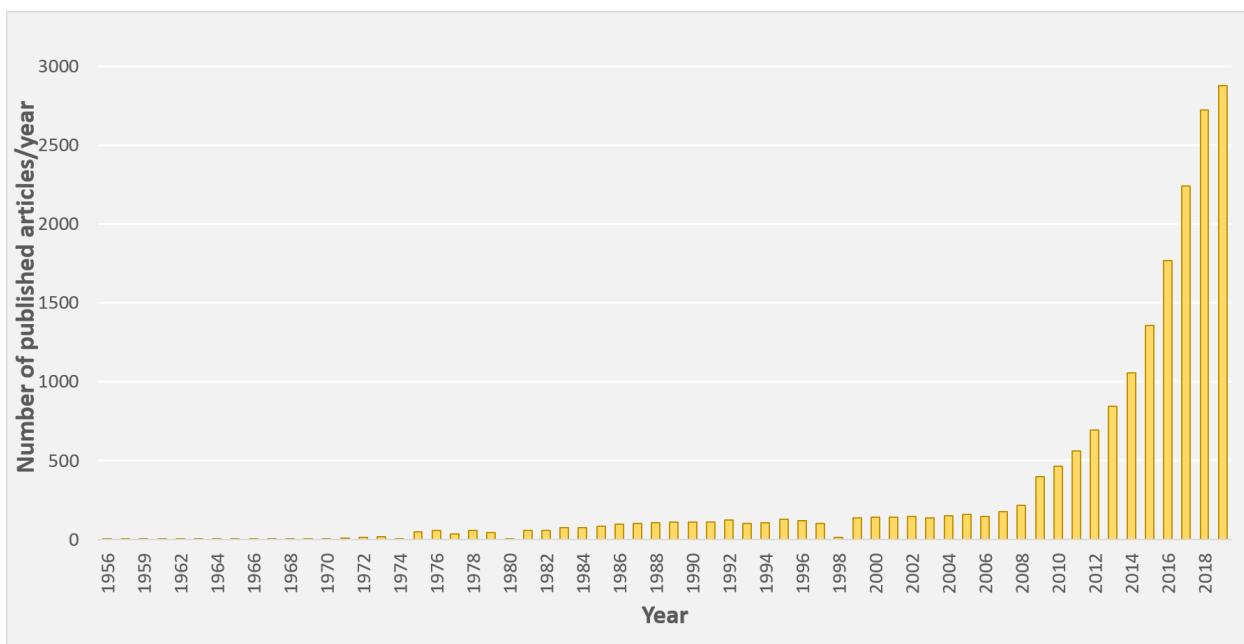


Figure 1.2: Graph showing the number of articles that are published every year on PubMed when searching the term “extra cellular vesicles”

Evs isolation has occurred in many body fluids and their role in the regulation of many physiological processes such as tissue repairing, blood coagulation, stem cell support, immune monitoring but

also in pathological functions has become more and more evident. They have been associated with tumorigenesis, the diffusion of viruses and pathogenic factors like HIV-1,  $\alpha$ -synuclein and amyloid- $\beta$  derived peptides which concern respectively Parkinson’s disease and Alzheimer’s disease but also the spread of prion protein PrPC found in the surface of pathogenic cells.

Thus, extracellular vesicles represent a new class of feasible therapeutic targets for tissue regeneration and regulation of immune response making them an enormous potential to be the future major breakthrough in the medical field given the arising tendency [2].

### 1.3 Classification

Many studies have reported that the size, the composition of the membrane as well as the constituents of extracellular vesicles consist of considerably dynamic and heterogeneous features and rely on the environmental and cellular source circumstances [19]. The term “extracellular vesicles” consists of a hypernym since it includes different groups of vesicles which derive both from prokaryotic and eukaryotic cells. EVs are most commonly classified according to their cellular origin or the biological function they possess, size, density, different centrifugation proprieties as well as based on their biogenesis [20]. In relation to the latter, the three main classes of extracellular vesicles consist of apoptotic vesicles, microvesicles (MVs) and exosomes.

Being the EVs field still in its youth, the nomenclature has not been very steady and consistent since the terms, exosomes, microvesicles, microparticles and EVs have been used indifferently. Extracellular vesicles, based on their origin and biological function, are also called argosomes, telerosomes, prostasomes, ectosomes, microparticles, oncosomes and many other terms as illustrated in *Fig. 1.3*.

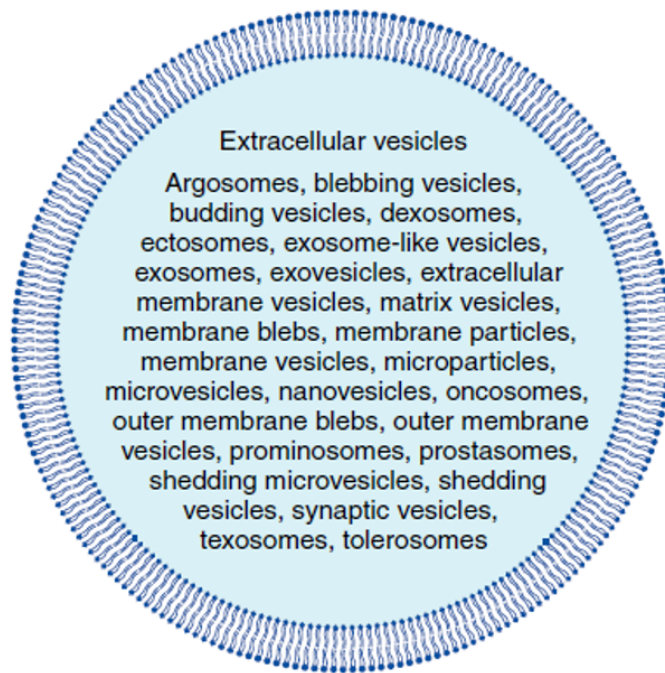


Figure 1.3: The wide nomenclature of extracellular vesicles [21]

The abundance of possible names for EVs is the reason why a discussion about standardization of the nomenclature is still ongoing [21]. Despite the confused nomenclature, some basic standards have been fixed from the International Society of Extracellular Vesicles (ISEV) [22].

In a general sense, we can describe EVs as being spherical nano-sized particles consisting of a bi-layer lipidic membrane with a size ranging from 30 to 2000 nm in diameter and have the particular characteristic of containing cargo such as nucleic acids, lipids and proteins, which originally were part of the parental cell from which they derived [23].

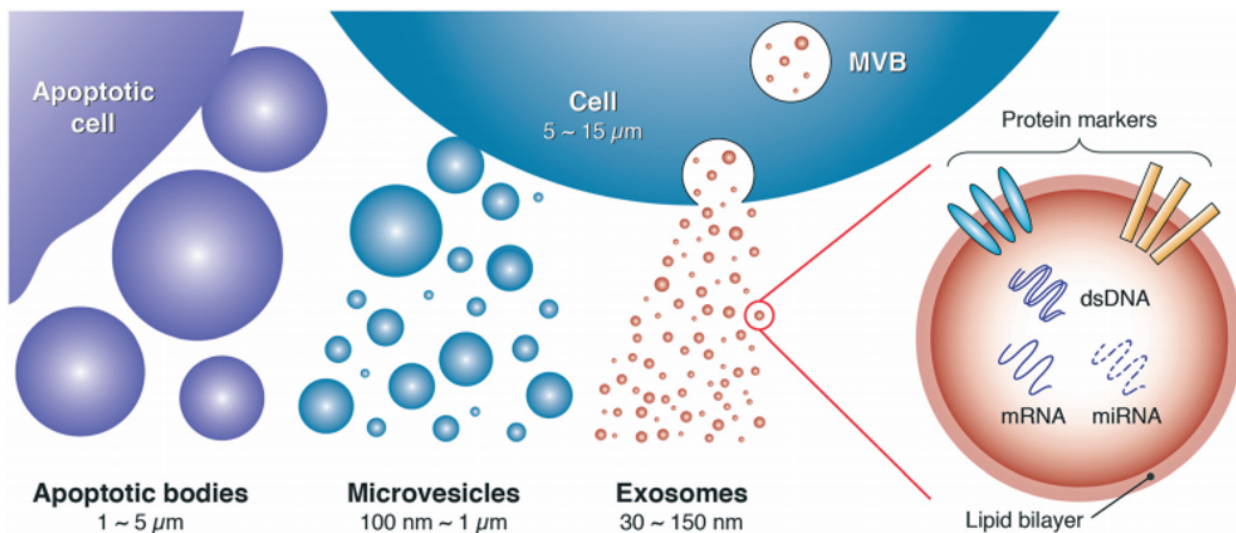


Figure 1.4: Illustration of the three main classes of extracellular vesicles adapted from [24]

Exosomes are the most studied among all EVs and they originate from the endosomal pathway and range between 40 and 120 nm in diameter and their density ranges from 1,13 g/ml to 1,19 g/ml [4]. Microvesicles present a more heterogeneous behavior with sizes ranging between 50 nm and 1 μm and are obtained from the direct cell membrane outward budding [23].

Apoptotic bodies, similarly to microvesicles, are released directly from the plasma membrane and present a larger size, measuring from 500 nm to 2 μm, but they derive from apoptotic cells blebbing into the extracellular environment. As a result, they may contain different sections of the dying cell of origin [23].

It is evident that the three different classes of EVs overlap between each other in relation to size, but they also do so in terms of protein content and density [21]. Such heterogeneity has become even more reinforced by the findings of different exosome populations which have indicated that some exosomes may carry certain features but may be deficient in other characteristics [25].

In this work, the emphasis will lay on the EV class which are commonly classified as exosomes, but the term small EVs will be used to refer to them, since, as mentioned above, the distinction between the EV classes are still ambiguous due to incomplete understanding of the vesicles biogenesis, discrepancies in the purification protocols and inadequacy of exhaustive characterization [23].

## 1.4 Biogenesis

### 1.4.1 Exosomes

As already mentioned, exosomes originate from the endosomal pathway which includes early to late endosomes, recycling endosomes and multivesicular bodies and has the function to operate as a categorization network in order to guide different intraluminal vesicles to adequate destination being that exocytosis, lysosomal degradation or cellular recycling [5].

After the early endosomes finish depositing content into recycling endosomes they turn into late endosomes and in the course of this transformation the inward budding of their membrane takes place, resulting into intraluminal vesicles (ILVs) packed inside with DNA, mRNA, microRNA, proteins and lipids ultimately forming the multivesicular body (MVB) [26]. The generation of MVBs through the invagination of ILVs represents the beginning of exosome biogenesis [27].

The operation that determines the destiny of a specific MVB to either merge with lysosome or fuse with the plasma membrane remains still not well understood [2].

It has been suggested that endosomes get directed into diverse destination by a series of various Rab GTPases, a family of proteins [28]. Moreover, different levels of cholesterol in MVBs also have been shown to control the path towards lysosome fusion or plasma membrane. In particular, a multivesicular body containing a high level of cholesterol secreted its content into the extracellular space while a MVB identical in morphology which was lacking of cholesterol was directed into the lysosomal department for degradation [29].

Although the precise mechanism is still not entirely understood, some evidence suggest that growth factors can stimulate the formation of MVBs and consequently the cell adjusts the production of exosomes accordingly to its needs [30].

### 1.4.2 Microvesicles

Microvesicles originate from an entirely different biogenesis pathway that, in comparison to the biogenesis of exosomes, is far less defined. The generation of MVs, as already mentioned, arrives from the external budding of the cell membrane, which is considered to be obtained by a mixture of mechanisms comprising the activation of cytoskeletal proteins and phospholipid rearrangement. Proteins and phospholipids are not distributed uniformly within the cell membrane. Such heterogeneity in the distribution and cluster formation is organized by aminophospholipid translocases which regulate the transport of phospholipids between the inner and outer leaflet ad vice versa [31].

The first phase in the microvesicles biogenesis has been proposed to initiate with the exposure of phosphatidylserine (PS) through a displacement to the outer leaflet [5]. Other studies have revealed that an increment in calcium levels provokes a reallocation of phospholipids which ultimately leads to the release of the microvesicles. The reallocation of phospholipids is followed by the budding process which takes place when the cytoskeletal proteins start to contract due to actin-myosin interactions [32].

In conclusion, the major distinction regarding exosome biogenesis, which occurs through the endocytic pathway, and microvesicle formation, which is carried out through the budding of the membrane and consequent rupture, is firmly recognized.

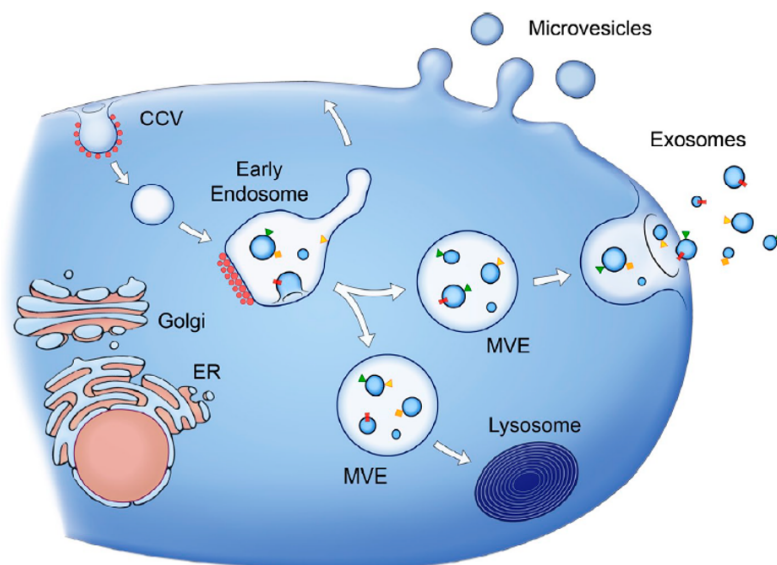


Figure 1.5: Figure illustrating the process of formation of microvesicles and exosomes deriving from the maturation of endosomes into MVBs adapted from [2]

### 1.4.3 Apoptotic bodies

Apoptosis, an event that occurs in both normal and cancerous cells, is an important mechanism of cell death. When a cell goes through such an event, it crosses different steps, starting from chromatin condensation in the nucleus, followed by the blebbing of the plasma membrane and progressing till the dissolution of the cellular content into separate and individual membrane-enclosed vesicles called, precisely, apoptotic bodies [5].

Microvesicles and exosomes are secreted during healthy cellular procedures, whereas apoptotic bodies are only generated when a programmed cellular death takes place. While apoptotic bodies present a size ranging from 500 nm up to 2  $\mu$ m in diameter and contain different organelles in the vesicles, small vesicles that are in size of 50 – 500 nm are also being secreted during the apoptotic event [5]. It is still uncertain whether such small vesicles are obtained as a result of the blebbing of the plasma membrane that takes place during the apoptosis. Moreover, current studies show that the blebbing of the membrane is partly mediated by the interaction of actin and myosin [5].

In *Fig. 1.6* is represented a summary table which includes the three main types of EVs, their size and biogenesis.

Type of EVs	Diameter	Origin
Exosomes	40 – 120 nm	Exocytosis from MVBs
Microvesicles	50 – 1000 nm	Outward budding of plasma membrane
Apoptotic bodies	500 – 2000 nm	Apoptosis

Figure 1.6: Summary table illustrating the three main types of EVs, their diameter and origin

## 1.5 Methods of isolation

One of the primary considerations that should be given utmost importance in order to identify extracellular vesicles consists in their isolation from extracellular fluids both conditioned cell culture media as well as body fluids. In reference to the latter, EVs have been efficiently purified from fluids such as saliva, blood serum and plasma, urine, bile, semen, breast milk, cerebrospinal and amniotic fluid and many others [22]. It is important that the EV-containing fluid collection is as gentle as possible in order to limit the disruption of cells. Indeed, mechanical rupture of cells can lead to the release of vesicles originating from compartments inside the cells, which would result in the decrease of EVs' purity. Therefore, the term "extracellular vesicles" would not be suitable to refer to samples isolated from such an approach [22].

The isolation process of EVs is technically challenging as a result of their small size, physicochemical properties, heterogeneity and often complicated surroundings. Moreover, the fluids from which the isolation takes place are complex and include, apart from EVs, proteins, lipoproteins, cell waste and nucleic acids among other contents [33].

At the moment there is no consensus on a gold standard isolation technique, but the most frequently used method is considered to be differential centrifugation including high speed ultracentrifugation to pellet exosomes [4]. This technique allows to separate subpopulations of EVs based on their size using different centrifugation speeds but is limited by high chances of co-sedimentation of non-EVs contaminants, low recovery and rupture of EVs [34]. Furthermore, ultracentrifugation is time-consuming, laborious and often results in aggregation of vesicles due to high gravitational forces [35]. Consequently, various other isolation techniques have emerged to replace or complement ultracentrifugation. These include precipitation techniques [36], density gradient separation [37], size exclusion through the use of filters or chromatography [38], immunoaffinity techniques [39] and microfluidic devices [40].

As already mentioned, the complexity of biological fluids and the overlap of biochemical properties between various EVs makes it difficult to generate isolation protocols that can easily differentiate the EVs distinct classes in a rapid, efficient, reproducible and clinically friendly manner thus future technical developments in this field are believed to bring about protocols and techniques that will result in better efficiency [27].

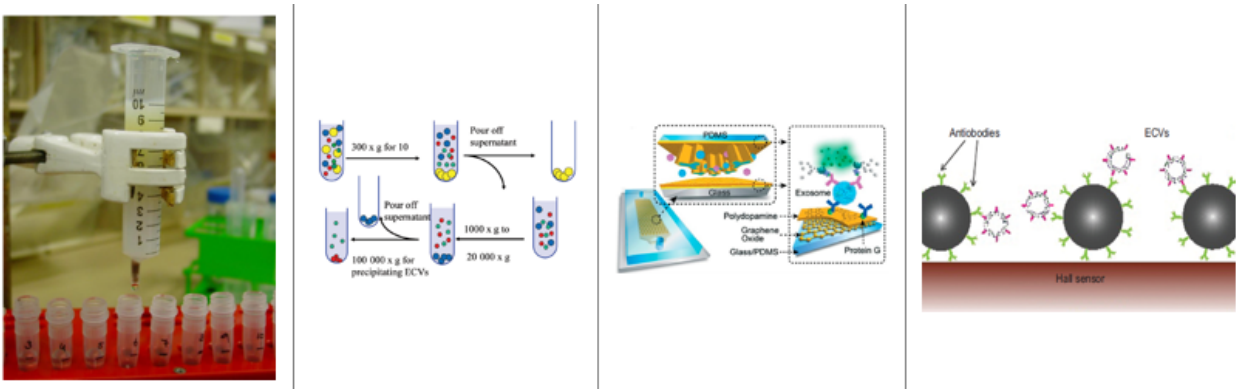


Figure 1.7: Some of the EVs isolation methods (chromatography, ultracentrifugation, microfluidic device, immunoaffinity technique) adapted from [35] [38] [41]

## 1.6 Molecular composition

The content and composition of extracellular vesicles are being largely unravelled through proteomics, lipidomics studies and in depth- characterization of nucleic acid. Significant databases like Vesiclepedia and Exocarta have been created to collect datasets and generate organized catalogues [42]. Despite the fact that EV content strongly depends on the culturing conditions, biogenesis, cell source and its physiological or pathological conditions, nevertheless, common characteristics such as composition of the outer lipid bilayer and various nucleic acids, lipids and proteins are shared between the various subtypes of vesicles [43].

### 1.6.1 Protein content

Proteins are significant components of the extracellular vesicles cargo and are often used as markers of characterization of EVs and their sub-types. Most of the commonly discovered proteins have an influence in the formation and biogenesis of the EVs. There has also been detected a collection of recurring proteins which have been categorized as common vesicular markers largely approved across the EV community [44].

Exosomes, as already mentioned, are originated from the endocytic pathway therefore they contain proteins connected to their biogenesis such as major histocompatibility complex class II (MHC II) and tetraspanins. Proteins belonging to the family of tetraspanins such as CD9, CD63 and CD81 have been discovered to be highly enriched on exosomes but they are also present on larger vesicles. More particularly, two tetraspanins that are believed to play an important role in exosome biogenesis involve CD9 and CD63 and for this reason they serve as most widely used exosome identifiers and consequently have been aimed for selective segregation [5]. The tetraspanins abundance derives as a result of the development of clustered microdomains along with other components such as syntenins and integrins that promote membrane budding either towards the MVBs lumen or toward the extracellular area [45].

In a similar way, the endosomal sorting complex required for transport (ESCRT) proteins such as TSG101 and ALIX, chaperone heat shock proteins such as HSP70 and HSP90, cytosolic proteins such as actin, tubulin as well as actin-binding proteins together with RAB proteins (RAB27A and RAB11B) which participate in the biogenesis of the multivesicular body, intracellular membrane fusions and transport are often found in exosomes. ALIX has been shown to cooperate with syndecan through the protein syntenin and with other protein complexes, including MHC molecules, assisting exosome biogenesis and guaranteeing cargo loading inside the vesicles [4].

Regarding microvesicles, there have been reports showing that they contain glycoprotein Ib, P-selectin and integrins in important quantities [46]. For example, melanoma-derived microvesicles grow rich with B1 integrin receptors and related membrane associated proteins like vesicle-associated membrane protein 3 (VAMP3). However, while transferrin receptors highly appear in exosomes, they are notably absent in microvesicles [5].

### 1.6.2 Lipid content

In terms of lipid composition there are not a large amount of data available so far [4]. Studying EV lipids has been a growing interest since 2002, when it was revealed for the first time that tumor derived EV lipids play a central role in angiogenesis [47].

Regarding lipid composition, taking into consideration the differences related to the origin of the cell type, EVs are mostly composed of phosphatidylserine, sphingomyelin, phosphatidyl-ethanolamine (PE), phosphatidylcholine, phosphatidylinositol, cholesterol and ceramides (GM3) [48]. It is firmly established that both inner and outer parts of the EV membrane possess an asymmetric lipid distribution that consequently determine the curvature of the membrane. From this prospective, the biggest difference compared to the plasma membrane of the cell is the presence of PE and PS on the outer layer of the exosomal membrane that appear to have a role in their biogenesis [48]. Moreover, the presence of PS in the outer leaflet of the exosomal membrane, which differentiates them from cellular membranes, also facilitates their internalization by recipient cells [49].

Lipids, in particular GM3 and sphingomyelin, have been shown not only to transfer higher stability and rigidity to the structural configuration of the vesicular membrane compared with that of cell membranes but to partake in cellular signaling pathways as well [50] [49].

### 1.6.3 Nucleic acids content

EVs have been shown to contain both RNA and DNA. A significant progress was the discovery that EVs included both microRNAs (miRNA) and messenger RNA (mRNA) and that the latter could be converted into proteins by recipient cells in vitro [2]. EVs transport RNA that is predominantly lower in size than the average cellular fraction (less than 200 nucleotides) and miRNA and transfer RNA (tRNAs) represent about 15% of EV-RNA [49]. EVs also contain a significant amount of a variety of other non-coding RNAs such as RNA transcripts overlaying with protein coding areas, structural RNAs, repeat sequences, vault RNA, tRNA fragments, Y RNA, and small interfering RNAs [2].

Furthermore, EVs may contain single-stranded DNA (ssDNA), transposable elements, amplified oncogene sequences and mitochondrial DNA [51].

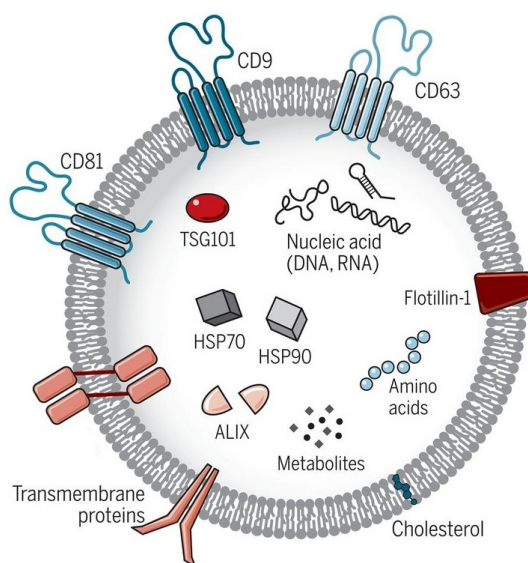


Figure 1.8: Extracellular vesicles molecular contents including various proteins, lipids and nucleic acids adapted from [52]

## 1.7 Characterization methods

The evaluation of EVs size, quantity or characteristics like the presence of particular surface markers have been employed and adapted by several optical and non-optical detection methods [33]. Currently, there are usually two different types of analysis carried out on already isolated vesicles consisting of physical analysis and compositional/biochemical analysis.

The former sheds light on the particles size and their concentration and usually is performed through tunable resistive pulse sensing (tRPS), dynamic light scattering (DLS), nanoparticle tracking analysis (NTA), flow cytometry and several microscopy methods including transmission electron microscopy (TEM), scanning electron microscopy (SEM), cryo-electron microscopy as well as atomic force microscopy (AFM).

The compositional/biochemical analysis is typically performed via immunoblotting (IB), proteomic analysis or staining and provides details about the isolated vesicles composition. Two usual techniques employed for molecular characterization of EVs are western blotting and flow cytometry [27].

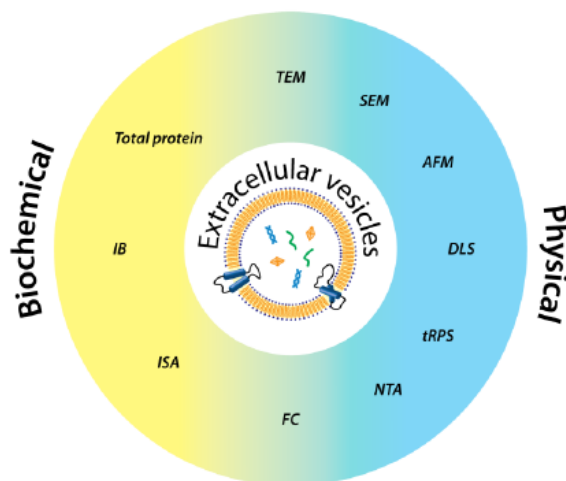


Figure 1.9: Schematic classification of the most conventional technologies for the analysis of EVs adapted from [53]

An important challenge in this field is establishing methods that can easily differentiate the various classes of extracellular vesicles, that are standardized and well multiplexed without difficulties. What makes it mostly challenging is the fact that whenever diverse isolation methods for the extraction of exosomes from the same cell line are utilized, the exosomes proteomic profiles are modified. Moreover, limitations in specificity as non-vesicular particles in the size range of EVs, such as protein complexes and lipid fragments, may wrongly be identified as extracellular vesicles. The microscopy techniques take into consideration subjective settings such as sample view, light intensity, pre- and post-acquisition thresholds of detection which inevitably influence the results and may impact the reliability and reproducibility of the measurement [19].

ISEV has outlined minimal requirement guidelines to follow during experiments in order to characterize EV preparations that might be used as a reference when deciding what characterization method to choose. Some of these minimal requirements involve the characterization of EV size and

possibly also morphology through at least two different methods as well as including the presence of different proteins associated with EVs. Moreover, there should also be evidence of the absence of proteins that are not expected to be found with vesicles. As long as the guidelines are followed, the optimal characterization method for EV analysis depends on the specific experimental goals and instrument accessibility [22].

Following, the most prominent methods are described.

### 1.7.1 Physical analysis

#### 1.7.1.1 Electron microscopy

Electron microscopy (EM) methodologies are well established and have been demonstrated very useful in the EV research field, able to determine the size and morphology even of single EVs thus supplying direct proof for the presence of extracellular vesicles [33] [53].

The two types of EM employed as detection methods are scanning electron microscopy and transmission electron microscopy. High resolution images of particles at the submicron level can be generated from both TEM and SEM using electron beam instead of light, but the difference between the two stands on the type of electrons that are detected [27]. In other words, in SEM, the electrons that are detected are the ones scattered while the electrons that travel through the sample are the only detected ones in TEM. More in detail, in SEM, the interaction of the electrons with the particles in the specimen causes them to get scattered and afterwards to be captured and detected, which generates the particles image. The sample in SEM imaging is required to be conductive and this is obtained through the coating with a thin layer of conductive material such as gold [54]. In TEM, on the other hand, electrons travel through the sample therefore not interacting with the particles and are finally detected employing a fluorescent screen. Dark regions, or shadows, are created by the particles on the fluorescent screen therefore generating an image [55].

Moreover, TEM is often combined with immunoglobulins which are attached to nanogold particles and are used in the detection of specific EV characteristics [33].

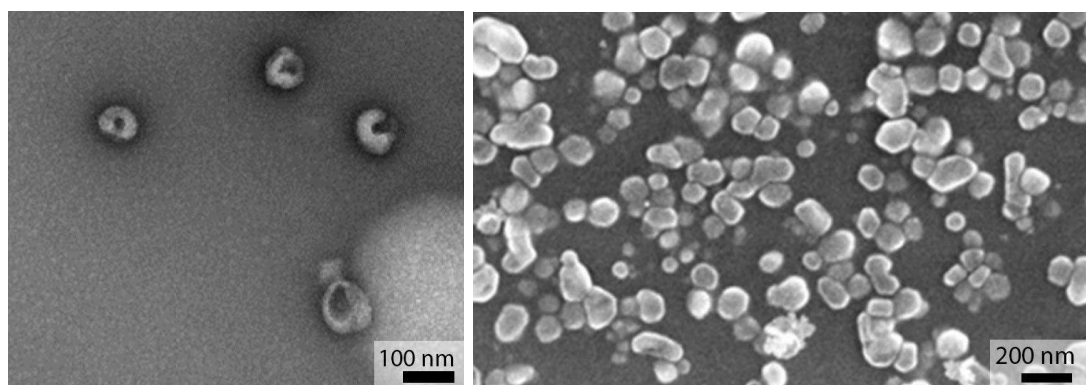


Figure 1.10: TEM (left) and SEM (right) images of exosomes adapted from [56] and [57]

The main restriction from using EM on biological targets is the essential requirement of imaging in vacuum which means that initial fixation and following drying of the sample are needed.

These sample preparation steps make the correlation between the observed targets and the original morphology of the biological objects more complicated. However, despite these limitations, regarding exosomes, both these EM techniques evidence comparable distribution in size, although the morphology appears slightly different [53]. Specifically, in TEM and SEM, exosomes typically are observed to have a sort of divot in the center. This is likely attributable to sample preparation such as the drying process involved in TEM and SEM analysis [57].

Furthermore, among the electronic microscopy devices used to investigate EV cryo-TEM is also included. This method depends on the imaging of ultra-thin vitrified film obtained through the very low temperature (-100 °C) flash-freezing of thin liquid layer of EV suspension [58]. Such a technique modification provides an opportunity for the EV analysis in frozen samples with the benefit of both eliminating dehydration effects and chemical fixatives as well. Cryo-TEM outcome have been reported to demonstrate that the cup-shaped form that exosomes display, as shown by various TEM studies, results from a preparation artifact as already mentioned above [33].

One of the biggest issues with EM analysis is the low number of EVs which gets analyzed which presents an issue in obtaining a representative population considering that EVs are very heterogeneous in terms of size and composition in both biological and clinical samples [53].

### 1.7.1.2 Atomic force microscopy

AFM is a type of scanning probe microscopy that enables the imaging of surface topology demonstrating lateral resolution of a few nanometers and a vertical resolution at the sub-nanometer scale. This is achieved without the requirement of any sample labelling through the scanning of an area with an extremely sharp tip to measure the force interaction between the tip and the sample. Such forces will cause the deflection of the cantilever which will ultimately be converted into the height of the surface using a reflected laser beam and a photodiode [54] [59].

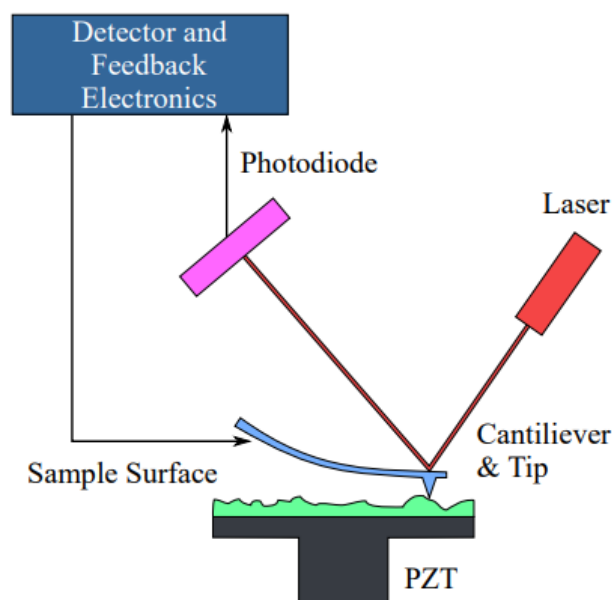


Figure 1.11: Atomic force microscopy schematics [60]

The acquisition of the topographical images can be achieved either in contact mode through the direct scanning of the surface with the tip or through a non-contact tapping approach where the resonance frequency variations of the cantilever can be monitored as a consequence of its vicinity to the surface. The tapping approach is usually applied to image gentle biological structures such as extracellular vesicles, since the possibility to induce deformation caused by the tip is very high. In such circumstances, applying tapping mode reduces placement or rupture when compared to the contact mode. Nonetheless, when employing atomic force microscopy to observe the morphology of EVs, one should take into account that during the preparation of samples, especially during the immobilization of the particles onto the substrate, vesicle deformation may occur which can change the appearance of the vesicles [54].

In the majority of the cases, the analysis is performed on dry and immobilized EVs which leads to the estimation of their size and structure, but this could cause sample damaging especially during the drying process. To prevent this EVs can also be analyzed in solution, firstly fixing them on a surface through electrostatic interactions or complementary antibodies. Moreover, AFM provides important data on the mechanical properties like for example stiffness and elasticity of EVs.

The biggest limitations on this technique consist of its low throughput and requirement of specific skills and machinery that prevent this method from being largely employed in the EV field [53].

### 1.7.1.3 Tunable resistive pulse sensing

tRPS, also known as scanning ion occlusion sensing, is another technique that allows to determine the size distribution and concentration of particles and can detect extracellular vesicles down to 50 nm. The classical setup is composed by a non-conductive nano-membrane dividing in half a fluid cell. The particle free electrolyte is contained in one half, while the other incorporates the suspension and the application of a potential through the two cells enables the particles to navigate through the membrane. This detection method is based on the measurement of the current drop, or resistive pulse, which happens when the nanoparticles pass through the elastic pores of the membrane. The particle's size can therefore be obtained from the length of the resistive pulse [27].

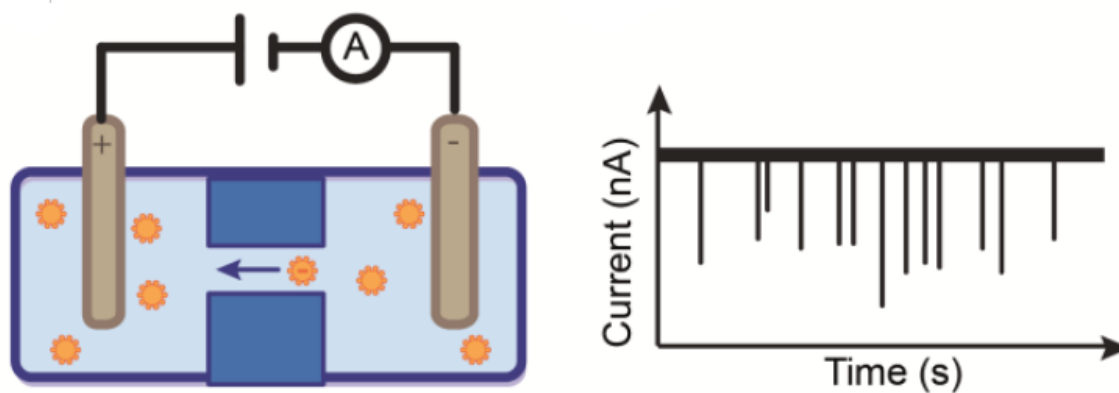


Figure 1.12: Schematic illustration of the setup of a resistive-pulse sensor [54]

Additionally, the concentration of the particles in a sample can be measured through the number of resistive pulses over a specified period [61].

This technique is notably suitable for the study of polydisperse mixtures since the size of the elastic pore can be tuned so in this way is possible to enhance the sensitivity in a major particle size range. It has been used as a tool for the characterization of EVs and for the protocol improvement of isolation methods for miRNA sequencing of EVs derived from blood specimen.

Moreover, it has also been employed as a technique to explore the properties of EVs concerned with the transmission of contagious prions and to characterize vesicles derived from leukemia [54].

#### 1.7.1.4 Dynamic light scattering

Similarly to NTA, DLS implements the light scattered from the particles due to Brownian motion upon illumination with a laser beam in order to calculate their size and concentration. However, there are some differences between the two methods in that DLS doesn't use the scattered light to estimate the diffusion coefficient but performs a fitting of the autocorrelation function of the fluctuations in the scattered light intensity through a mathematical model to establish the particle's size distribution assuming that all the particles have spherical shape [54].

Moreover, contrary to NTA, DLS needs less volume, is easier to use with only a small number of parameters to optimize [62].

An illustration of this detection method is shown in *Fig. 1.13*.

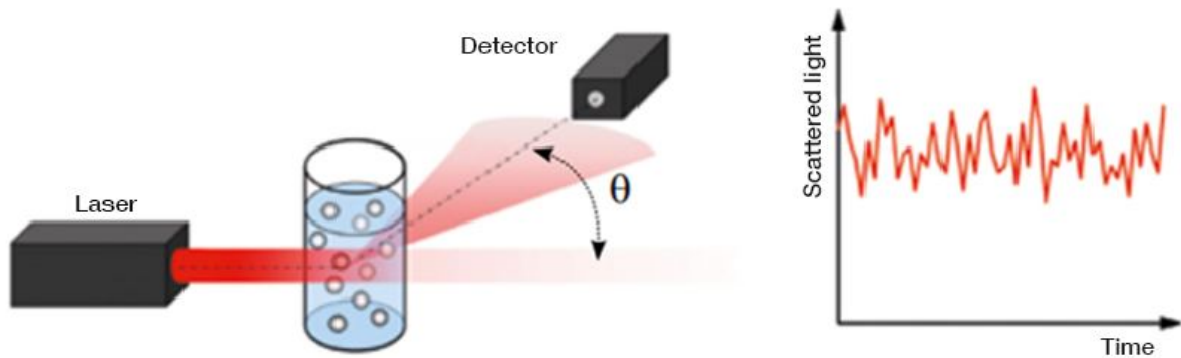


Figure 1.13: Basic setup principles of a Dynamic Light Scattering measurement system [63]

While there are some advantages that DLS has over NTA, its biggest drawback is its ability to analyze heterogeneous mixtures. In particular, the scattered light intensity is proportional to the sixth power of the diameter of the particle, making it this way harder for smaller particles to be detected thus producing data with a skewed distribution towards particles with bigger size when the mixture analyzed contains different sizes of suspended particles.

For this reason, NTA is the method to use in case of heterogeneous groups of particles [64].

### 1.7.1.5 Nanoparticle tracking analysis

NTA is the commercial name for the optical tracking technology that enables to determine both concentration and particle size [33]. This is due to the fact that size is calculated through the Stokes-Einstein equation by obtaining the hydrodynamic diameter. Moreover, the Brownian motion of the particles within the experimental chamber is related to the diffusion coefficient [65]. The light from a laser beam is scattered as the particles in suspension interact with it in the confined chamber and ultimately is collected by a microscope with an attached CCD camera fixed to it. The camera captures the moving particles in video and consequently calculates the particle size and since the particles can be directly visualized, knowing the sample volume, the concentration can also be calculated both in body fluids and conditioned media [66] [54].

A schematic of the NTA optical configuration is shown in *Fig. 1.14*.

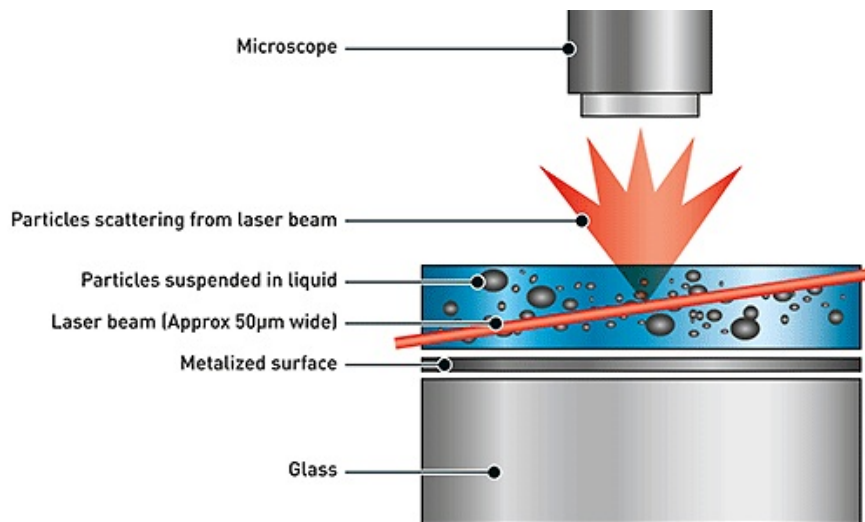


Figure 1.14: Schematic illustration of the NTA optical configuration [67]

Despite the fact that standard NTA does not allow the detection of chemical composition of EVs or their cellular origin, analysis of fluorescently labelled vesicles can also be investigated through this technology, but it requires optimization as it is not used very frequently.

Before proceeding with NTA analysis of biofluids or cell cultured media, isolation of vesicles is essential in order to get rid of protein complexes, lipoprotein particles and other substances that can be in the size range of EVs and thus have similar Brownian motion [33]. NTA is able to determine particle size as small as 50 nm up to 1000 nm in diameter [66]. The issues with nanoparticle tracking analysis are that it represents a drawback when analysing small EVs which include also vesicles smaller than the lower limit and also the instrument measures the moving particles as if they were point of light and for this reason the amount of EVs larger than 500 nm can be underestimated [54] [49]. Moreover, it has the disadvantage that it doesn't distinguish between vesicles and protein aggregates if they have the same size range of EVs [33].

Lastly, for an accurate analysis of the size and number of a heterogenous group of particles, an improvement in the data collection, camera optimization and analysis parameters is required [27].

### 1.7.1.6 Flow cytometry

Flow cytometry can account on the one hand as a physical form of analysis given that permits EVs to be visually observed and on the other hand as a compositional analysis since information about protein composition can also be acquired [27]. This detection method is based on a technology that registers both the fluorescence signal and the scattering that are generated by the particles upon illumination with a laser beam while navigating through a nozzle as it is shown in *Fig. 1.15*

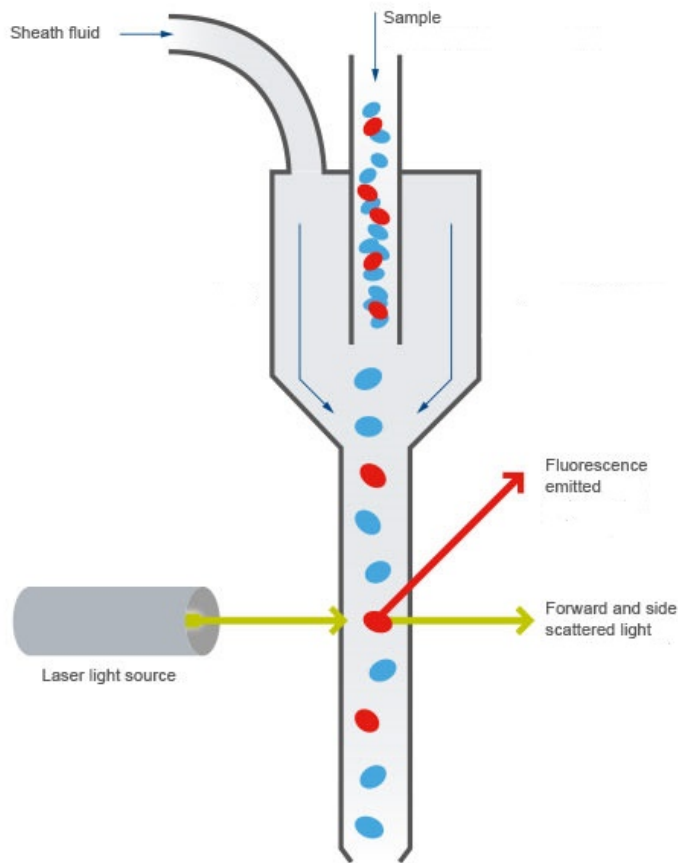


Figure 1.15: Schematic illustration of the setup of a flow cytometer [68]

In a flow cytometer, the particles of interest are brought through a fluidic system to the location point where the laser light can intercept the stream. The fluorescence and scattering signals generated are therefore collected and analyzed as a result of the positioning of light detectors [54].

For objects possessing a size bigger than the wavelength of light, particularly cells, the scattering signal which is detected in a forward direction off-axis of the laser beam can be used for the size determination [54]. For smaller objects instead, for example EVs, the dimension of the objects being scattered can be obtained from the deconvolution of the side scattering signal as long as the refractive index is known. Nevertheless, EVs heterogeneity puts a lot of uncertainty to this strategy. Alternately, it has been suggested that beads of known dimension and refractive index

possess scattering intensity that can be used as internal calibration for the determination of various extracellular vesicles sizes [69].

Flow cytometry is a quickly advancing technology having new instruments with low detection limits (100–200 nm) although detection limits of 300–500 nm, which results in a much higher range than the size of exosomes, have been observed in most of the instruments. The challenging aspect of flow cytometry in the EV field is that, although there have been a lot of latest developments, a single particle suspension it still needed but might be difficult to obtain in the case of high exosomes' concentration, or in the case of exosome aggregation in the isolation procedure which leads to inaccurate data. The immobilization of exosomes on beads surface of can be a valid method to overcome this issue. The exosome immobilization is followed by their exposure to fluorescently conjugated antibodies against an antigen that has been reported to be displayed on their surface. Before the flow cytometry, an epifluorescent microscope can be employed for the observation of the beads and the vesicles conjugated to the fluorescent antibody. Subsequently, when the sample passes through the flow cytometer laser beam, it radiates a fluorescent signal which can be detected. This method not only allows a high throughput exosome analysis but also classification of exosomes based upon their antigen expression [27] [70].

## 1.7.2 Biochemical analysis

### 1.7.2.1 Immunoblotting

IB in the EV field consists of lysing purified extracellular vesicles in order to release their proteins and subsequently two methods can be employed. Either there can be a direct spotting on a membrane in the case of dot blot assay or the other method regards the separation of the proteins using SDS-PAGE. This last method is called Western blotting (WB) and is the main technique used in the EV field [53]. It can be employed to prove the presence of proteins that are relevant in extracellular vesicles or in EV subgroups such as CD9, CD63, ALIX, TSG101 as suggested by the MISEV2018 guidelines, however, is not an adequate method for establishing EV quantity [53] [33].

The principles behind western blotting, are related to the binding affinity of an antibody that specifically recognizes the antigen which in the case of extracellular vesicles are target proteins [27]. Contrary to flow cytometry, WB does not permit to observe the vesicles when they are intact but rather, the EVs are lysed which lead to the denaturation and reduction of the proteins during the sample preparation [71]. After being denatured, the proteins get separated by SDS-PAGE followed by the transfer to a nitrocellulose or polyvinylidene fluoride membrane. The pores on the membrane that remain open are consequently packed with detergent and/or some protein derived from non-fat milk. In a second step, an antibody against a specific antigen that would be specifically recognized on the membrane surface is exposed. Next, a secondary antibody which is the antibody of the initial one is displayed on the membrane. A fluorescent tag on the secondary antibody enables it to be detected, or another method used is by the second antibody bound to the horseradish peroxidase/alkaline phosphatase group [27].

Western blotting is among the most used methodologies for EV analysis due to its wide accessibility, ease of use and the capacity to identify both internal and surface proteins. However, is crucial to lay emphasis on the fact that this method alone is not able to determine whether detected proteins are from EVs, and, most importantly, the enrichment of a specific marker does not exclude the presence of contaminants [33].

Despite the fact that western blotting permits EV protein detection in a quick and simple manner, it is important to underline once again that this method is only semi quantitative and possesses the restrictions of a bulk assay and furthermore fails to supply protein content details on single EVs [53]. The major drawback consists of the lack of multiplexed optimization and the fact that the reproducibility and specificity are circumscribed to the amount of antibody used. This leads to the utilization of huge protein quantities from EVs in order to gain little amount of information [27]. These limitations can partially be resolved through assays that are able to capture specific EVs which are currently being developed [53].

Nevertheless, western blot remains a useful instrument in the detection of proteins derived from purified samples [33].

To summarize, EVs heterogeneity regarding origin, size, and composition together with the issue of telling them apart from biological objects such as lipoproteins and viruses which are often found in the samples, complicates the process of standardization of physical and biochemical approaches employed to characterize EVs [53]. No matter the large range of techniques developed and applied in the EV field of research, each of the detection techniques described offers both potential and limitations in the throughput, accuracy, and application for the analysis of certain EV characteristics [72].

Currently, there is no single technology that can give full coverage of the EV analyses. In fact, although many physical detection methods are not able to identify EVs deriving from different sources the employment of flow cytometry by applying detection antibodies provides the protein analysis and vice versa biochemical detection methods lack in size, concentration and heterogeneity information that can be integrated by means of electronic microscopy or other physical analysis [53].

Furthermore, EVs protein quantification presents some limits since extracellular vesicles that derive from different sources (patients, tissues or cell lines) introduce differences in terms of composition as a result of the heterogeneous expression of proteins. This indicates that although equal levels of protein can be measured by two different methods, the EV concentration of the samples can still differ. For this reason, nowadays, biochemical detection methods are often integrated with other absolute quantification techniques in order to normalize the achieved expression data [53].

ISEV advises to combine imaging of isolated EVs in high-resolution employing EM or AFM, combined with size and concentration analysis, which can be provided by NTA or flow cytometry. Moreover, in the 2018 paper that expresses the position statement of ISEV it was strongly suggested that all experimental details are to be reported including instrumental details such as software, version and brand, as well as the settings utilized during the data acquisition (e.g., camera settings, flow rate, sample dilution, image threshold) and details about calibration and controls.

Lastly, a special care should go to the analysis description for each method employed for EV analysis [44].

## 1.8 Role of EVs in physiological and pathological conditions

Extracellular vesicles can apply their impact on important biological processes through the direct activation of receptors on the cell membrane surface by employing their proteins and lipid ligands or through the delivery of their cargo into the receiving cells. Consequently, EVs are involved in processes aimed at maintaining the normal physiology such as immune surveillance, stem cell maintenance, blood coagulation and tissue repair rendering them important multifunctional signaling complexes [23].

As far as we know, one of the first papers which reported the functional communication between EVs, and cells, is the one explaining the promotion role that prostasomes have in the mobility of sperm cells [73]. During the course of the past years, several biological functions have been assigned to EVs, thus making the role of exosomes and MVs as significant vehicles of intercellular communication commonly accepted [2].

Concerning the immune responses regulation, EVs can on the one hand activate adaptable immune reactions and on the other hand inhibit inflammation by tolerogenic means. Regarding the last, it has been demonstrated that EVs provide immune suppression through different mechanisms such as via the function enhancement of the regulatory T cells, the suppression of natural killers, the differentiation inhibition of monocyte into dendritic cells as well as through the interference in the maturation of the last. On the flip side, the immune activation impacts are seen in the mediation of EVs in the survival and proliferation of haematopoietic stem cells and in the activation of B lymphocytes cells, monocytes, and natural killer cells. Regarding blood circulation, EVs partake in the coagulation stream of events by supplying an area where the clotting factors can be assembled [23].

Inside the nervous system, neurons, microglia and oligodendroglial cells, excrete EVs which can be directed from one cell kind to the other [2]. Additionally to the well-known synaptic neurotransmission, neurons can also communicate through the secretion of EVs which can participate to a variety of neurobiological functions comprising local and distal synaptic plasticity. This occurs through their enhanced release while showing neurotransmitter receptors from neurons in the cortical area which results as a consequence of increased glutamatergic activity [74]. Moreover, EVs have recently been suggested to contribute in neuronal survival, myelin creation, and neurite development [2].

Extracellular vesicles have also been shown to be involved in the cell phenotype modulation such as the phenotype conversion of haematopoietic stem cells into liver cells and the transcriptome and proteome shift from bone marrow cells to lung phenotype in vivo. Several studies have implicated EVs in stem cell maintenance and plasticity, stating also how extracellular vesicles derived from stem cells have a significant role in tissue regeneration as a result of their anti-apoptotic factors, neoangiogenic properties, and cell proliferating and stimulating features [23].

Functions of EVs have also been studied in epithelial cells. They seem to be engaged in antigen display under inflammatory conditions when released apically or basolaterally by the epithelial cells in the intestinal system, and as a result EVs can give static epithelial cells the possibility to perform at a distance. In the respiratory system, EVs found in the bronchoalveolar fluid may enhance the secretion of proinflammatory cytokines by means of the epithelial cells in human patients suffering from asthmatic conditions [2].

Nevertheless, the similar properties that emphasize the essential functions of extracellular vesicles in maintaining the normal physiology can also result in their engagement in pathological

conditions [23].

One of the leading and better-known roles of EVs in the disease area is the part they play in tumor biology. Various papers have demonstrated their involvement in activating the creation of a pre-metastatic tumor niche [75]. Extracellular vesicles possess the capacity of tumor progression stimulation. This ability is carried out through different processes such as cell proliferation induction, which consequently leads to a direct stimulation of tumor growth, angiogenesis stimulation, metastasis induction. Other procedures include, matrix remodeling promotion through the secretion of matrix proteases, and immune escape facilitation by controlling T cell activity [23].

EVs excreted by tumor cells were recognized to have direct or indirect procoagulant activity even years before demonstrating that they were involved in tumor spreading, thus connecting thrombosis induced by vesicles with cancer expansion. An important study linking EVs and tumor invasion of healthy tissues in glioma cells showed how an activated mutated epidermal growth factor receptor (EGFRvII) has proven to be highly enhanced in vesiculation causing the formation of angiogenic factors like vascular endothelial growth factor (VEGF) [76].

EVs excreted by tumor cells were recognized to have direct or indirect procoagulant activity even years before demonstrating that they were involved in tumor spreading, thus connecting thrombosis induced by vesicles with cancer expansion. An important study linking EVs and tumor invasion of healthy tissues in glioma cells showed how an activated mutated epidermal growth factor receptor (EGFRvII) has proven to be highly enhanced in vesiculation causing the formation of angiogenic factors like vascular endothelial growth factor (VEGF) [76].

Similar outcomes were reported by another study, where it was shown that EVs contain not just EGFR, but also diverse miRNAs that can lead to tumor growth stimulation and angiogenesis [77]. Tumor-derived extracellular vesicles were also demonstrated to transport EGFR in an activated form to endothelial cells in vitro and in vivo, thus promoting VEGF expression and causing angiogenesis stimulation through the autocrine activation of VEGF receptor 2. In this study it was also reported how the growth rate of the tumor could be markedly reduced via EV phosphatidylserine blockade [78].

Overall, the results of these studies indicate how EVs can trigger tumor growth through the stimulation of cancer cells proliferation by provoking an angiogenetic effect in the nearby endothelial cells [23].

Tumor-secreted extracellular vesicles influence other systems such as the immune functions where they can promote the evasion of tumors from the immune control by promoting the growth of regulatory T cells and therefore inducing the apoptosis of CD8+ T cell. Moreover, EVs are also involved in pathologies associated with tumor like thrombotic occurrences due to the enrichment in tissue factor that tumor derived EVs possess.

This factor is a main component of the blood coagulation process and combined with PS exposure provides an adequate surface for clotting and consequently drives the prothrombotic action [23].

Besides cancer, EVs also contribute to the spread of several pathogenic agents such as HIV-1, Epstein-Barr virus through the transport of viral miRNAs in non-infected cells, prions through the selective distribution of PrP but especially to the propagation of neurodegenerative diseases. Neurons not only can communicate via EVs in a local range modality as already mentioned above but they also permit a wider communication range inside the central nervous system and can possess an important effect on static neuronal networks even at a certain distance [74].

Such phenomenon is shown in the Alzheimer's disease case, where amyloid- $\beta$  peptides are discharged together with exosomes facilitating their spread to other brain areas. Along the same

lines,  $\alpha$ -synuclein protein has been found in EVs which consequently can serve as local spreading vehicles of Parkinson's disease between enteric neurons and the brainstem or bigger cortical centers [79].

A summary of EVs involvement in health and diseases is illustrated in *Fig. 1.16*.

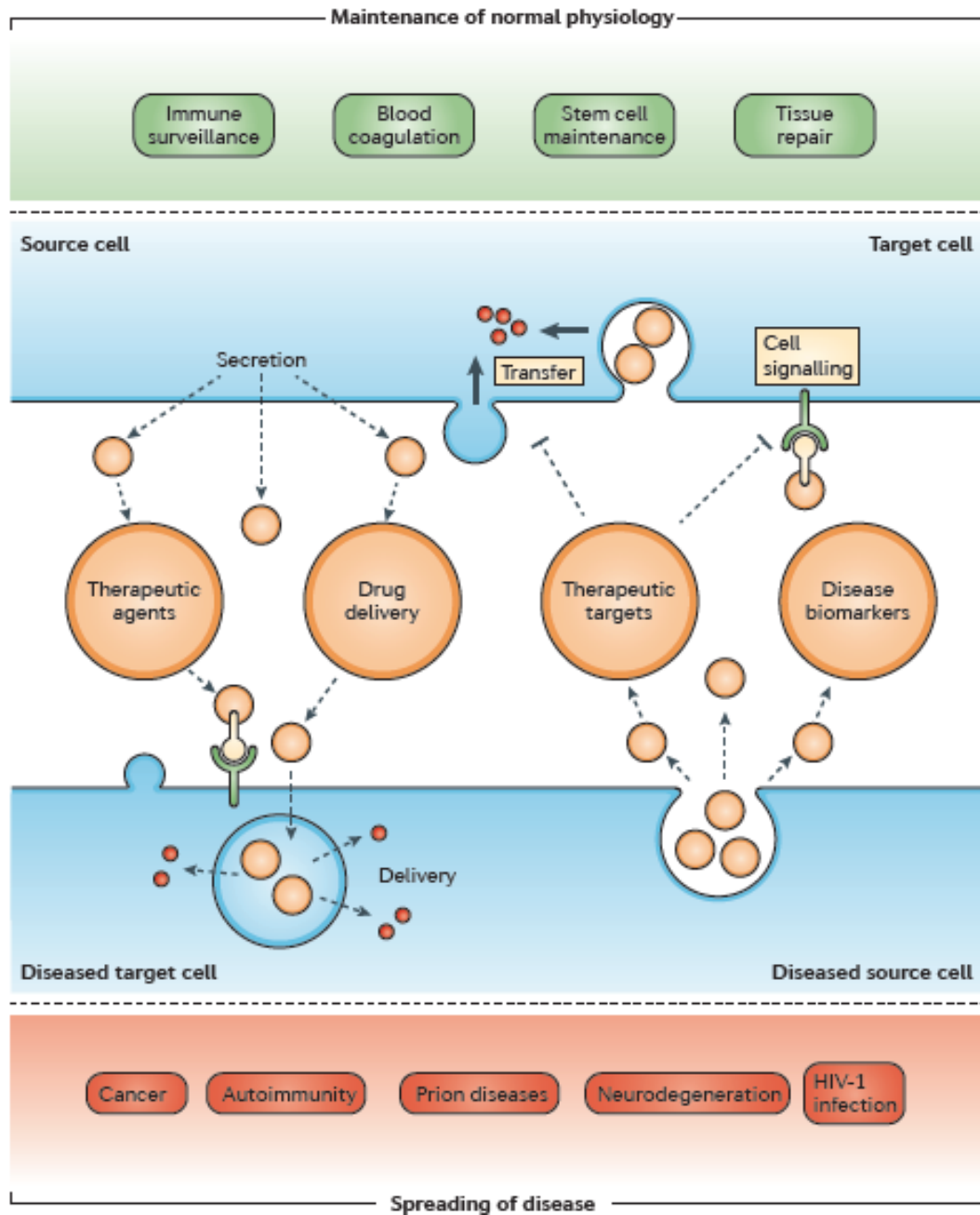


Figure 1.16: A summary figure showing the main roles that EVs play in conditions of normal physiology and disease pathogenesis [23]

All the beneficial impacts given the pleiotropic signaling effects that extracellular vesicles possess might be converted into treatments by employing them as therapeutic factors in regenerative medicine, in vaccine development, in immunotherapy thanks to their immune modulation and in tissue repair. EVs, being biological structures, are properly accepted in the human body, possess a long circulating half-life, and are able to penetrate the cell membranes and thus targeting specific types of cells, which causes them to be good candidates for immunological applications [27]. Tissue repair involves EVs capacity to transfer growth factors, bioactive lipids, soluble proteins, genetic material like miRNA, non-coding RNA and mRNA as demonstrated in the infraction of the myocardial and in cases of reperfusion injury due to ischaemia [23].

It has been also studied the capacity that the mesenchymal stem cell exosomes possess in being able to operate as therapeutic objects to assist tissue injury reduction [27].

Moreover, since EVs are secreted by most cell types, contain RNAs and have the capacity to transmit their cargo to recipient cells shows how they are extremely fitting candidates for drug delivery, in particular the one concerning therapeutic nucleic acids [23].

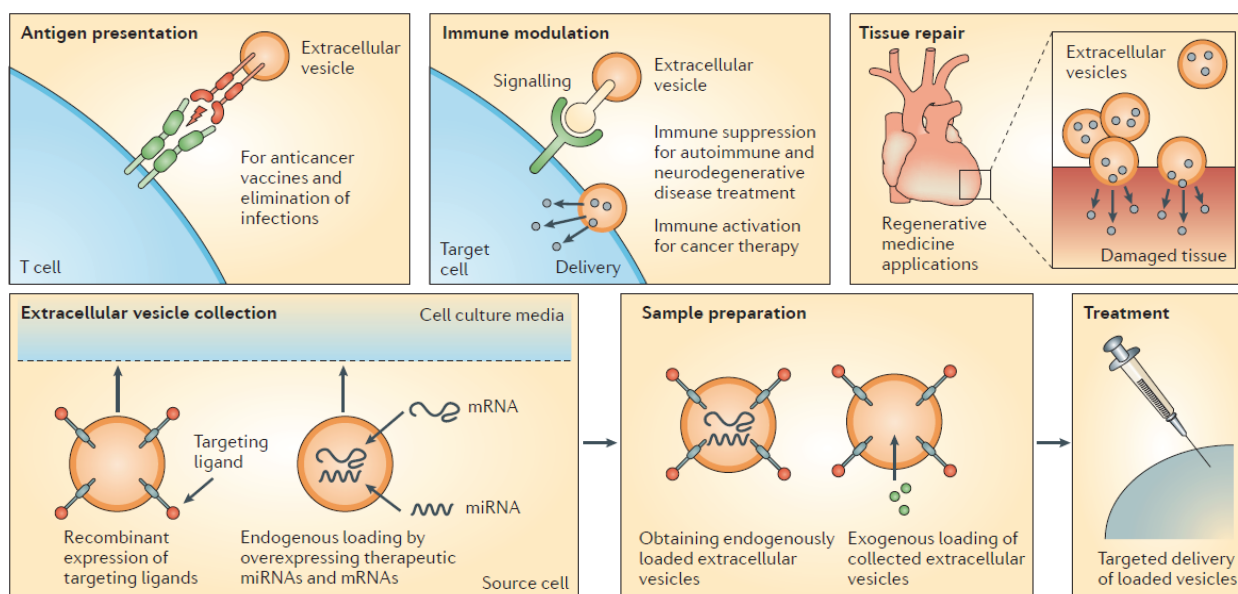


Figure 1.17: Therapeutic targeting and exploitation of extracellular vesicles adapted from [23]

In the EV research field, a recent interest in examining their potential to behave as biomarkers for several diseases has surfaced. Recent studies have concentrated on extracellular vesicles as biomarkers of glioblastoma, of acute kidney injury, pancreatic cancer and lung cancer as well [27] [80]. Utilizing EVs to diagnose cancer is ideal due to the fact that they are easily located in many body fluids which enables to perform non-invasive liquid biopsy approaches not only for diagnosis purposes but also to track the response to treatment for a specific patient. More in details, this is related to the possibility to discover if a certain disease marker could be directly correlated to a disease state and in the eventuality that the patient's therapy is successful if consequently there is a change in the behavior of biomarkers as the patient is subjected to therapy [27].

The role of EVs as biomarkers will be focused especially on lung cancer as discussed hereafter.

### 1.8.1 Lung cancer

In 2019, the American Cancer Society estimated that a number of 606,880 American citizens would have died from cancer during that year, which corresponded to nearly 1,700 deaths every day. In men, cancers of the lung, prostate, and colon & rectum are the cause of the majority of deaths while in women of the lung, breast, and colon & rectum. [81].

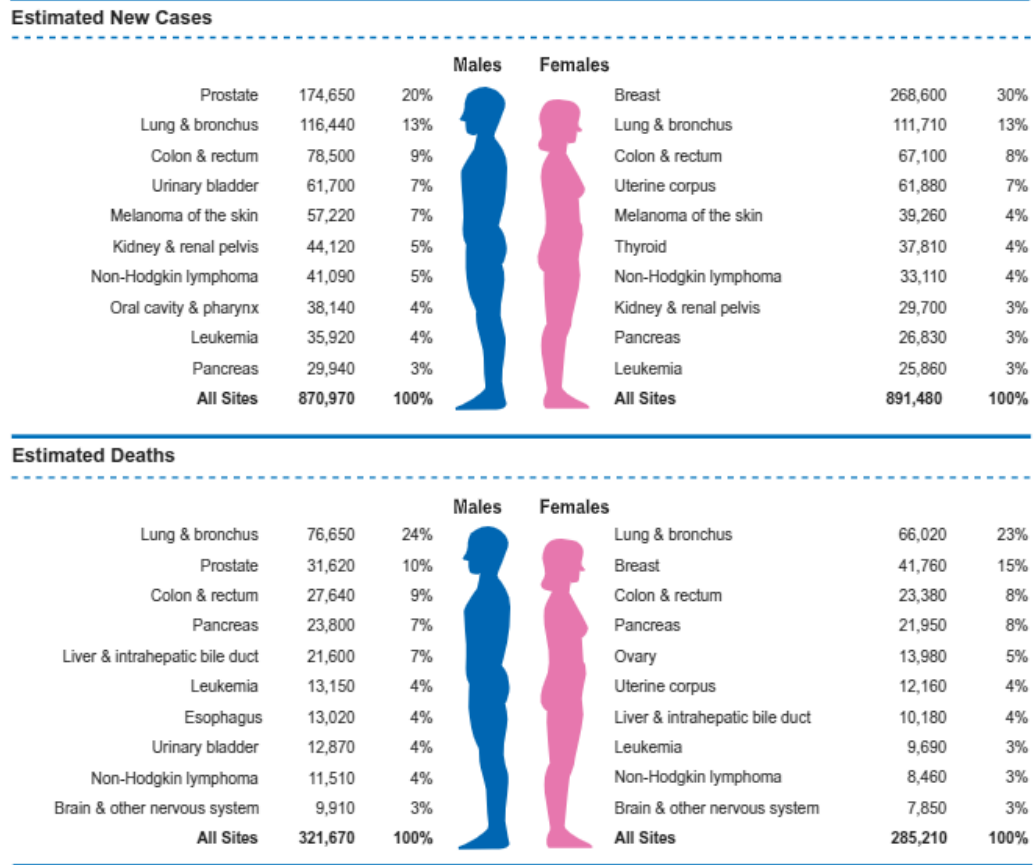


Figure 1.18: Indication of the ten leading cancer types in the United States in 2019 in relation to the estimated new cancer cases and deaths divided by sex [81]

Lung cancer is responsible for about 25% of deaths related to cancer in the United States each year reaching 170'000 victims, and ranges currently as the second most frequently diagnosed cancer in both men and women worldwide. Among men, the amount of lung cancer deaths exceeds two times that of prostate cancer deaths while, lung cancer deaths in women, in comparison to that of breast cancer, are almost double the amount.

In Europe, the number of people diagnosed with lung cancer every year rank about 213,663 for men and 98,982 for women which makes lung cancer the second and third most diagnosed cancer in Europe for male and females, respectively. Also in Europe, lung cancer is the main cause of cancer deaths, with a recorded number of 267,700 deaths in 2012 counting for nearly one fifth of all cancer deaths [82].

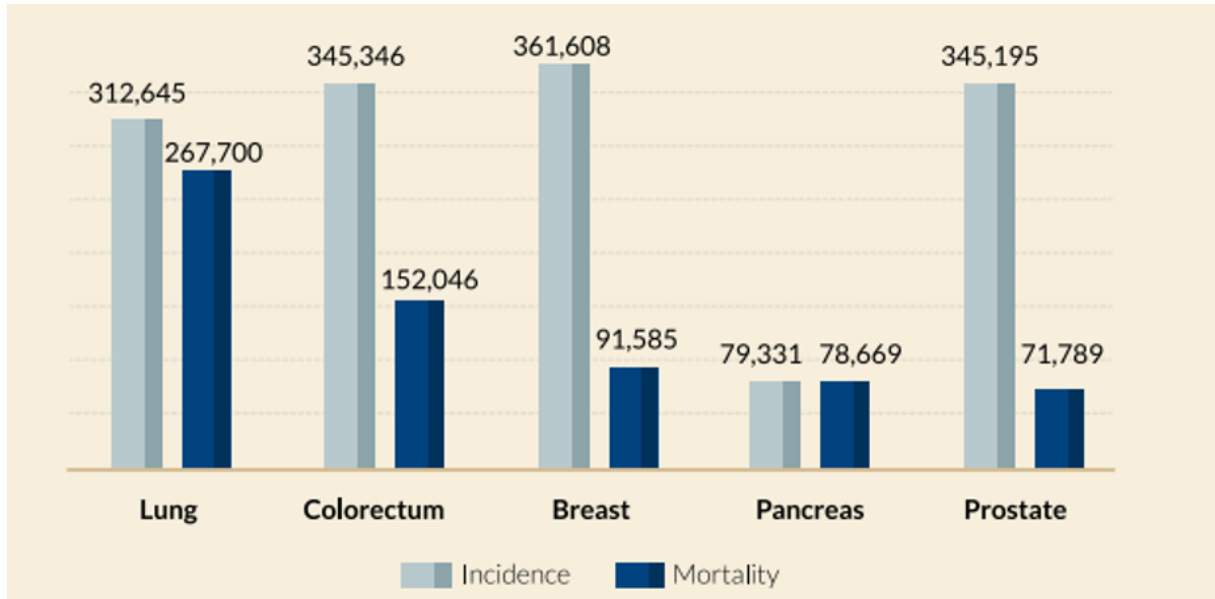


Figure 1.19: Five highest mortality cancers in the European Union [82]

Nearly 80% of lung cancer cases are of non-small cell lung cancer (NSCLC) type while the other 20% are small cell lung cancer (SCLC) [83]. When diagnosed with lung cancer, more than half of the patients die within the first year of diagnosis while the five-year survival rate, without holding distinctions between the subtypes, is 17,8%, percentage which rates through the lowest among all cancers types [84]. For many cancer types there has been observed a steady increase in survival but this sort of behavior hasn't been applied for lung cancer because over 50% of the cases are diagnosed at an advanced or metastatic stage [81] which makes curative treatments not applicable in up to 90% of the cases.

The delay in diagnosis is to blame to first symptoms which appear when the cancer has already spread to other organs which mostly include bones, brain, liver, adrenal glands, pleura and the other lung. Even when cancer symptoms appear since the beginning, in many cases, they are associated with less serious causes such as smoking effects or various infection. Thus, early detection would have a nominal influence on survival [82].

In this situation, EVs, especially exosomes, have obtained recent attention for their role in simplifying early detection and diagnosis and giving improvement in cancer treatment outcomes [85] [86]. EGFR represents a potential cancer and angiogenesis target since it has been observed that this receptor is widely lacking in normal endothelial cells nevertheless is frequently overexpressed in a selective way by the tumor-related vasculature [78].

The dysregulations that occur on the EGF receptor engage in a variety of cancers in different ways. In the NCSLC type, EGFR mutations and the consequent increased protein expression are the main developments that take place and this overexpression has been implicated in the pathogenesis of the disease. The EGFR triggering promotes cell proliferation, apoptotic threshold increase, cellular motility increment and consequently metastasis, neoangiogenic enhancement, and ultimately chemotherapy and radiation resistance [87].

For these reasons EGFR can be considered a valid NCSLC biomarker.



## Chapter 2

# State of the art

### 2.1 Liquid biopsy detection methods

Proteins found in EVs' surface, as already mentioned, have recently been emerging as important biomarkers for cancer diagnosis. Regarding lung cancer, exosomes' proteins, such as LG3BP, LRP1, and more importantly EGFR have been associated with stages of such tumor as well as metastasis. To measure the expression levels of the extracellular vesicles' proteins different techniques can be employed such as, the previously mentioned western blotting and flow cytometry based on immunobeads, enzyme-linked immunosorbent assay (ELISA) and mass spectrometry. The issue concerning these methods relates to their bulkiness, time and cost consuming effects, other than the fact that, currently, these techniques cannot be adapted to clinical use, especially from a point-of-care view [88]. Therefore, in this context, liquid biopsy biosensors have been proposed to overcome these challenges. In fact, liquid biopsy not only consist of a simple and minimal invasive approach, but also, is able to provide more extensive tumor information at different time stages that tissue biopsy cannot deliver. For these reasons, its employment could be advantageous in many fields such as diagnosis, precision medicine, cancer screening and treatment evaluation. Moreover, the majority of biosensors proposed to detect EVs are miniaturized or integrated in portable platforms of sensing and deliver quick and cost-effective analysis demonstrating a good potential in cancer diagnostics [88].

Regarding the detection methods, the biosensors are based on three major fields: immunofluorescence, surface plasmon resonance (SPR) and electrochemistry.

Examples for each category will be shown below.

#### 2.1.1 Immunofluorescence-based detection

This type of detection is one of the most commonly employed for the detection of exosomal protein, since it allows to be easily integrated in microfluidic platforms and also enables sensing at a multiplexed level.

One of the most used strategies for this type of detection is to capture exosomes using magnetic beads conjugated with antibodies. The application and removal of a magnet can comfortably, therefore, retain or release the extracellular vesicles in the microfluidic channel. Once the exosomes are captured, their protein markers' expression levels can be analysed through immunofluorescence techniques.

The design of a microfluidic biochip using such an approach is shown in *Fig. 2.1*. The first capture step consists in the isolation of the exosomes through the immunomagnetic technique. Secondly, the exosomes are lysed in order for their internal proteins to be released since the biochip is designed for both intra-vesicular and surface protein detection. The last capture step consists in the protein capture through magnetic beads and lastly they are characterized via chemifluorescence detection [88].

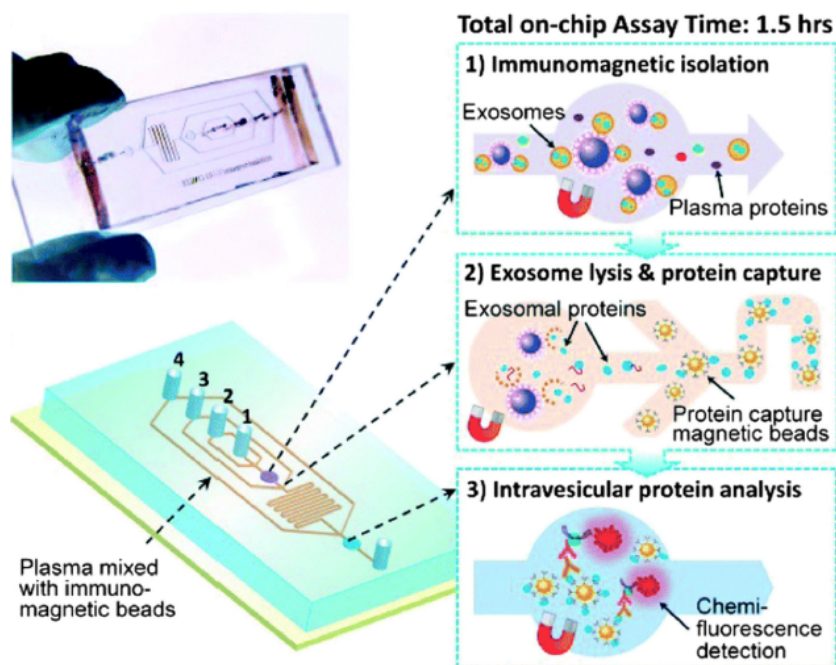


Figure 2.1: Photo and schematics showing the main steps for exosome immunomagnetic isolation and further protein immunofluorescence detection performed by a microfluidic biochip [88]

The improvement of the previous chip into a multiplexed biomarker detection is shown in *Fig. 2.2*.

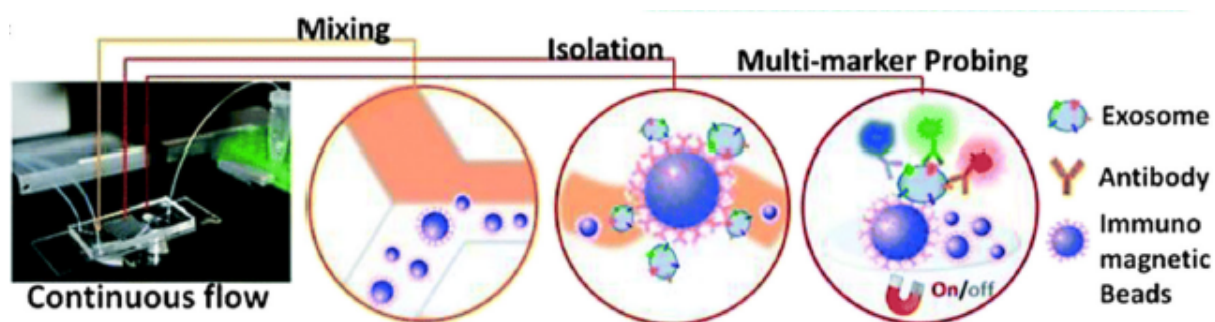


Figure 2.2: Main steps for multiplexed exosomal protein detection performed by the ExoSearch biochip [88]

The design, called ExoSearch biochip, in addition to improving the exosomal capture by the magnetic beads conjugated with antibodies performed on chip instead of the previous off-chip plasma premixing, allowed also the multiplexed detection of exosomes' surface proteins, performed through a mix of antibodies labeled with various fluorescent dyes [88].

Another strategy that doesn't require the employment of magnetic beads consists in the detection of exosomes through photosensitizer beads. The assay, called ExoScreen involves acceptor beads that present an antibody and free biotinylated antibodies both reacting with non-purified serum samples. The goal is to capture exosomes that present both of the correspondent surface proteins to the previous antibodies. Subsequently, the addition of donor beads coated with streptavidin is combined in order for such beads to interact with the biotinylated antibodies previously applied and, thus, create acceptor-exosome-donor bead complexes. The signal deriving from the fluorescent acceptor beads can be detected and therefore, the protein expression can be measured.

Approaches that don't rely at all on the employment of capture systems have also been developed and they concern the functionalization of microfluidic chips with antibodies. Following the immunofunctionalization process, the protein detection is performed through fluorescence techniques [88].

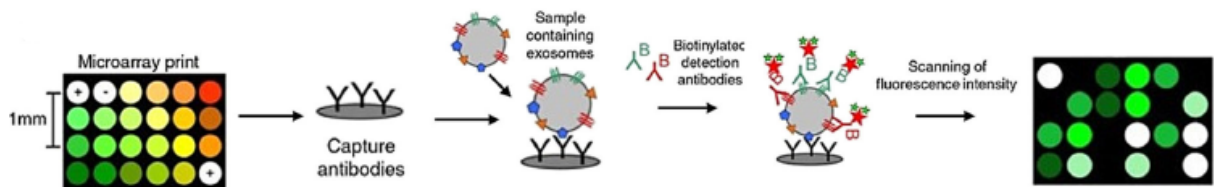


Figure 2.3: Example for exosomes' protein detection performed through an EV array [88]

### 2.1.2 Surface plasmon resonance-based detection

Surface plasmon resonance (SPR) consists of an optical, sensing technology that performs measurements in real time and without the employment of labels. The detection method is used in the case of biomolecules immobilized on metal surfaces, usually gold.

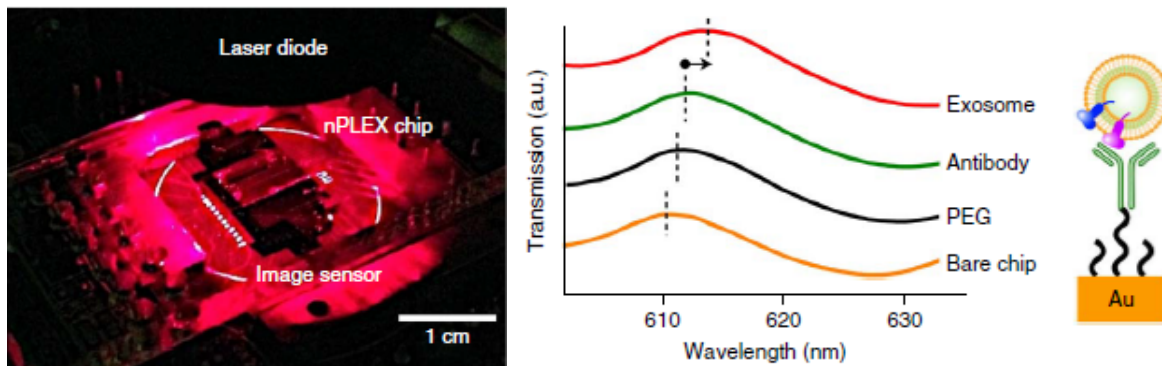


Figure 2.4: Photo of the nPlex biochip device (on the left) and relative spectral shifts (on the right) adapted from [89]

When the target molecules are bonded to the immobilized receptors the refractive index locally changes, affecting thus the optical proprieties which leads to a signal change that can be measured. This detection method can be very sensitive and selective and in particular requires small sample volumes.

As an example, the photo of a device called nPlex biosensor that employs SPR detection is shown on the left side of *Fig. 2.4*. It consists of nano-holes that are patterned periodically to create an array into a metal film. The spectral shifts that occur when the surface protein of exosomes bind to the affinity agents are shown on the right side of *Fig. 2.4*. These shift reflect the laser light change of intensity which vary proportionally to the expression level of the exosomes' proteins [88].

### 2.1.3 Electrochemical-based detection

This type of detection can result in very encouraging results since it can produce good sensor sensitivity with also the possibility to be incorporated in solid platforms as well as the potential to lead to multiplexed sensing.

The majority of the sensors employs horseradish peroxidase for the target labeling. The reaction that occurs between the mentioned compound and a chromogenic substance called 3,3',5,5'-tetramethylbenzidine is of the redox type. This allows amperometric systems to detect such reaction as a signal and can also be employed for the concentration calculation of the target molecules.

As an example, a device named iMEX designed for a portable and integrated magnetic-electrochemical detection of exosomes is shown in *Fig. 2.5*. A magnet was enriched in the sensor electrodes in order to capture exosomes that were conjugated with antibody-magnetic bead complex. The detection of surface proteins on the exosomes occurred through the redox reaction mentioned above. The sensor can perform multiplexed measurements up to eight channels [88].

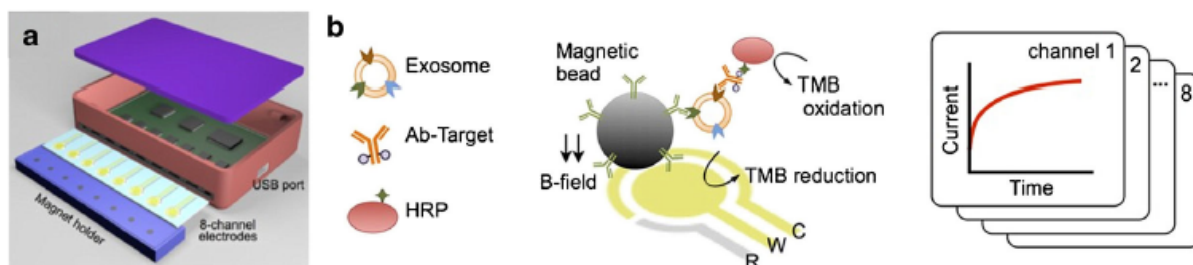


Figure 2.5: a) Schematics of the device showing the magnetic holder and b) sensing mechanism [88]

## 2.2 Aim of the thesis

The need for label-free detection capable of targeting a wide variety of molecular targets performed by a simple and inexpensive sensor has been long researched and as a result has encouraged the development of novel techniques taking into account the immense potential that this hold in the monitoring of personal health as well as in the diagnostics field. Among various detection methods, the attention has been often focused on label-free sensors based on semiconductor technology since

they have been shown to possess certain advantages being that the capacity to allow devices that are ultra-sensitive, portable as well as easy-to-use at a low cost [90].

Recently, a wide interest has grown for exosome-based liquid biopsies. This can be traced to the huge advantage that the liquid biopsies provide since the cancer presence and treatment feedback can have a direct and frequent monitoring in various body fluids, among which pleural effusions, contrary to traditional tissue-based biopsies [91]. In fact, tumor cells already at an early stage can release exosomes in the extracellular space, and ultimately they can travel in body fluids. This allows liquid biopsies performed on exosomal surface markers to be a great tool in the early detection of cancer [91].

The platform and the setup have already been tested for one-channel measurements and they have showed positive results [91]. In addition, it is well known that in order to bring a device to clinical settings it is important to scan as many markers as possible, simultaneously, as this could lead to time and costs saving results. Moreover, the employment of the same device to scan different markers in parallel produces less chance of error.

For these reasons, the first aim of this work is to investigate and further validate the efficacy of a platform for multiplexed EV detection and profiling using simple, low cost and label-free electrokinetic sensors. The method of detection is based on the streaming current from which the zeta potential  $\zeta$  is calculated permitting the monitoring of markers' binding dynamics from a solution under laminar flow. The goal is to successfully detect and profile EVs derived from lung cancer cells both from engineered cell line and directly from patients' pleural effusions using a multiplexed platform capable to investigate more than one channel at a time by targeting their membrane proteins CD9, CD63 and EGFR, considered to be important set of representative surface biomarkers for lung cancer.

This multimarker analysis of EVs surface proteins exploits the surface potential change that occurs due to the binding between the proteins and the targeting antibodies on functionalized silica capillaries. Control measurement should also be carried out in order to test the influence of non-specific binding (NSB).

The second aim of this work is to employ the sensor, possibly with the four-channels platform in the testing of clinical samples. Since the sensor has never been tested on such samples, it is important to assess its performance, for the fact that clinical samples are more impure than the ones derived from engineered cell lines. This is due to the harder difficulty in the isolation and purification techniques and contamination from proteins, lipids could interfere with the measurements and result in false outcomes.



## Chapter 3

# Experimental method

In this chapter the methods and materials adopted in order to perform the experiments as well as the theoretical principle behind the detection procedure will be reported. As already mentioned, the analysis method employed is based on the detection of unlabeled proteins measured from the streaming current variations within a microfluidic channel upon the application of a pressure gradient.

### 3.1 Electrokinetic phenomena

Electrokinetic phenomena can be identified as all those phenomena involved in tangential fluid movement that is situated near a charged surface. They represent evidence of the electrical properties found in interfaces under steady-state and isothermal conditions and often portray the only origin of information accessible [92]. Taking into account the fact that when a solid surface engages with a liquid it carries a surface charge, it is understandable to conclude that this effect increases significantly in nanochannels, due to their high surface-to-volume ratio.

Surface charge results from surface groups separation and specific surface adsorption of ions that are found in the solution. The charge density of the solid surface could be either positive or negative depending on the number and type of acid and basic groups in the solution but the surface could also carry zero net charge, called "point of zero charge", that occurs at a certain pH of the solution. The surface charges cause electrostatic forces that are essential in the interactions between the surface in liquid itself and different molecules as they control the transport in nanofluidic structures.

In fact, van der Waals forces play an important role at small distances providing the attractive interaction in dissolved particles while repulsive electrostatic forces can prevent coagulation. Moreover, van der Waals forces do not undergo any changes due to variations in pH and electrolyte concentration, which cannot be said the same for electrostatic forces [93].

An opposite charge area of counterions is developed in the liquid as a consequence of the well-established surface charge created at the solid surface in order to maintain the electroneutrality at the interface between liquid and solid. This kind of charge distribution has historically been called electrical double layer (EDL) and is composed of one layer of fixed charge in the solid surface and another layer of excess of counterions some bound and other diffused while the co-ions (same charge of the fixed surface) present a deficit [92].

On account of these phenomena, molecules can be monitored as a result of their charge in

nanochannels due to the electrostatic interactions they have with the EDL, that consists of a shielding structure, naturally originated at the solid-liquid interface near a charged surface [93].

### 3.1.1 Zeta potential

In the Helmholtz model, EDL was originally delineated as a simple capacitor. Chapman and Gouy addressed one of the charge layers as uniformly spread on a planar surface while submerged in an electrolyte solution while Stern regarded that the model explaining the solvent as a unstructured dielectric holding a constant permittivity and the electrolyte ions being as point charges was not satisfactory thus introducing the Stern layer which is situated between the inner and outer Helmholtz planes in which the potential distribution and charge are presumed to have a linear trend, and a diffuse layer situated at a distance from the wall in which the Gouy-Chapman model is employed instead [93].

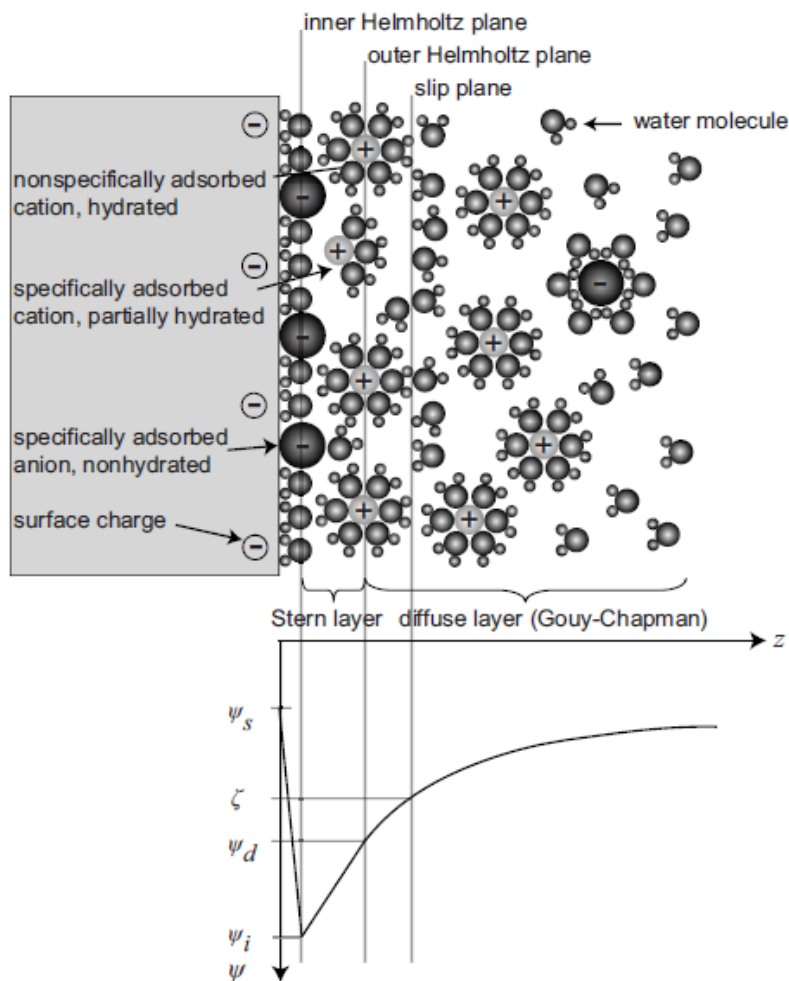


Figure 3.1: Graph showing the solid-electrolyte interface according to the Gouy-Chapman-Stern model [93]

The representation of such model is illustrated in *Fig. 3.1* which as can be seen is divided into three layers.

The first one holds the  $\psi_i$  potential and is situated at the inner Helmholtz plane, containing non-hydrated counterions and co-ions which consequently are absorbed specifically on the surface. The second layer holds the  $\psi_d$  potential and is delimited by the outer Helmholtz plane and is composed of hydrated, partially hydrated and bound counterions while the third and more exterior layer is called diffuse layer in which the slip plane bearing the  $\zeta$  potential is located and it consists of counterions and mobile co-ions [93].

On many occasions, since the slip plane and outer Helmholtz plane are located close by from one another  $\psi_d$  is often approximated to  $\zeta$  for practical reasons.

The slip plane, also known as the shear surface, consists of an imaginary plane which divides the ions that are mobile in the solution from those that are immobile close to the solid surface and its  $\zeta$  potential can be obtained through experiments making it a significant parameter for the determination of particles balance in colloid science and for the description of fluid flow in microchannels in micro-total analysis systems.

Moreover, the  $\zeta$  potential depends on the pH and ionic strength of the solution resulting in a decrease of its absolute value with increase in concentration of ions in the solution as shown in *Fig. 3.2* [93] [94].

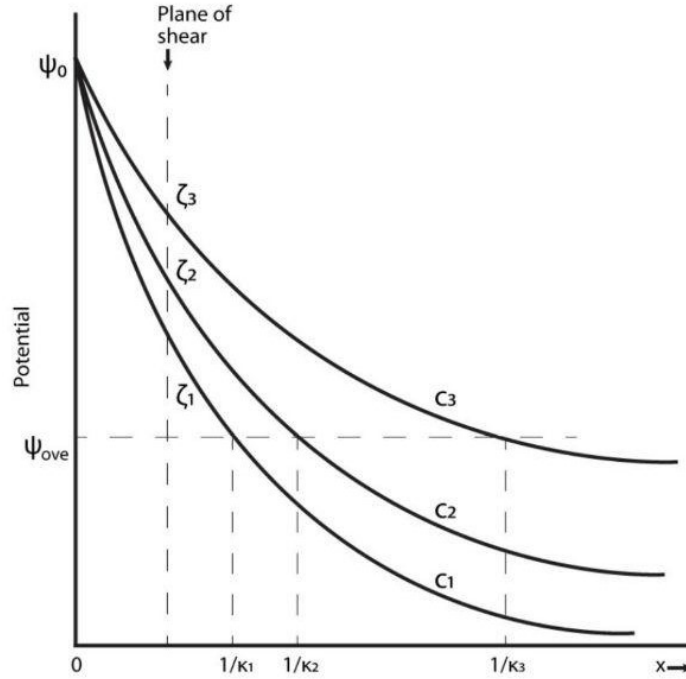


Figure 3.2: Effect of the concentration of electrolyte on the  $\zeta$  potential with  $c_1 > c_2 > c_3$ ;  $\zeta_1 < \zeta_2 < \zeta_3$  adapted from [94]

Thus, the range of application of the streaming current method is confined by the ionic strength. The upper and lower boundaries rely on the electrode and electronic circuit quality employed in the

detection of the direct current. It is suggested from experimental studies that the ionic strength for the zeta potential analysis of solid surfaces should be 0.001 mol/l [95].

$\zeta$  potential measurements are largely employed in the colloid science field mostly for the importance this investigation has on the state of their stability. However, they remain still poorly unexamined in regards to solid surfaces and practically uninvestigated in the case protein absorption.

The  $\zeta$  potential could be used for the description of surface charging behavior, providing information concerning the surface charge in function of pH, the isoelectric point, the reactivity and absorption processes of the surface [96].

### 3.1.2 Streaming current

The streaming current or potential is a phenomenon that arises in plugs and capillaries and emerges as a result of the displacement of charge within the EDL due to the application of a pressure gradient which causes the liquid phase to shift tangentially in respect to the solid phase [92].

During the flow of the liquid through a small capillary the ions situated in the mobile zone of the EDL are transported downstream. This results in the creation of the streaming current which flows parallelly to the liquid advancement. With the increasing ion collection downstream arises an electric field generation which induces another current, called conduction current, to move in the opposite direction. A stable state is obtained when these two currents equal each other.

The streaming potential, on the other hand, is the electrostatic potential resulting from the difference between the two end zones of the capillary [93].

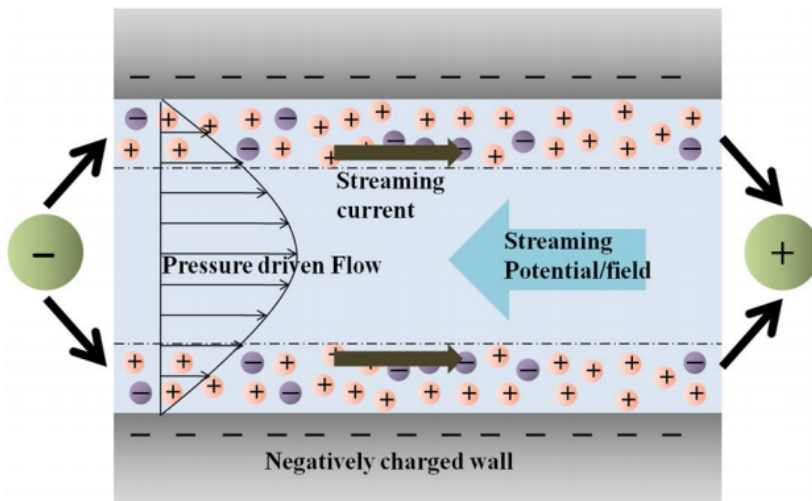


Figure 3.3: Schematic representation of how a pressure driven flow leads to the generation of a streaming current [97]

The detection of the streaming current can be carried out through the direct measurement of the electric current flowing between two locations, one situated upstream and the other downstream using non polarizable electrodes at each location attached to an electrometer possessing a low in-

ternal resistance. The streaming current  $I_{st}$  in a circular cross-section capillary is obtained through the following equation [92]:

$$I_{st} = -\frac{\epsilon_{rs}\epsilon_0\pi a^2}{\eta} \frac{\Delta P}{L} \zeta \quad (3.1)$$

where  $\eta$  is the dynamic viscosity,  $\epsilon_{rs}$  and  $\epsilon_0$  the relative permittivity of the dispersion medium and vacuum,  $L$  and  $a$  are the length and radius of the capillary,  $\Delta P$  the pressure difference between the two end zones of the capillary produced externally [92].

In order to monitor the streaming current, the extremes of the capillary should be connected in short-circuit conditions meaning that the external circuit should possess a low resistance. This is an important condition which if not respected, therefore in the case of an open circuit with high resistance, could lead to the transport of ions and consequent charges accumulation of opposite signs between the two end zones of the capillary causing the emergence of the streaming potential  $U_{str}$  which ultimately generates the conduction current,  $I_c$  [92]:

$$I_c = K_L \pi a^2 \frac{U_{str}}{L} \quad (3.2)$$

with  $K_L$  being the bulk liquid conductivity.

## 3.2 Capillary surface functionalization

In this section, a surface functionalization protocol prepared to achieve in-capillary immobilization of EVs will be described. The protocol represents a crucial procedure in the detection of EVs thus allowing their capture and further investigation.

The protocol consists of the following steps:

**1) Cleaning:** Deionized water (DIW) was passed through the length of the capillary for a few seconds.

**2) TL1 cleaning:** A solution consisting of a mixture of DIW, hydrogen peroxide ( $H_2O_2$ ) and ammonium hydroxide ( $NH_4OH$ ) in 5:1:1 volume proportion was passed through the capillary at  $88^\circ C$  for 10 minutes. This mixture is highly corrosive and consists of a powerful oxidizing agent, removing not only all the impurities that may be present inside the capillary but also hydroxylating the surface by adding OH groups.

Afterward, the capillary surface was rinsed with DI water and then ethanol, for a few minutes.

**3) Silanization process:** Metal oxide surfaces such as the silicon oxide obtained from the previous step can go through this process, since they contain OH groups which react and exhibit the alkoxy groups on the silane creating a covalent -Si-O-Si- bond.

For this purpose, a solution consisting of 5% w/v of APTES ((3-Aminopropyl) triethoxysilane) and 95% ethanol (EtOH) was prepared and flowed into the capillary for 10 minutes.

As it can be observed in *Fig. 3.4*, APTES enables the exposition of  $\text{NH}_2$  groups.

Afterward, the capillary surface was rinsed with ethanol and then DIW, for a few minutes, to remove the unbound silane from the surface.

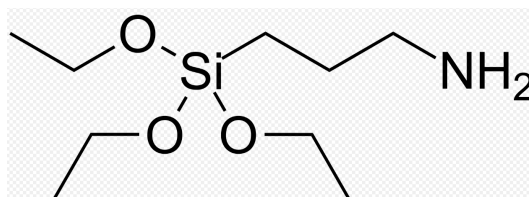


Figure 3.4: APTES chemical formula [98]

**4) Glutaraldehyde (GA) incubation:** This compound is often used in the biochemistry field as an amine-reactive crosslinker and fixative. In fact, GA operates as a linker thanks to the presence on both sides of a carboxyl ( $\text{COOH}$ ) group that binds on the one side with the amine present in APTES from the previous step and on the other side remains available for the following step.

1% w/v GA was mixed with 0.01 M phosphate buffered saline (1xPBS) and flowed for 1 hour, followed by rinsing in 1xPBS for a few minutes.

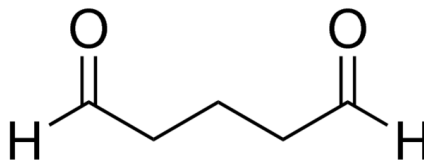


Figure 3.5: GA chemical formula [99]

**5) Capture probes immobilization:** The antibodies or affibodies were immobilized into the capillary surface at a concentration of 50  $\mu\text{g}/\text{mL}$  dissolved in 1x PBS for 2 hours. This incubation was skipped in the case of control measurements in order to test the capillary surface without capture probes for non-specific binding.

To prevent agglomerations from happening, the sample containing the capture probes was vortexed for 20 seconds after the dilution step. The dilution rate relies on the initial concentration of the antibodies stock.

The 2 hours immobilization time was followed by rinsing in 1xPBS for a few minutes.

**6) GA deactivation:** A solution of tris-ethanolamine (tri-ETHA: 0,1M tris-buffer and 50 mM ethanolamine at  $\text{pH} = 9,0$ ) is employed for the deactivation of the NSB sites of GA that are not attached to the capture probes.

Without this step, the EVs binding during the experimental measurements would result in a non-specific one since EVs would not only bind to the specific capture probes but also to the free GA.

The incubation time was 30 minutes, after which tri-ETHA was washed with 1xPBS for a few minutes.

**7) Casein saturation** : The last step of the functionalization process consisted of preparing a casein-based blocking solution (0,05 w/v % in 1xPBS) in order to minimize and saturate the residual free binding sites. For this purpose, the solution was flowed for 2 hours. At the end of the incubation the capillary was rinsed by 1xPBS for a few minutes.

At the end of these steps the functionalized capillaries were stored under  $N_2$  into vials until use. For more details on the chemical reactions of each step the Appendix can be consulted.

Each of the microcapillaries employed in the functionalization process aforementioned were cut at a length of about  $\sim 12$  cm allowing to obtain two microcapillaries to be utilized during the experiments reducing the functionalization period which could be time-consuming.

### 3.2.1 Control functionalization

The steps described above refer to a functionalization with capture probes in order to target a specific protein. In case of control measurement some changes were applied.

The procedure remained the same until step 4 while capture probes immobilization was not applied since the capillary surface without capture probes was used to test the influence of non-specific binding. Therefore, GA incubation was followed by GA deactivation also for 30 minutes in this case while the saturation in step 7 was performed for 4 hours instead of 2 hours to compensate for the time the capture probes were incubated in the normal functionalization process.

In *Fig. 3.6* a schematic of the final result of the functionalization procedure applied to the inner capillary surface is shown.

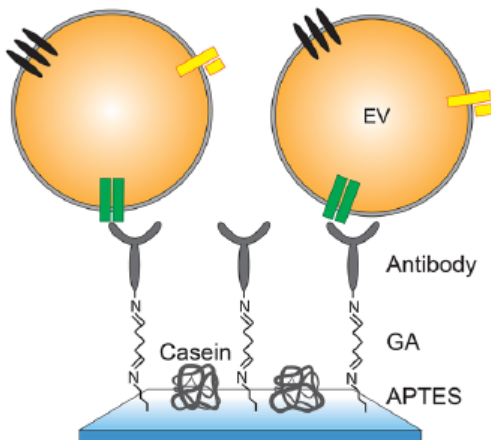


Figure 3.6: Schematics of the functionalization strategy applied to the inner surface of the microcapillary, displaying how the immobilized antibodies act as affinity reagents capturing EVs by their surface proteins [91]

### 3.3 Experimental setup

The detection method was based on the measurement of the streaming current caused by the pressure-produced flow of phosphate-buffered saline (PBS) buffer or sample containing EVs within a hollow silicon-made functionalized micro-capillary.

The experiments were conducted using micro-capillaries with an inner diameter of 25  $\mu\text{m}$  and a length between 4,6 and 4,8 cm.

A flow sensor (Elveflow, MFS3) was positioned at the inlet of the capillary in order to manage the monitoring and correct maintenance of the flow rate. For the measurement of the streaming current, two platinum electrodes at the inlet and at the outlet of the micro-capillary were used.

A constant train of periodic trapezoid pressure pulses with a duration of 30 seconds and 1,5 bars of height switching from 1,5 bars to 3 bars was produced thanks to the employment of a commercial pumping system (Elveflow, OB1) in order to achieve the flow of the solutions into the micro-capillary. In particular, the applied pressures produced flow rates of 3  $\mu\text{l}/\text{min}$  and 6  $\mu\text{l}/\text{min}$ , respectively, considering a one channel measurement. The flow rates increased linearly when more channels were recorded.

Since the streaming current changes with pressure  $\Delta I_{st}$  can be calculated. The pressure switching was performed in order to compensate for electrode polarizations. In fact, if only one pressure were to be applied, the value of the streaming current might significantly change over time, because of platinum electrode polarization.

Therefore, with the application of two pressure pulses, the change due to polarization results the same for both pressures, thus, when  $\Delta I_{st}$  is calculated the contribution of polarization is eliminated.

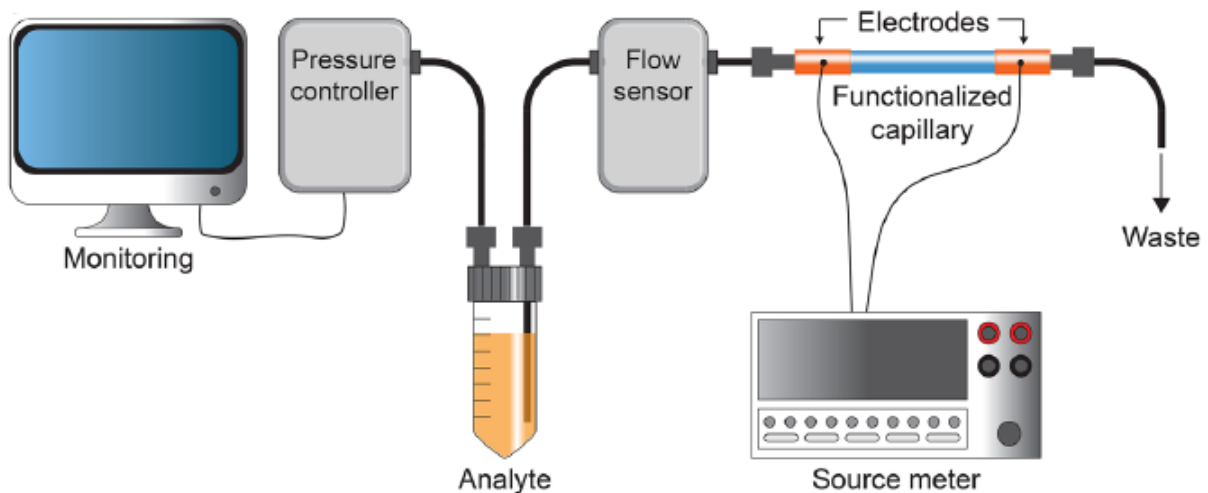


Figure 3.7: Schematics of the experimental setup [91]

Lastly, a source meter enabled the recording of the changing streaming current due to the periodic pressure pulses and was later transformed in apparent zeta potential ( $\zeta^*$ ) in accordance with the following equation:

$$\zeta^* = \frac{\Delta I_{st}}{\Delta P} \frac{\eta}{\epsilon \epsilon_0} \frac{L}{A} \quad (3.3)$$

where  $\frac{\Delta I_s}{\Delta P}$  is the modification that occurs in  $I_s$  with pressure,  $\eta$  the viscosity,  $\epsilon \cdot \epsilon_0$  the permittivity, and  $\frac{L}{A}$  the length and cross-section of the capillary, respectively.

This equation results from an evaluation approach by Helmholtz and Smoluchowski (HS). In order to apply the HS equation, precise knowledge of the streaming capillary geometry is required [95].

Considering that proteins exhibit a larger size than the charge determining ions found in the PBS buffer, during protein binding on the capillary the hydrodynamic flow could be modified in the region nearby its surface.

For this reason, the  $\zeta$  potential measured following protein binding may result in a reduced value compared to the real surface potential. Thus, the term "apparent  $\zeta$  potential ( $\zeta^*$ )" is used in reference to this lower  $\zeta$  potential measured [90].

The data collected from the experiments were processed by a custom-designed software.

The functionalization procedure on the inner micro-capillary surface was performed with capture probes that are affinity reagents against particular membrane proteins situated on EVs. Upon injection, the sample containing EVs progressively diffused to the capillary surface, permitting surface proteins to interact with the immobilized capture probes. This interaction resulted in a modification of the surface charge of the functionalized capillary and consequently in a variation of the streaming current, whose measurement was directly performed thanks to the setup described above and shown in *Fig. 3.7*.

The experiments were carried out at room temperature with PBS at pH 7.4. In order to decrease the concentration of counterions, the PBS buffer was diluted to 0.1xPBS, which corresponds to the recommended ionic strength of 0.001 mol/l resulting in an increment in the magnitude of the measured  $\zeta^*$ .

### 3.4 Experiment conduction

Without any major distinction between measurements involving one, two or four channels, the experiments were essentially carried out in five main steps.

1) The first step included a **caseination process** of the tubes, connectors and electrodes included in the setup for the duration of two hours. This process was performed for the same reason as in the functionalization procedure of the silicon capillary: to reduce non-specific binding of the EVs to the setup components.

This process in the case of, respectively, a two-channels and a four-channels measurement is shown in *Fig. 3.8* and *Fig. 3.9*.

2) **Initial 0.1xPBS injection** until a stable flow rate was reached in order to measure the first  $\Delta I_{st1}$  baseline. The use of 0.1xPBS was preferred to the 1xPBS because the thickness of the EDL is higher in the first case, enabling, thus, to sense the charge from a larger area occupied by the EVs and thus resulting in a higher sensitivity.

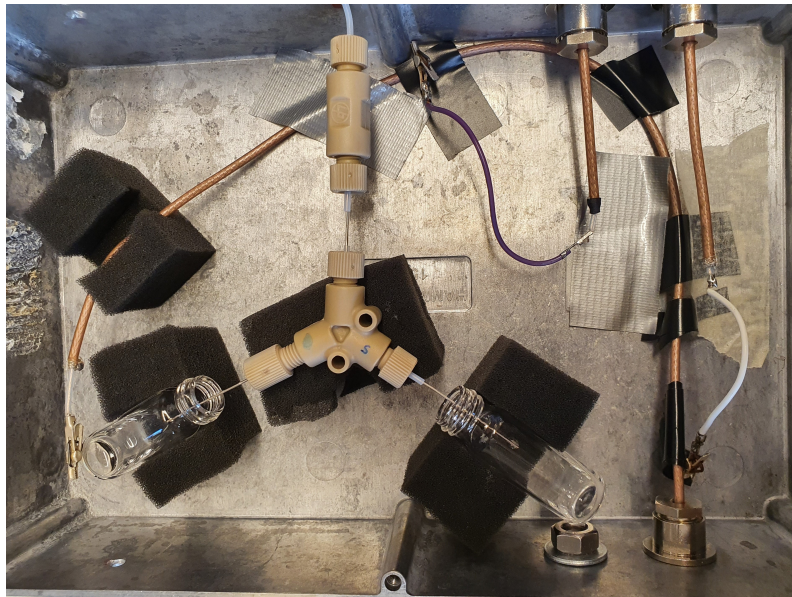


Figure 3.8: Caseination process during a two-channels measurement

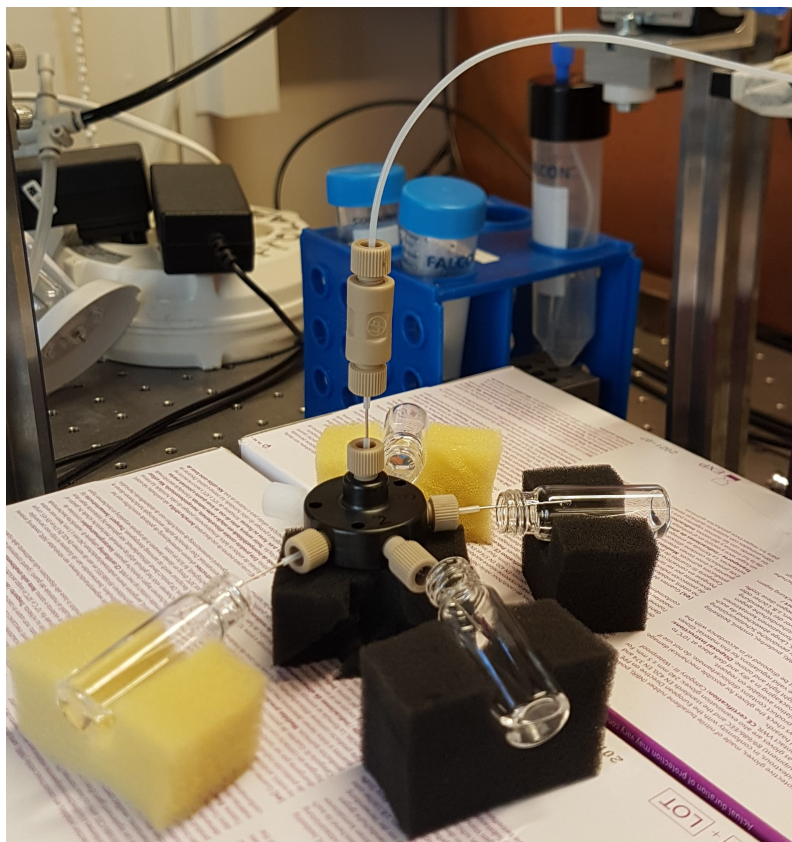


Figure 3.9: Caseination process during a four-channels measurement

In *Fig. 3.11* the first streaming current baseline schematics can be observed in region 1. It is important in this step to ensure stable and constant pressure pulses and flow rates with the intention of avoiding current drifting which could inevitably result in an uncorrect measurement.

**3) EVs incubation.** In order to minimize the EV sample consumption while maximizing its binding, the EVs were incubated following a different pressure pulse approach. A square wave pressure pulse at a 10% duty cycle shifting between 0 and 1.5 bars in a 360 seconds period, as shown in *Fig. 3.10* was applied.

The EVs sample was incubated inside the capillary for a total duration of two hours. The streaming current during the experiments was only recorded during the PBS buffer injections that occur in step 2 and 4. This kind of approach is called end-point detection.

The EVs sample concentration ranged in the order of  $10^9$  particles/ml.

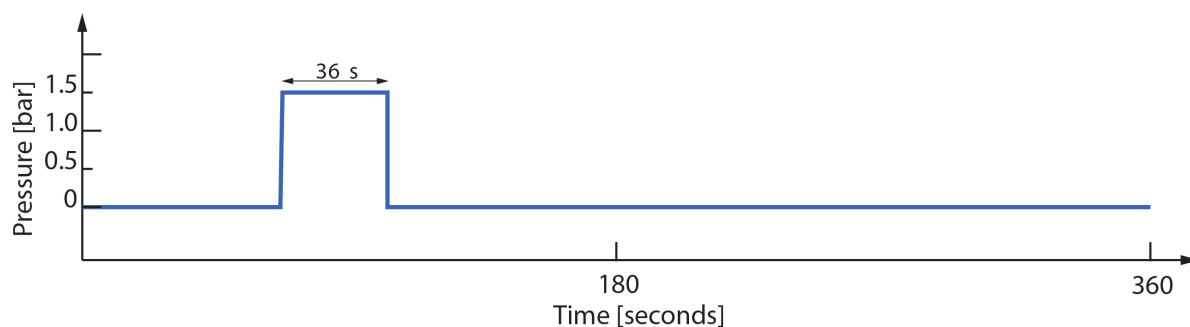


Figure 3.10: Square wave pressure pulse performed during EVs incubation time

**4) Final 0.1xPBS injection** for the measurement of the second streaming current baseline ( $\Delta I_{st2}$ ) as well as for the removal of unbound or vaguely bound EVs. The measurement is performed holding the same considerations of step 2 and  $\Delta I_{st2}$  is shown in the schematics of *Fig. 3.11* in region 2.

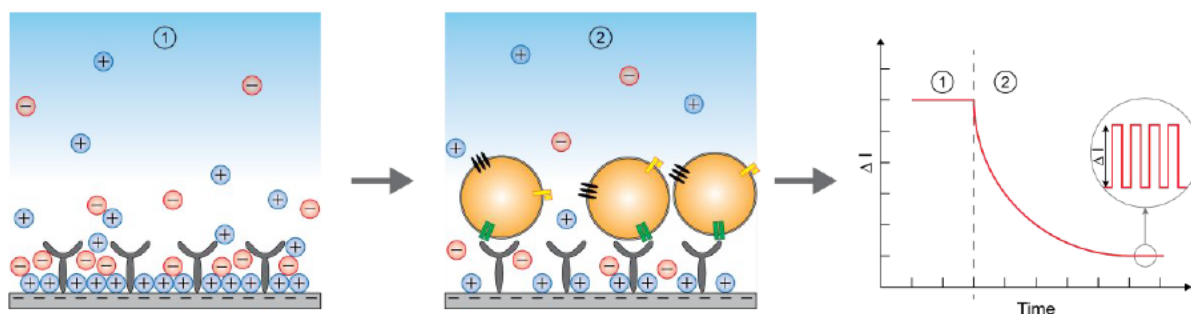


Figure 3.11: Schematics displaying the change in the streaming current difference ( $\Delta I_{st2} - \Delta I_{st1}$ ) between final (region 2) and first PBS injection (region 1) [91]

Following the end-point measurement approach for this electrokinetic detection technique, during

the experiments, the difference between the two streaming current PBS baselines ( $\Delta I_{st2} - \Delta I_{st1}$ ) was calculated. Considering that real-time measurements that can be employed in different kinetic analyses, require a large amount of sample volumes ( $\sim 400 \mu\text{L}$ ) they result in restricted application in practice [91].

Therefore, on all the performed experiments, an end-point measurement approach was followed. Since the binding between EVs and the affinity agents is a non-covalent interaction, there are association and dissociation events occurring upon the injection of the second baseline. Thus, the signal is considered only after 30 min of injection of the second baseline, in order to have a stabilization of the baseline but also avoid too much binding dissociation.

**5) Setup cleaning** applying a cleaning solution, acetone and isopropanol.

The connectors were cleaned separately from the setup with acetone, isopropanol and water using an ultrasonic bath 5 minutes for each step and dried with  $N_2$  before being stored.

### 3.5 Data analysis

The following graphs on the step-by-step method of data analysis will be shown for an informative purpose, evidencing how the important parameters that have been highlighted in this chapter, such as streaming current and zeta potential, are numerically obtained from each experiment. Special emphasis will be addressed to the zeta potential parameter in the next chapter.

The electrokinetic detection data acquired during a one-channel measurement experiment from the custom-designed software and plotted in MATLAB is shown in *Fig. 3.12*.

The experiment was carried out following the steps described in the previous section using a micro-capillary functionalized with immobilized anti-EGFR affibodies interacting with EVs sample but the data analysis method is performed in the same manner even with other antibody employment. In the upper part of *Fig. 3.12* three main areas can be observed.

The first area refers to step two of the experiment conduction section and represents the first streaming current baseline. The middle area with the growing trend represents the EVs incubation time while the last region refers to the recording of the second streaming current baseline. It can be observed how the sample injection induces a gradual variation of the streaming current which is equally reflected in the  $\zeta^*$  change.

In the lower part of *Fig. 3.12*, instead, a close-up of the first streaming current baseline is shown. As it can be observed the trapezoid pressure pulses switching from 1.5 and 3 bars employed during the recording of baselines also produce trapezoid streaming current pulses.

As already pointed out, ensuring that the pressure pulses, and therefore the flow rates, are constant in this phase represents an important factor in order to obtain a stable current recording.

Following the end-point measurement approach for this electrokinetic detection technique, as already mentioned in the previous section, during the experiments, only the recoding of the two streaming current PBS baselines will be taken into consideration.

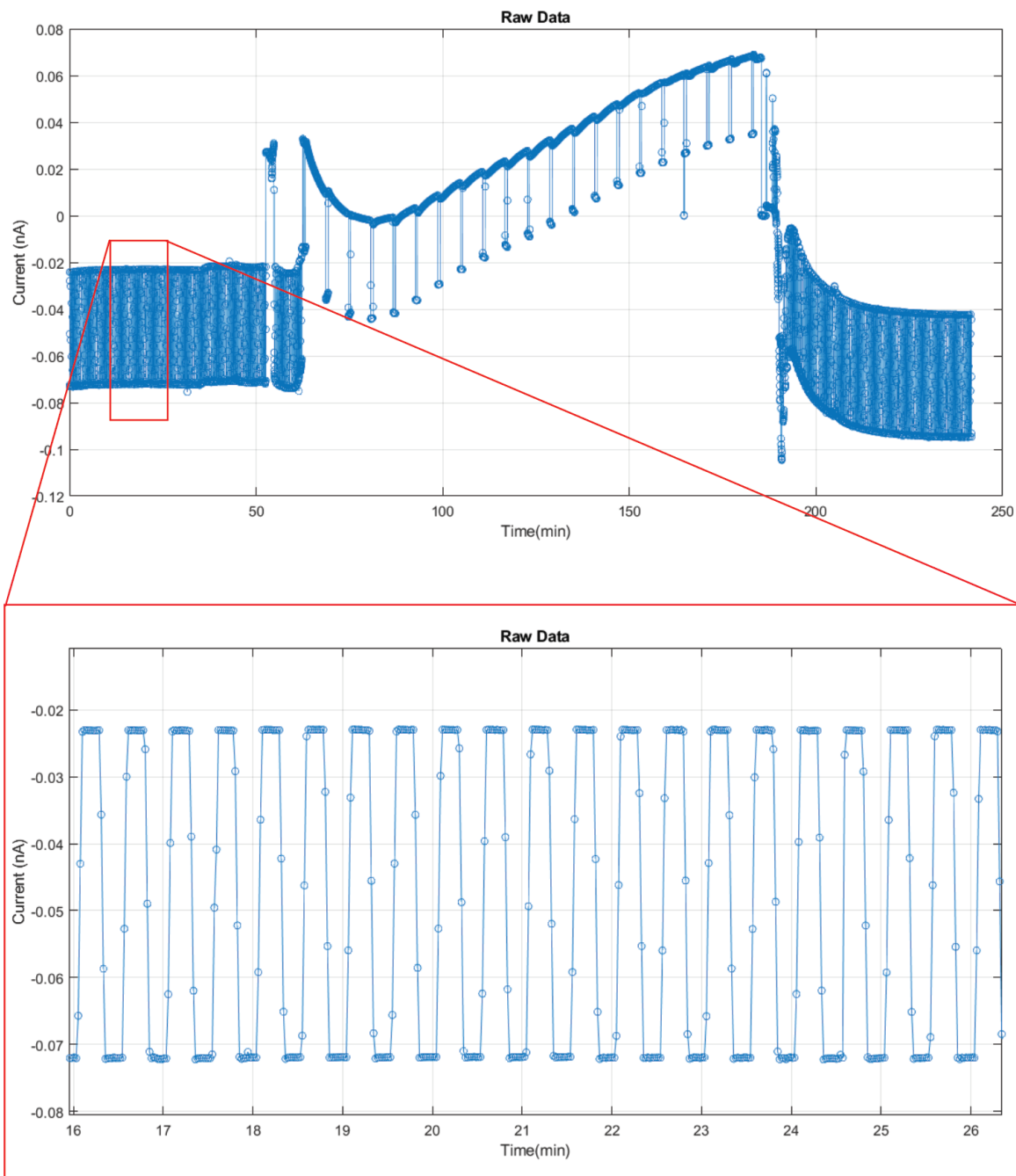


Figure 3.12: Raw data and close-up of a one-channel experiment on a microcapillary functionalized with anti-EGFR affibodies

The first step in obtaining the streaming current parameter is to isolate the two baseline areas especially the streaming current values which are recorded when the pressure hits 1,5 and 3 bar as shown in *Fig. 3.13*.

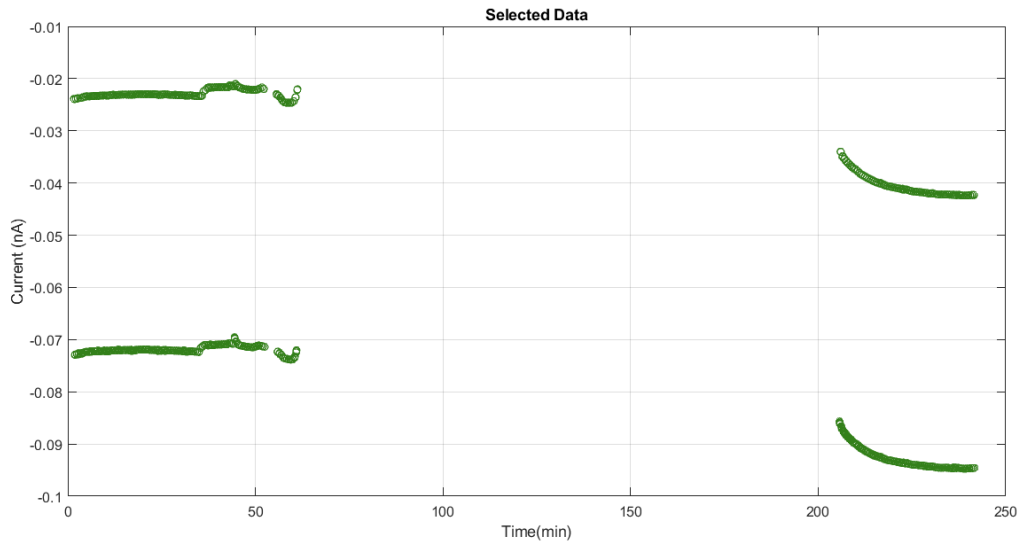


Figure 3.13: Selection from the raw data of the highest and lowest streaming current values of the two baseline areas

The average streaming current values for both high and low pressure from the previous selected values are calculated.

In order to obtain a continuous data set and not a discrete signal, a fitting of the data of both high and low values shown in blue and purple respectively in *Fig. 3.14* was carried out.

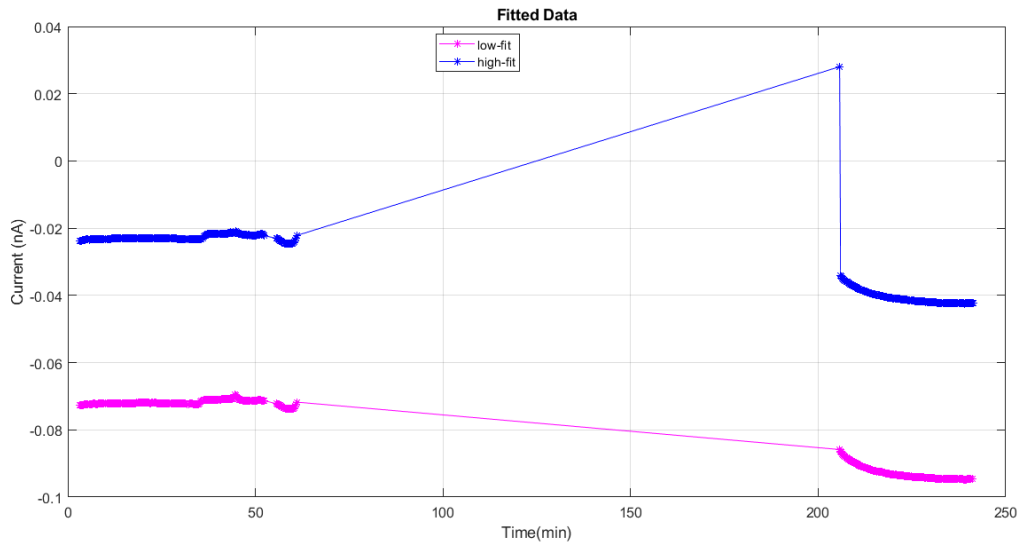


Figure 3.14: Plot showing the fitting of the data for the obtaining of a continuous signal

Next, the difference  $\Delta I_{st1}$  and  $\Delta I_{st2}$  between high and low values in both baselines is obtained for every set of pulses and *Fig. 3.15* shows the plot.

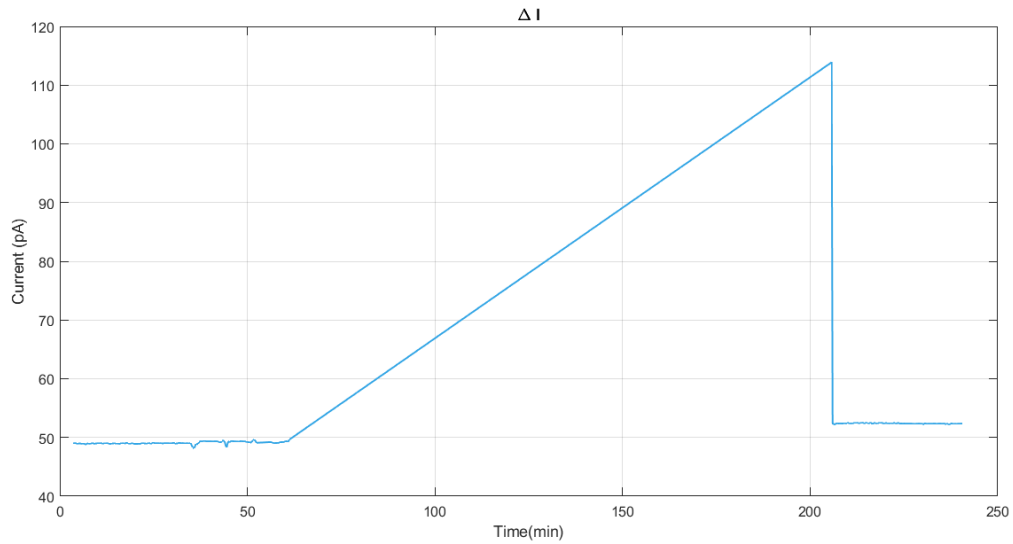


Figure 3.15: Plot showing  $\Delta I_{st1}$  and  $\Delta I_{st2}$  calculated for each pulse

In *Fig. 3.15* is immediately noticeable the change in streaming current between the first and second baseline since EVs injection was placed in the middle of these recordings and the interaction between the EGFR affibodies (in the case of this experiment) immobilized on the internal microcapillary surface and the EGFR surface proteins on the extracellular vesicles can be accountable for the produced effect.

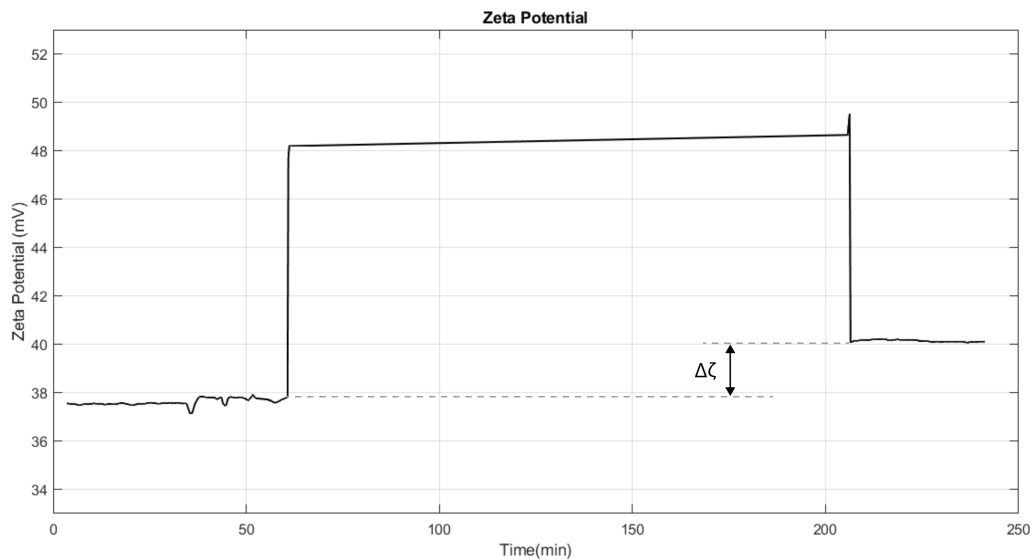


Figure 3.16:  $\zeta^*$  potential obtained from equation 3.3 showing the potential change that occurs after sample injection resulting in  $\Delta\zeta^*$

It is also important to notice that the sudden current change recorded at the beginning of the

second baseline was merely due to an artifact in the data processing code and not to a EV binding process.

Lastly, the  $\zeta^*$  potential is obtained through the streaming current values through the use of *Equation 3.3* as shown in *Fig. 3.16*. The important parameter which will be largely used in the Results chapter is the potential change that occurs after the sample injection due to the interaction between EVs surface proteins and the correspondent affinity agents. Such difference is shown in *Fig. 3.16* as  $\Delta\zeta^*$ .

### 3.6 EV characterization

As mentioned above, the thesis focused on EVs derived from lung cancer cell lines, with the aim of analyzing both common surface markers, i.e. tetraspanins, and cancer specific markers such as EGFR. The purified tumor derived EV samples, provided by the Karolinska Institutet, were obtained from NSCLC H1975 cell line which is known to present a mutant expression of EGFR (L858R and T790M) [91]. The vesicles were isolated using size exclusion chromatography and were characterized using NTA, in order to evaluate their particle counts and distribution in size, while for the investigation of their morphology, SEM was employed. With regard to the biochemical analysis WB was performed for the examination of protein expression.

The EVs analysed with the SEM technique were not performed in their physiological solution (PBS) but were covalently immobilized onto a silicon wafer through APTES and GA linker. Next, EVs were then sputtered with Au/Pd before carrying out sample imaging in order to prevent surface charging which can cause lower resolutions and image artifacts.

As mentioned in the Electron Microscopy section, EVs appear to have a more cup shape when imaged in SEM or TEM. As can be observed from *Fig. 3.17*, the EVs appear to have a spherical shape and a diameter of 100 - 200 nm. This results from an x-y plane prospective although crushes in the z direction can not be evaluated from the images.

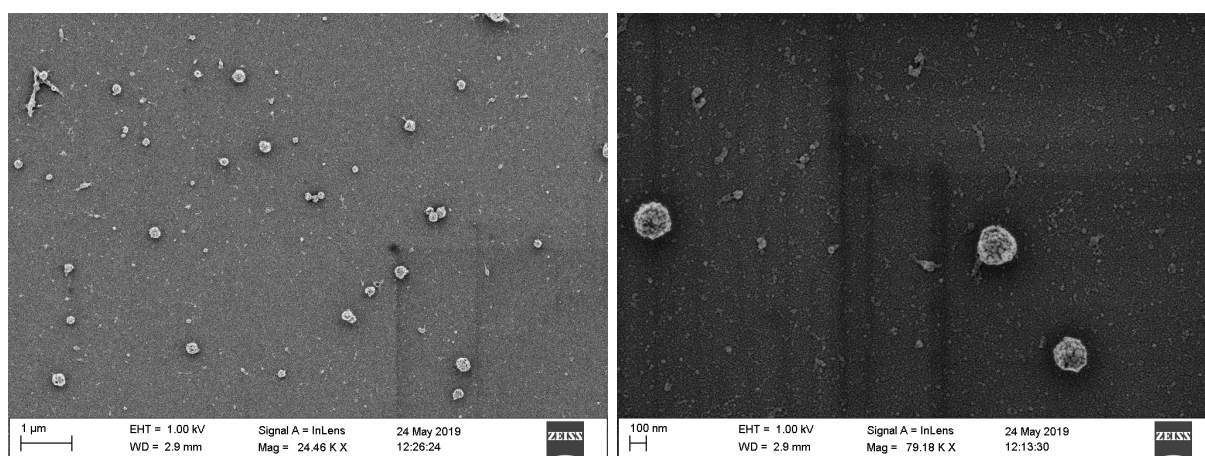


Figure 3.17: SEM-images of sEVs derived from the H1975 cell line: images were taken using Inlens detector and a voltage of 1kV

NTA analysis was performed for the eletrokinetic detection measurements on EVs sample that were diluted 1:50, analyzed on NS300 (Malvern Panalytical, UK) using a blue laser at 488 nm as well as the following settings: syringe pump speed set at 100, camera level set at 14, threshold for detection set at 5. *Fig. 3.18* shows that the EVs ranged from 50 nm to around 300 nm in diameter, with peaks located around 100 nm.

In the figure on the left, the three different colours indicate that the analysis was performed three times on the same sample, while in the figure on the right, the black line represent the mean of the particle size, while the red error line represent the standard deviation.

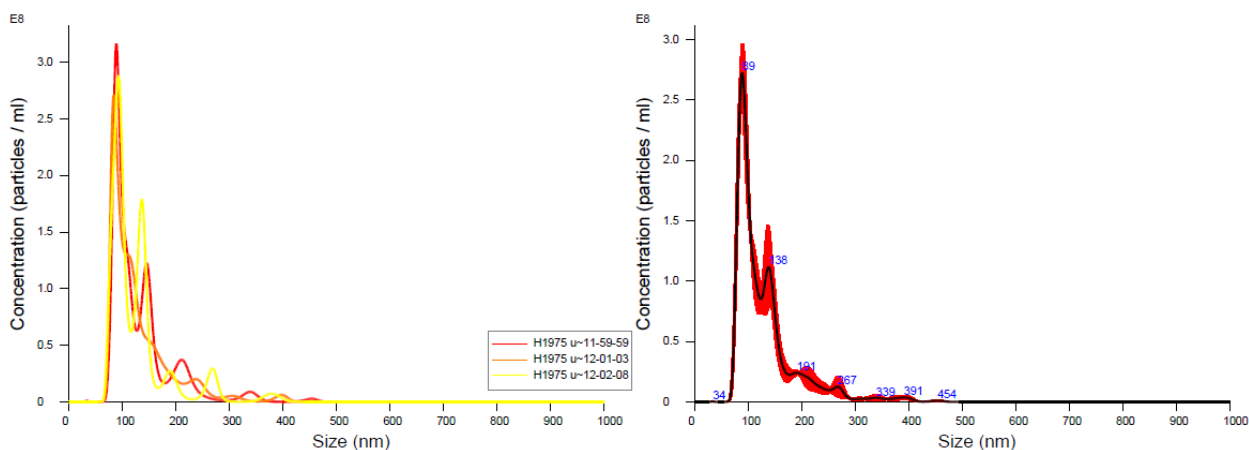


Figure 3.18: NTA analysis of EVs sample

In the case of an EV analysis derived from cells cultured *in vitro*, their biochemical composition should preferably be confronted with that of the parental cells in order to gain a better understanding of the enrichment level that the EV components possess [22].

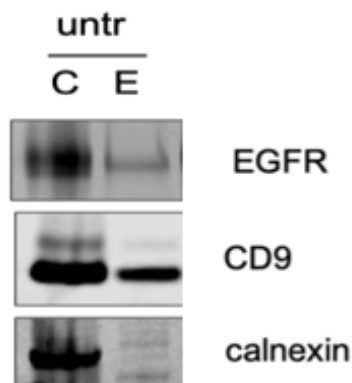


Figure 3.19: Western blot analysis of EGFR, CD9 and calnexin expressions on H1975 cells "C" and their corresponding EVs "E"

When dealing with negative controls the ISEV recommends some control mechanisms, which should be performed at least on one of the following markers such as Grp94, calnexin (which are both endoplasmatic reticulum markers), cytochrome C (mitochondrial marker), GM130 (Golgi marker), argonaute (RISC complex marker) and histones (nuclear marker) which are known to be absent or under-represented in EVs [22].

The western blot analysis was performed for EGFR, CD9 and calnexin expressions on untreated, H1975 parental cells marked with “C” and their corresponding EVs marked with “E” as shown on *Fig. 3.19*.

It can be observed that the analysis validated the presence of EGFR and CD9 both on the NSCLC H1975 cells and on the derived EVs, while the expression absence of calnexin on the extracellular vesicles, which serves as the negative control, functions as a confirmation of EVs sample purity.



## Chapter 4

# Results and Discussion

### 4.1 Preliminary characterization

This section of the Results will be focused on the preliminary experiments which were carried out on the measurement set-up with the intention of checking the correct functioning of all the equipment and software before employing the application of EVs samples given the limited amount and relative difficulty of isolation and characterization.

Moreover, the experimental results that will be shown in this section were intended with the purpose of practicing with the conduction of the experiments as well as possessing initial data of first  $\zeta^*$  potential baselines and  $\Delta\zeta^*$  potentials in certain conditions.

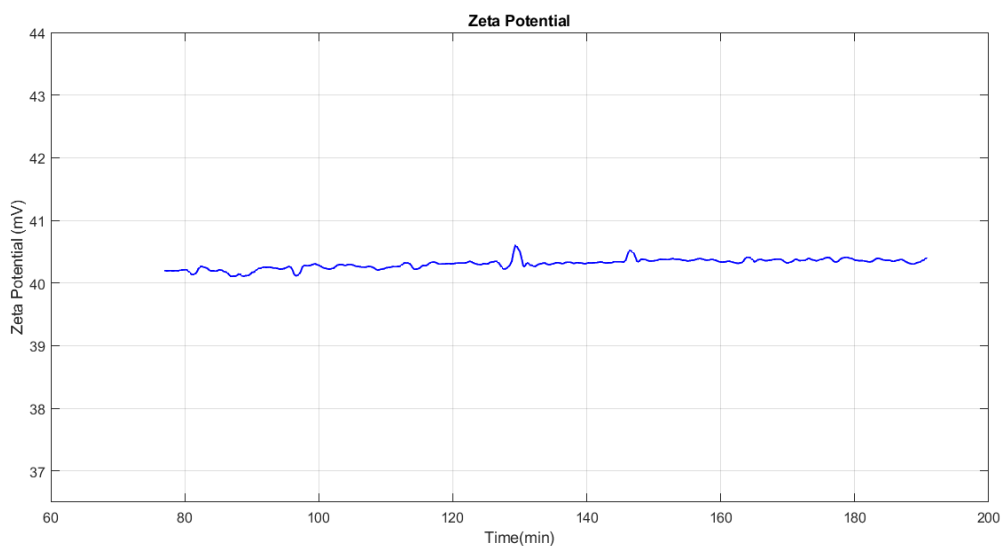


Figure 4.1:  $\zeta^*$  potential obtained during a one-channel, first baseline measurement, using a micro-capillary functionalized with anti-EGFR antibodies

In *Fig. 3.1* the  $\zeta^*$  potential obtained during a one-channel measurement experiment, carried out

using a microcapillary functionalized with immobilized anti-EGFR affibodies can be observed. The plot shows that the  $\zeta^*$  potential of the first and only baseline is pretty stable for the duration of the experiment (around 3 hours) and the average value is 40,3 mV with a signal drifting of 0,3 mV which is acceptable as it can come as a result of minor changes in the flow rate or negligible changes in the capillary functionalization due to the detachment of some molecules from the surface. However, changes are negligible compared to the duration of the baseline and the signals obtained.

In order for this value to be considered adequate, the measurement should be reproducible and this issue will be addressed in the next section not only for the EGFR affibody but for the other antibodies as well.

With the intention of investigating the change in the zeta potential that takes place before and after a certain period of time, measurements with totally non-functionalized capillaries were performed. The steps described in the experiment conduction section were simulated as similarly as possible, with the only difference however of not employing the EVs injection step.

As a matter of fact, 0.1xPBS was flown instead, using the square wave shown in Fig.X for 30 minutes instead of the usual 2 hours period.

The two experiments were carried out separately through one-channel measurement using two totally non-functionalized microcapillaries, presenting both a 4,6 cm length.

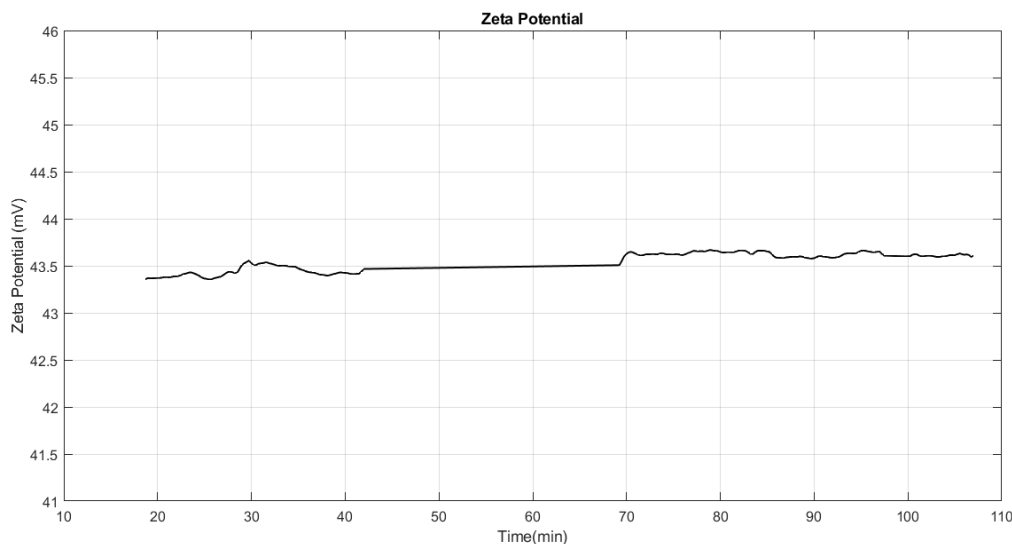


Figure 4.2:  $\zeta^*$  potential of the first non-functionalized capillary obtained during a one-channel measurement

As can be seen from *Fig. 4.2* and *Fig. 4.3* the zeta potentials recorded in the two capillaries seems reproducible and the baselines are pretty stable and in average range between 43,4 mV and 44,3 mV, while the  $\Delta\zeta^*$  potential between the second and first baseline is about 0,2 mV, a value considered almost irrelevant as signal drifting of this magnitude have also been observed in other experiments.

Therefore, it can be concluded that the change in zeta potential during the course of a two-hour measurement is practically zero if non-functionalized capillaries are used.

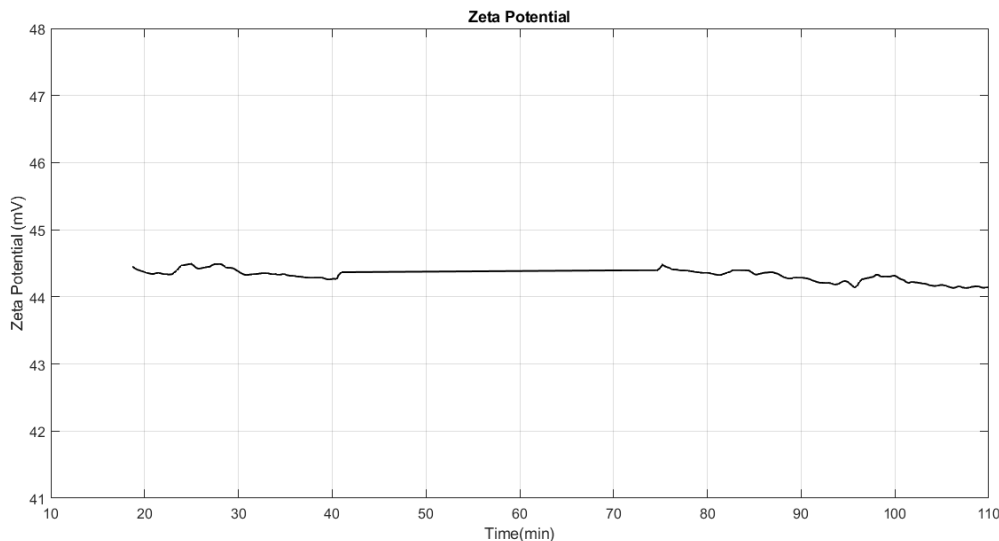


Figure 4.3:  $\zeta^*$  potential of the second non-functionalized capillary obtained during a one-channel measurement

In conclusion, considering both this experiment performed on two totally non-functionalized capillaries as well as the previous one carried out during a one-channel measurement using a microcapillary functionalized with anti-EGFR affibodies it can be observed how the  $\zeta^*$  potential results overall stable with a minor signal drifting in the range of 0,2-0,3 mV during a 2-3 hours time range throughout the application of constant  $\Delta P$  in both functionalized and non-functionalized capillaries.

In *Fig. 3.4* the  $\zeta^*$  potential obtained during a one-channel measurement experiment, carried out using a microcapillary functionalized with immobilized anti-EGFR affibodies can be observed. The current plot has already been shown in the Data Analysis section with the intention of demonstrating how the  $\Delta\zeta^*$  potential is obtained from the raw data.

In this measurement the Experiment Conduction steps were followed precisely and a concentration of  $3 * 10^9$  part/mL of H1975-derived EVs was used.

It's immediately noticeable that the sensor displayed a distinct change in the signal of the zeta potential between the first and second baseline resulting in a  $\Delta\zeta^*$  potential value of 2,5 mV. Since EVs injection occurred between the baseline recordings it's reasonable to assert that the interaction between the EGFR affibodies immobilized on the internal microcapillary surface and the EGFR surface proteins on the extracellular vesicles can be held accountable for the produced  $\Delta\zeta^*$  potential. The above mentioned outcome is in accordance with the western blot analysis that confirmed the presence of EGFR in the sample. However, in such an experiment, a direct association between the the precise amount of EGFR and signal strength is hard to establish but,

nonetheless, relative EGFR expression levels could be compared among different EVs. Thus, for practical reasons, such a measurement can be employed as a semi-quantitative method of analysis for the expression of the surface marker EGFR.

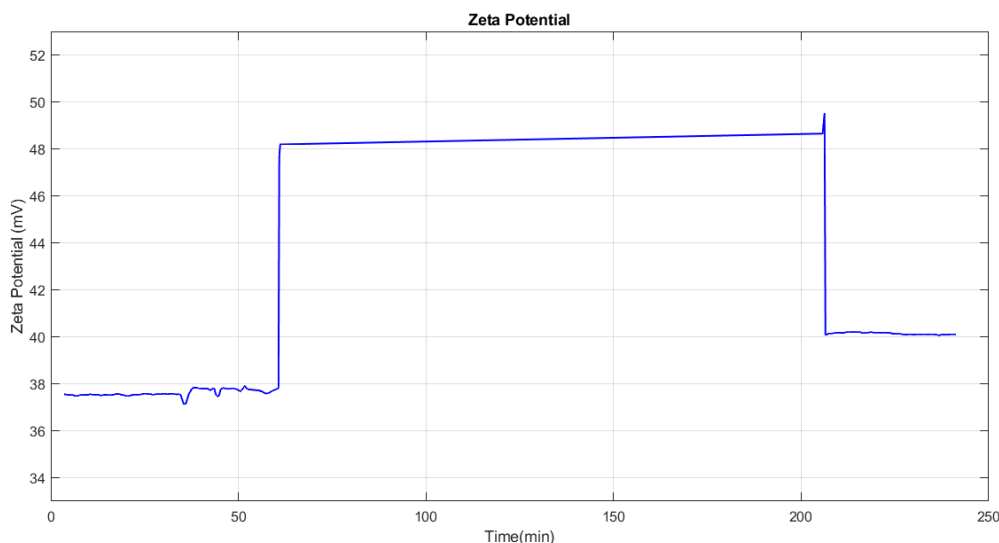


Figure 4.4:  $\zeta^*$  potential obtained during a one-channel measurement using a microcapillary functionalized with anti-EGFR affibodies interacting with NSCLC H1975-derived EVs

## 4.2 Capture probes' baseline characterization

Before starting the part of the thesis work focused on the multiplexed electrokinetic sensor detection of protein markers such as CD9, CD63 and EGFR a thorough characterization of the captures probes employed in the microcapillaries functionalization was conducted first.

The characterization consisted on the recording of the first baselines on capillaries functionalized with the capture probes in question in order to evaluate their stability and reproducibility.

The first one to be examined was the EGFR affibody provided by the Department of Protein Science at the Royal Institute of Technology.

1° multiplexed EGFR-affibody	2° multiplexed EGFR-affibody
39,9 mV	35,1 mV
42,3 mV	35 mV
34,7 mV	39,8 mV
33,5 mV	41,1 mV

Figure 4.5: First baseline  $\zeta^*$  potential averaged values of microcapillaries functionalized with anti-EGFR affibodies

For the purpose, a total of eight microcapillaries were tested.

As shown in *Fig. 3.5* the average values of the  $\zeta^*$  potentials of the first baselines obtained from microcapillaries functionalized with anti-EGFR affibodies range from a minimum of 33,5 mV and a maximum of 42,3 mV spanning thus a wide range of values.

The  $\zeta^*$  potentials are shown also in *Fig. 3.6* and a peculiar trend can be noticed. The plots appear to go pair-wise around two average values: either 34,5 or 40,7 mV.

It can be however observed that the  $\zeta^*$  potentials result overall stable with a minor signal drifting of about  $\pm 0,3$  mV, a value that has been found in many other experiments and thus considered acceptable.

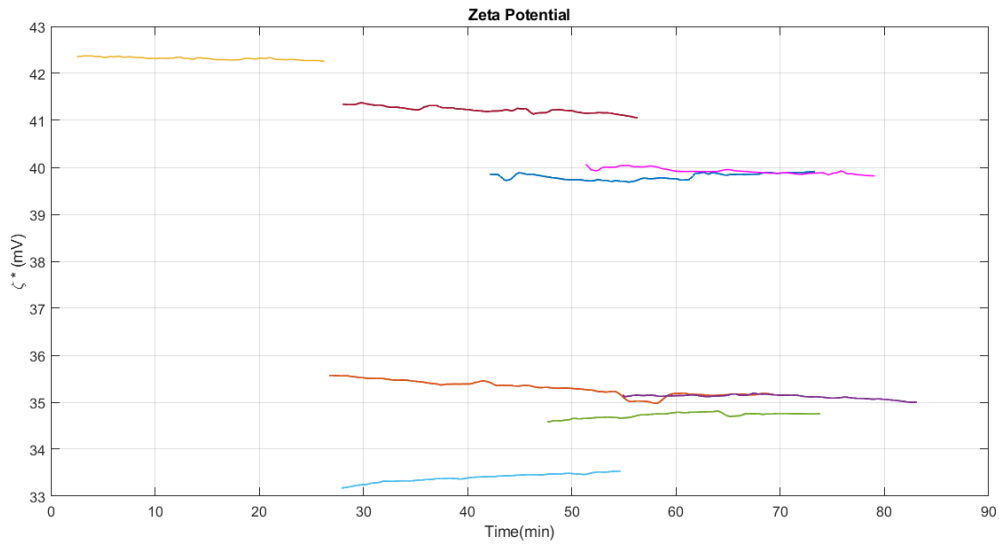


Figure 4.6: First baseline  $\zeta^*$  potentials of microcapillaries functionalized with anti-EGFR affibodies

Given the non-consistency of the results, the convenience of using the affibodies instead of the commercial product Cetuximab, widely used as a monoclonal antibody which binds to EGFR, was questioned.

Cetuximab
22,7 mV
22,9 mV
24,2 mV
29,3 mV

Figure 4.7: First baseline averaged  $\zeta^*$  potentials of microcapillaries functionalized with anti-Cetuximab antibodies

In order to get more validation on the results obtained with the affibodies, the baselines for capil-

larities functionalized with Cetuximab were measured, and the results are shown in *Fig. 3.7*. It can be observed that compared to the EGFR affibody, with Cetuximab three out of four capillaries show similar values, and, overall, the baselines seem to be more reproducible considering that the capillary with the highest baseline may be due to a problem in the functionalization process. However, the difference is lower if compared to the EGFR affibody and for this reason it was decided to proceed with the Cetuximab antibody instead of the affibody. Moreover, in *Fig. 3.8* it can be noticed that also in this case the  $\zeta^*$  potentials result overall stable with the usual minor signal drifting of about  $\pm 0,3$  mV.

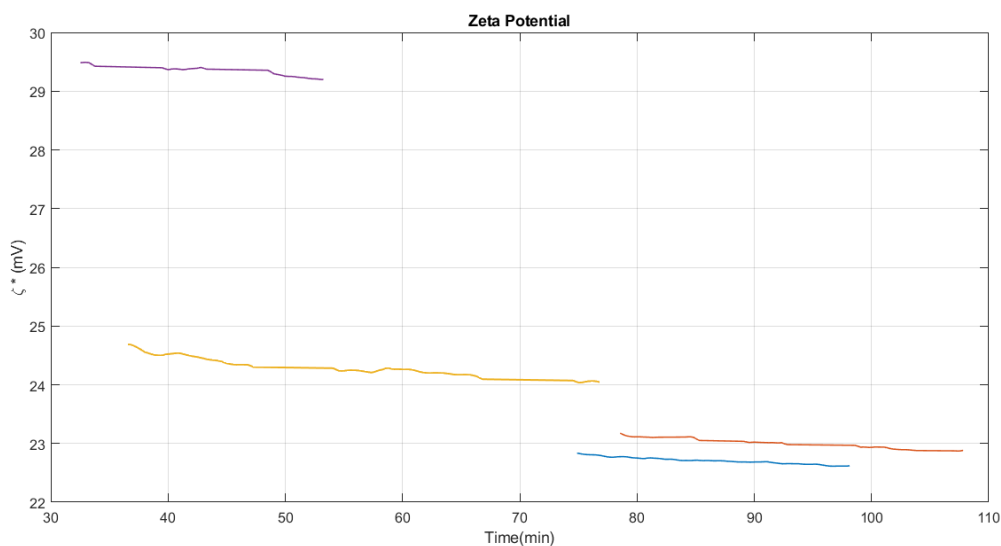


Figure 4.8: First baseline  $\zeta^*$  potentials of microcapillaries functionalized with anti-Cetuximab antibodies

The experiments on the microcapillaries functionalized with anti-CD9 and anti-CD63 were performed in the same manner and their average values of the  $\zeta^*$  potentials of the first baselines are shown in *Fig. 3.9*.

CD9	CD63
29,4 mV	26,8 mV
30,5 mV	28,1 mV
24,4 mV	25,6 mV
26,7 mV	25,5 mV

Figure 4.9: First baseline averaged  $\zeta^*$  potentials of microcapillaries functionalized with anti-CD9 and anti-CD63 antibodies

The range of the  $\zeta^*$  potential values results smaller on the CD9 and even lower on CD63 if compared with EGFR affibody but comparable with Cetuximab.

As already stated for the microcapillaries functionalized with anti-EGFR affibodies and anti-Cetuximab antibodies the  $\zeta^*$  potentials shown in *Fig. 3.10*, also in the case of CD63 and CD9, result generally stable with the usual minor signal drifting of about  $\pm 0,3$  mV.

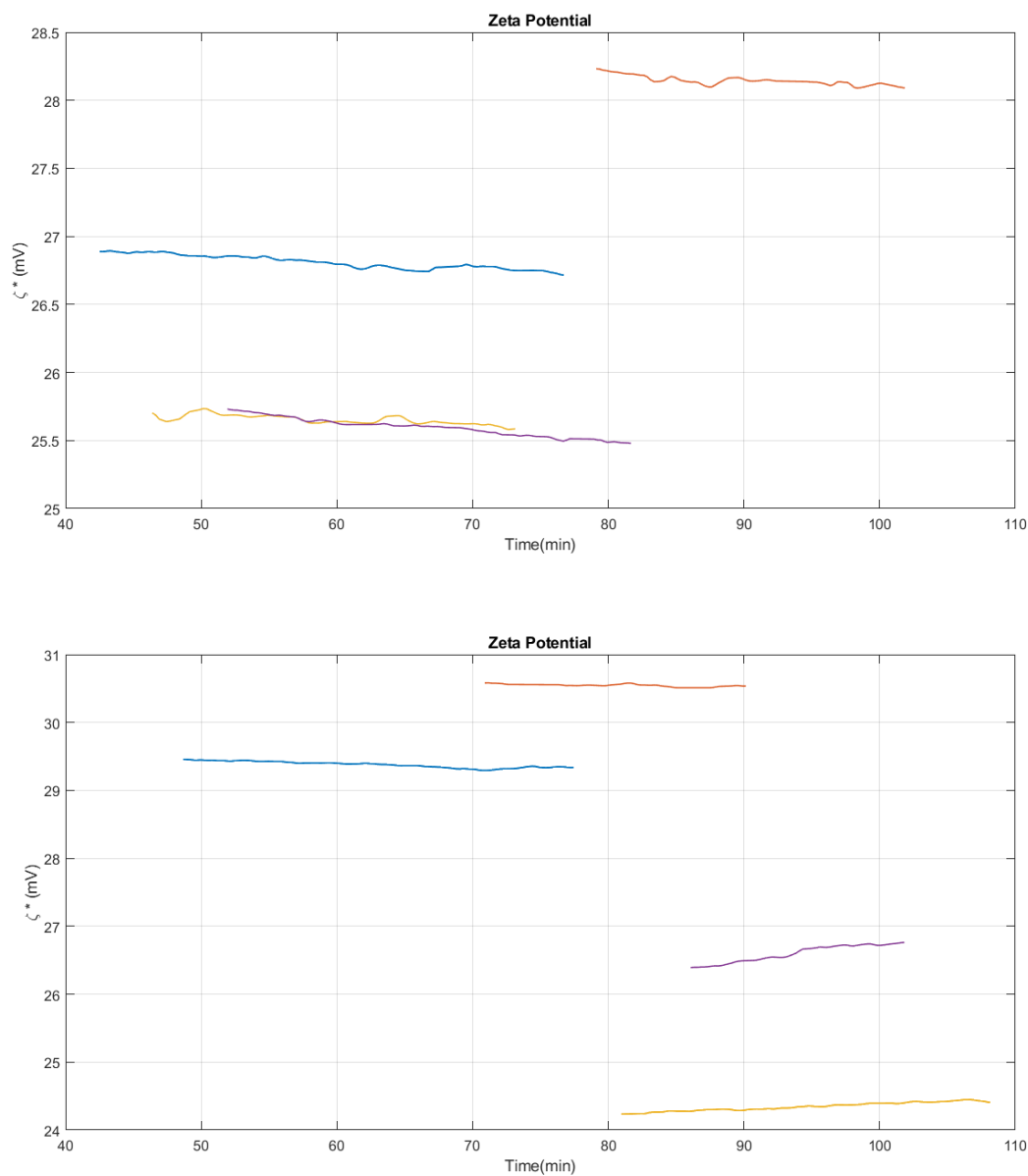


Figure 4.10: First baseline  $\zeta^*$  potentials of microcapillaries functionalized with anti-CD63 (above) and anti-CD9 antibodies (below)

The summarized results are shown as barplots in *Fig. 3.11*, indicating the average first baseline  $\zeta^*$  potentials and correspondent standard deviation for the main markers aforementioned.

The capillaries functionalized with different capture probes show different average baselines. This is in accordance with the theory, as each probe brings a different charge and therefore modifies the streaming current flowing inside the capillaries in different ways. Moreover, the data show that the highest mean value for the  $\zeta^*$  potential corresponds to the EGFR affibody with an average of 37,7 mV while the other three antibodies have mean values more closely to each other with measurements corresponding to 27,7 mV for CD9, 26,5 mV for CD63 and 24,8 mV for Cetuximab.

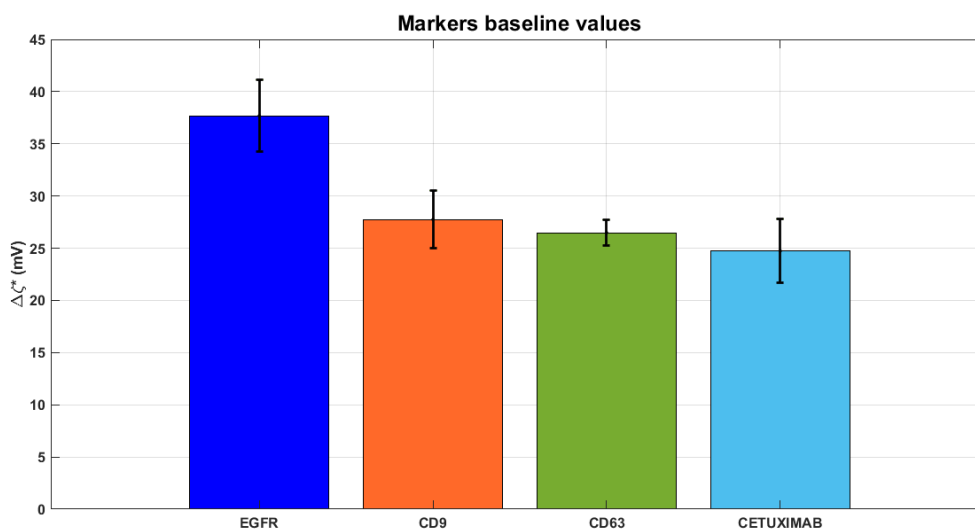


Figure 4.11: Barplots showing the mean values of the first baseline  $\zeta^*$  potentials and corresponding standard deviation of microcapillaries functionalized with EGFR affibody, CD9, CD63 and Cetuximab antibodies

Moreover, the standard deviation is also the highest in the case of EGFR affibody amounting to 3,4 followed by Cetuximab with a value of 3, CD9 with 2,7 and lastly CD63 with 1,2.

Being the reported standard deviation a measure of uncertainty and precision of those measurements, overall, it can be established that the capture probes' baselines showed good reproducibility with standard deviations under the 10% of the overall signals, for the majority of cases. More importantly the experiments showed stable baselines over time for the same measurement without drifting which could compromise the final signal.

Despite the good reproducibility, a further elucidation for this outcome can be traced to the experiment assessment. Small changes in the flow rates between the measurements were observed and since the baselines depend on the flow rates, this can lead to small shifts.

Moreover, since the immobilization of the antibodies happens randomly and not in an oriented manner, there can be changes in their orientation on the surface of the micro-capillary that can therefore lead to changes in the overall capillary charge resulting ultimately in small variations in the baselines.

To be exhaustive and complete, the values of the  $\zeta^*$  potential of the first baseline of control capillaries (as described in Control functionalization section) that were obtained in the course of several experiments are also reported in *Fig. 3.12*.

The mean  $\zeta^*$  potential values of the control capillaries resulted 40,7 mV and its standard deviation 1,3 thus having, overall, a better and stable outcome than EGFR, CD9 and Cetuximab but a standard deviation comparable with the CD63 one.

Considering the bigger number of repetitions, the values of the control capillaries result more stable than the markers, probably due to the absence of the capture probes, either affibodies or antibodies. This seems to confirm the hypothesis of the variability of the baselines due to the random capture probe immobilization.

Moreover, the mean value results higher than the EGFR affibody one but even the maximum value of the control  $\zeta^*$  potential (42,8 mV) is however lower than the ones found in the completely empty capillaries described in the Preliminary characterization section (*Fig. 3.2* and *Fig. 3.3*).

CONTROL		
40 mV	42,8 mV	37,6 mV
41,4 mV	41,2 mV	40,8 mV
40,5 mV	40,9 mV	41,9 mV
42,3 mV	39,1 mV	39,6 mV
41,2 mV	40,7 mV	

Figure 4.12: First baseline averaged  $\zeta^*$  potentials of non-functionalized microcapillaries serving as control capillaries obtained from various experiments including two-channels measurements, four-channels measurements as well as patient sample measurements

### 4.3 Two-Channels Measurements

Before extending the platform for multichannel measurements, it was proceeded gradually by firstly carrying out two-channels experiments in order to verify and validate the multiplex electrokinetic detection method at a lower scale.

The first experiment was performed on two micro-capillaries, one of which was functionalized with anti-EGFR affibodies while for the other one was used a control capillary as described in the Control functionalization section of Chapter 3.

NSCLC H1975-derived EVs were injected at a concentration of  $3 * 10^9$  particles/mL and both of the capillaries were cut at a length of 4,7 cm.

The  $\Delta\zeta^*$  potentials were calculated, leading to values of 1,3 mV for the control capillary and 3,3 mV for the micro-capillary functionalized with anti-EGFR affibodies, therefore resulting in almost an increase of 154% in the latter case.

A visual comparison plot of the  $\zeta^*$  potentials between the two capillaries employed in this experiment is shown in *Fig. 3.13* where it can be clearly noticed that in the case of the micro-

capillary functionalized with the anti-EGFR affibodies the  $\zeta^*$  potential signal is higher after the EVs injection period if compared to the control signal.

The averaged  $\zeta^*$  potential of the first baseline in the case of the anti-EGFR functionalized micro-capillary was calculated being 37,6 mV which is a acceptable value since it is in close proximity to the mean value of anti-EGFR functionalized micro-capillaries (37,7 mV) obtained in the Capture probes' baseline characterization.

In the case of the control capillary, its first baseline  $\zeta^*$  potential was recorded being 40,1 mV, this value also being acceptable as consistent with the range of values recorded for the control capillaries.

In conclusion, the sensor clearly displayed a 2,5-fold higher change in the signal of the  $\zeta^*$  potential between the first and second baseline in the case of the micro-capillary functionalized with the anti-EGFR affibodies compared to the control capillary.

However, as already mentioned before, in such an experiment and the ones that will follow, a direct connection between the expression levels of EGFR and signal strength is difficult to determine since only the relative amounts between different patients or samples can be compared. Only in such conditions, a lower signal would mean lower EGFR expression in general.

Nevertheless, for practical reasons, such a measurement can be employed as a semi-quantitative analysis method for the EGFR expression level.

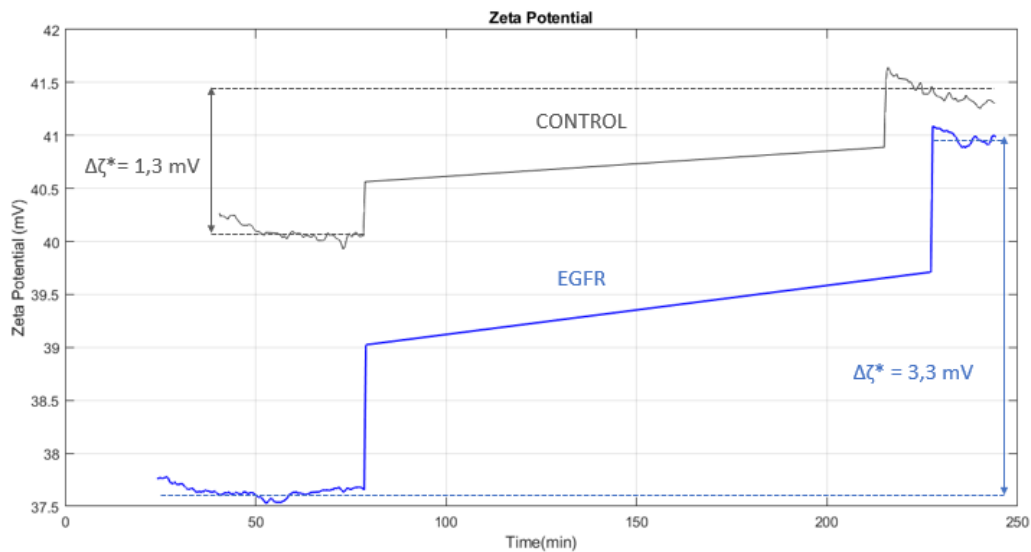


Figure 4.13: Plot showing the comparison between the  $\zeta^*$  potentials and relative  $\Delta\zeta^*$  obtained during a two-channels measurement using a micro-capillary functionalized with anti-EGFR affibodies and a control micro-capillary interacting with NSCLC H1975-derived EVs

In *Fig. 3.14* is shown another comparison between the  $\zeta^*$  potentials and the relative  $\Delta\zeta^*$  obtained during a two-channels measurement using a micro-capillary functionalized with anti-EGFR affibodies and a micro-capillary functionalized with anti-CD9 antibodies.

NSCLC H1975-derived EVs were injected at a concentration of  $3 \times 10^9$  particles/mL and the capillaries were cut at a length of 4,1 cm and 4 cm.

The  $\Delta\zeta^*$  potentials were calculated, leading to values of 0,2 mV for the anti-EGFR functionalized micro-capillary and 5,9 mV for the anti-CD9 functionalized microcapillary.

In this experiment, the anti-EGFR functionalized micro-capillary exhibits a  $\Delta\zeta^*$  comparable to the empty capillaries shown in *Fig. 4.2* and *Fig. 4.3* and the averaged  $\zeta^*$  potential of the first baseline was calculated being 35,4 mV.

Moreover, the averaged  $\zeta^*$  potential of the first baseline in the case of the anti-CD9 functionalized micro-capillary was recorded being 26,4 mV which is an acceptable value since it is not that far from the mean value of anti-CD9 functionalized micro-capillaries (27,7 mV) obtained in the Capture probes' baseline characterization.

It can be hypothesized that the low signal of  $\Delta\zeta^*$  for the anti-EGFR functionalized micro-capillary was due to the fact that either some kind of error took place during the functionalization procedure that caused a low interaction between the EGFR surface proteins and the immobilized affibodies on the inner surface of the capillary, or that the EVs sample employed presented generally low levels of EGFR as surface proteins, which seems a less likely possibility.

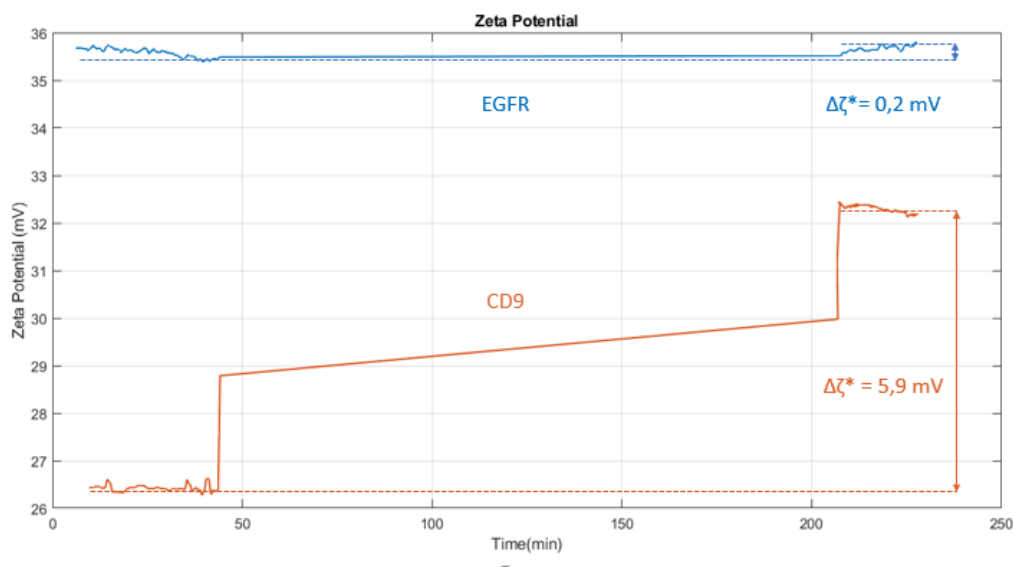


Figure 4.14: Plot showing the comparison between the  $\zeta^*$  potentials and relative  $\Delta\zeta^*$  obtained during a two-channels measurement using a micro-capillary functionalized with anti-EGFR affibodies and a micro-capillary functionalized with anti-CD9 antibodies interacting with NSCLC H1975-derived EVs

To demonstrate the effects of capillary functionalization procedure and how the performance changes in the experiment, a comparison between a 1-2 days old functionalized capillary and a capillary functionalized almost 1 week before was performed through a two-channels measurement of two micro-capillaries both functionalized with anti-EGFR affibodies.

NSCLC H1975-derived EVs were injected at a concentration of  $3 \times 10^9$  particles/mL and the capillaries were both cut at a length of 4,7 cm.

As shown in *Fig.4.15* the two capillaries show very distinct behaviours. The  $\Delta\zeta^*$  potentials were calculated, leading to values of - 0,5 mV for the old EGFR functionalized micro-capillary and 1,2

mV for the fresh EGFR functionalized one, resulting thus, in a 2,4-fold larger signal in comparison to the former value.

The averaged  $\zeta^*$  potential of the first baseline in the case of the old functionalized micro-capillary was recorded being 41,8 mV while the fresh one exhibited an averaged  $\zeta^*$  potential of 38,2 mV.

Moreover, it is undoubtedly noticeable that in the case of the old capillary the first baseline is by far less stable than the fresh one showing a 0,6 mV peak to peak value from the averaged signal which results doubled if compared to the freshly functionalized microcapillary peak to peak value of 0,3 mV.

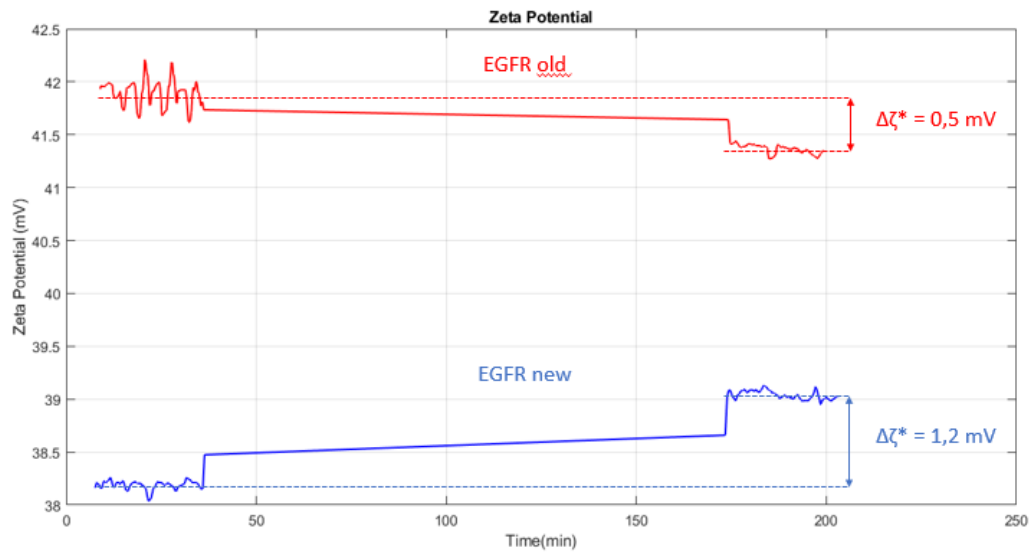


Figure 4.15: First plot showing the comparison between the  $\zeta^*$  potentials and relative  $\Delta\zeta^*$  obtained during a two-channels measurement using a fresh microcapillary functionalized with anti-EGFR affibodies and an old microcapillary also functionalized with anti-EGFR affibodies interacting with NSCLC H1975-derived EVs

At a first analysis, looking at the results of this experiment, it seemed that a value of the  $\zeta^*$  potential of the first baseline farthest from the mean value of anti-EGFR functionalized micro-capillaries (37,7 mV) obtained in the Capture probes' baseline characterization might have suggested that it could be referred to more unstable capillaries as in the case of the old microcapillary functionalized with anti-EGFR affibodies but a replication of this experiment denied this hypothesis.

As a matter of fact, in *Fig.4.16* is shown a second experiment employing a two-channels measurement of two micro-capillaries both functionalized with anti-EGFR affibodies.

Both old and fresh micro-capillaries displayed averaged first baseline  $\zeta^*$  potentials of, respectively, 39,6 mV and 39 mV, values that, although being very similar to each other, produce nonetheless very distinct outcomes.

Also in this case, the old capillary's first baseline is less stable than the fresh one showing a 0,7 mV peak to peak value from the averaged signal which results more than doubled if compared to the freshly functionalized microcapillary peak to peak value of 0,3 mV.

The calculated  $\Delta\zeta^*$  potentials, lead to values of - 0,2 mV for the old EGFR functionalized microcapillary and 2 mV for the fresh EGFR functionalized one, resulting thus in a 10-fold larger signal in comparison to the former value.

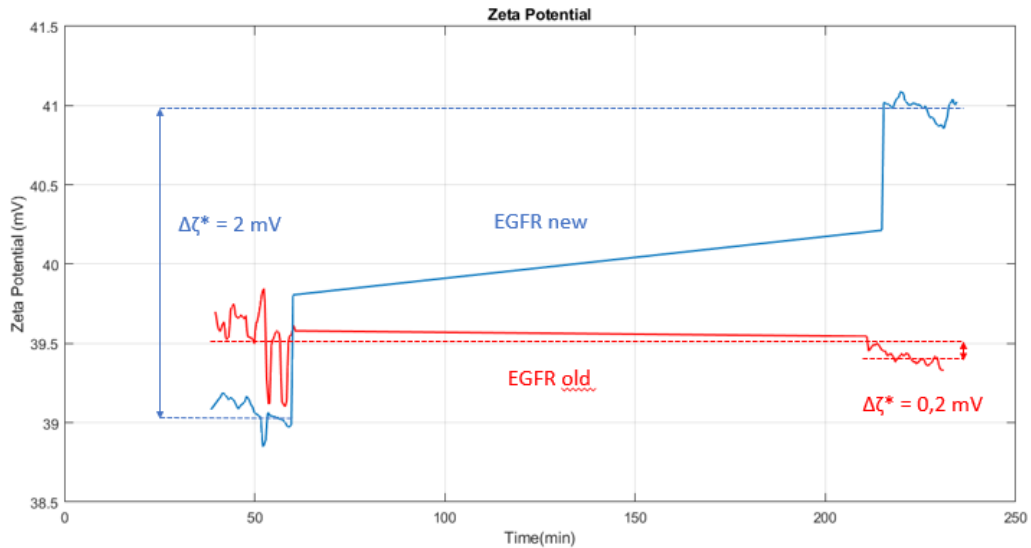


Figure 4.16: Second plot showing the comparison between the  $\zeta^*$  potentials and relative  $\Delta\zeta^*$  obtained during a two-channels measurement using a fresh microcapillary functionalized with anti-EGFR affibodies and an old microcapillary also functionalized with anti-EGFR antibodies interacting with NSCLC H1975-derived EVs

It can be therefore concluded that in the case of experiments carried out with freshly functionalized micro-capillaries there is a considerable increase in the  $\Delta\zeta^*$  signal compared to old micro-capillaries functionalized with the same type of antibodies. This suggested the importance to conduct the measurements with freshly functionalized capillaries in order to get more reliable results.

An attempt to enhance the  $\Delta\zeta^*$  signal was performed during a two-channels measurement using a micro-capillary functionalized with anti-EGFR affibodies and a control micro-capillary, both interacting with NSCLC H1975-derived EVs.

The experiment was carried out employing precisely the usual Experiment Conduction protocol, although some other steps were further added. After the EVs incubation period and second baseline recording there were included another incubation period and a third baseline recording.

During the second incubation period that lasted around 1,5 hours a solution containing anti-EGFR affibody conjugated with DNA was flowed. Since DNA is negatively charged, the hypothetical idea was that by binding to the EVs, the EGFR affibodies could further change the overall charge of the surface and resulting in a higher signal.

NSCLC H1975-derived EVs were injected at a concentration of  $3,5 \times 10^9$  particles/mL and the capillaries were both cut at a length of 4,7 cm.

As can be observed in *Fig.4.17*, the usual  $\Delta\zeta^*$  potentials that were calculated as the  $\zeta^*$  potential difference between second and first baseline, resulted in values of 0,7 mV for the control capillary

and 4,3 mV for the micro-capillary functionalized with anti-EGFR affibodies, therefore reaching almost an increase of 514 % in the latter case.

The averaged  $\zeta^*$  potential of the first baseline in the case of the anti-EGFR functionalized micro-capillary was calculated being 34 mV which is within the range of values found in anti-EGFR functionalized micro-capillaries described in the Capture probes' baseline characterization. In the case of the control capillary, its first baseline  $\zeta^*$  potential was recorded being 40,5 mV, this value also being acceptable as consistent with the range of values recorded for the control capillaries.

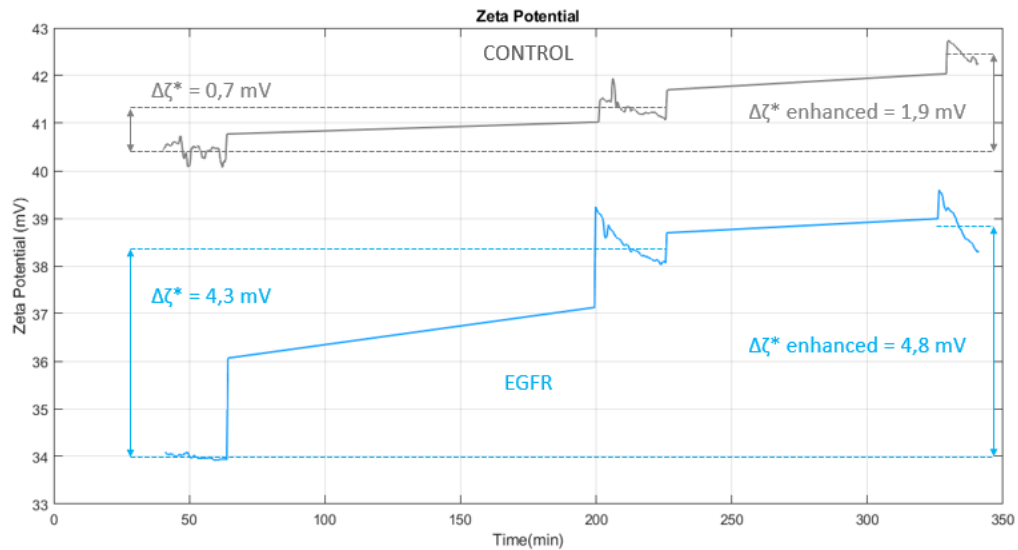


Figure 4.17: Plot showing the comparison between the  $\zeta^*$  potentials and relative  $\Delta\zeta^*$  obtained during a two-channels measurement using a micro-capillary functionalized with anti-EGFR affibodies and a control micro-capillary interacting with NSCLC H1975-derived EVs

The first baseline averaged  $\zeta^*$  potential results less stable in the control capillary showing a peak to peak value of 0,6 mV instead of the more steady EGFR baseline which reaches a maximum of 0,2 mV, a value considered almost irrelevant as it happens to be the minimum signal drifting.

A serious challenge was faced during the recording of the second baseline, since the signal drifting established was very high reaching 0,9 mV in the control capillary and 1,2 mV in the anti-EGFR functionalized one.

The same challenge was also encountered in the third baseline recording thus the accuracy of the experiment results impaired.

After the enhancement steps the  $\Delta\zeta^*$  enhanced potentials were calculated, leading to values of 1,9 mV for the control capillary and 4,8 mV for the anti-EGFR functionalized micro-capillary resulting in an increase of, respectively, 171 % and 11,6 % compared to the usual  $\Delta\zeta^*$  potential.

Therefore, it can be concluded that the experiment did not lead to a successful outcome due to the poor stability of the second and third baseline, in addition to the fact that the signal enhancement resulted inadequate in the target anti-EGFR functionalized micro-capillary in contrast to the control capillary which had an almost 15-fold higher  $\Delta\zeta^*$  enhanced signal. Experiments in this direction need further studies and investigation.

Overall, except for a few minor complications, the two-channels platform appeared to be functioning well, since the flow rates remained stable for all the duration of the measurements and in most cases the signals behaved as expected.

Moreover, it should be noted that, due to the difficulties in EVs isolation and purification, some of the measurements were performed with different EV batches, leading to differences in the signals for the same marker (i.e. EGFR) and EV concentrations.

## 4.4 Four-Channels Measurements

After having carried out experiments in the two-channels platform, measurements of four channels at the same time were performed in order to further test and evaluate the multiplexed electrokinetic detection method.

In *Fig.4.18*, the bar-plots displaying the mean and standard deviation calculated from two four-channels measurements can be observed. The two multiplexed measurements were carried out employing the two halves on the same functionalized micro-capillaries and NSCLC H1975-derived EVs, withdrawn from two different batches, were injected in both cases at a concentration of  $3,5 \times 10^9$  particles/mL.

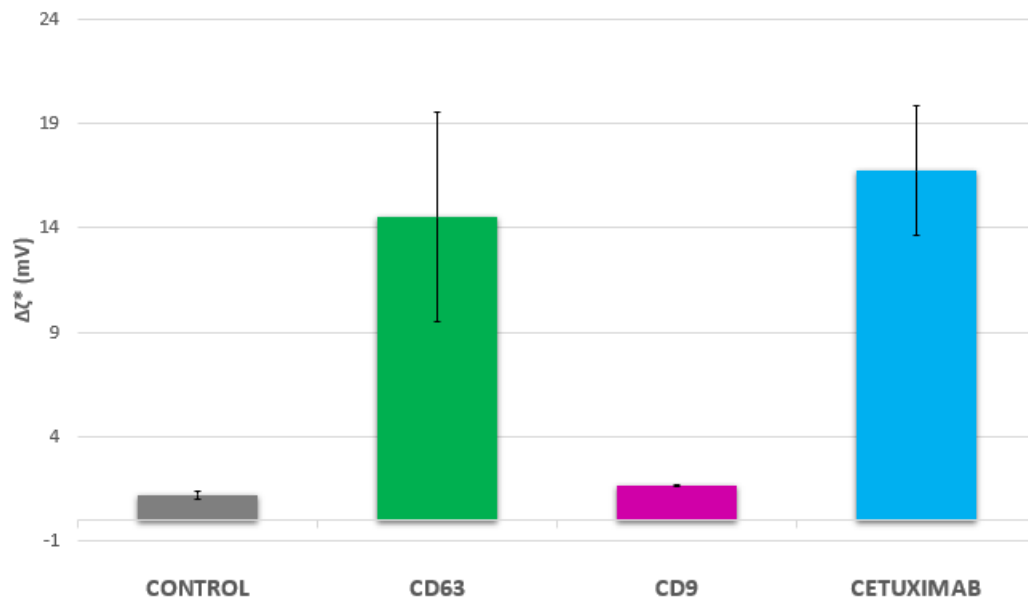


Figure 4.18: Bar-plots showing the mean  $\Delta\zeta^*$  and the relative standard deviation obtained during two four-channels measurements of a control micro-capillary and three micro-capillaries functionalized with Cetuximab, anti-CD63 and anti-CD9 antibodies interacting with the same batch of NSCLC H1975-derived EVs

It is immediately noticeable that the mean and standard deviation of the control capillaries result very low, with values, respectively, of 1,2 mV and 0,2. The anti-CD9 functionalized micro-capillaries are situated very close to the control values holding a mean value of 1,65 mV and a extremely low standard deviation of 0,05.

Opposed to this pair of capillaries can be found the micro-capillaries functionalized with Cetuximab and anti-CD63 which express not only  $\sim 10$ -fold higher mean values but higher standard deviation as well. The mean values are 14,5 mV for the anti-CD63 functionalized micro-capillaries and 16,7 mV for the Cetuximab ones while their standard deviations are, respectively, 5 and 3,1.

The reproducibility can not be considered overall optimal and this is believed to be traced to the experiment assessment. During the measurements carried out on the four-channels multiplexed platform with the introduction of the third but particularly of the fourth capillary a certain difficulty in obtaining a constant flow rate was observed. This is thought to be due to a non-equal flow distribution as a consequence of the 5-outlet valve employment, which results blocked in one of the outlets in order to obtain the four-channels configuration.

In conclusion, the worsened reproducibility of these results compared to the two-channels measurements might be attributed to the fact that two different batches of EVs samples have been used in the case at hand, which therefore, might suggest that there could be present a probable batch to batch difference between the different samples.

In addition to this fact, the aforementioned non-equal flow distribution that leads to complications and not quite reliable results could also be overlaid on obtaining such an outcome.

Another attempt to enhance the  $\Delta\zeta^*$  signal was performed during a four-channels measurement using a control micro-capillary and three micro-capillaries functionalized with anti-EGFR affibodies, anti-CD63 and anti-CD9 antibodies, all interacting with NSCLC H1975-derived EVs at a concentration of  $3,5 \times 10^9$  particles/mL.

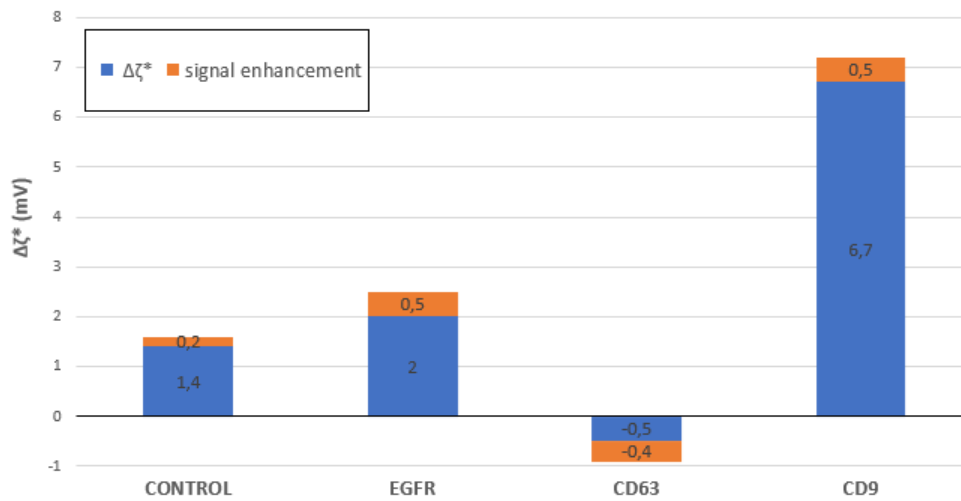


Figure 4.19: Bar-plots showing the  $\Delta\zeta^*$  and the relative signal enhancement obtained during a four-channels measurement using a control micro-capillary and three micro-capillaries functionalized with anti-EGFR affibodies, anti-CD63 and anti-CD9 antibodies interacting with NSCLC H1975-derived EVs

Compared to the two-channels enhancement attempt, in this experiment the second incubation period lasted around 1 hour during which a solution containing Cetuximab was flowed instead and

the results have been summarized in the form of bar-plots in *Fig.4.19*.

The  $\Delta\zeta^*$  value regarding the anti-CD9 functionalized micro-capillary indicates a good presence of the marker in the EVs sample while the anti-EGFR one is considerably lower and closer to the control value. The negative value of the anti-CD63 functionalized micro-capillary recalls the same outcomes of the old micro-capillaries functionalized with anti-EGFR affibodies seeming to suggest the non-reliability of the result.

Moreover, it can be noticed that the signal enhancement, which was measured as the difference between the third and second baseline, is very low in absolute value although quite uniform in all of the micro-capillaries, ranging from a minimum of 0,2 mV to a maximum of 0,5 mV thus finalizing the ineffectiveness for this enhancement attempt as well.

## 4.5 Clinical samples

After having tested the platform with EVs from the lung cancer cell line H1975, the performance of the platform for EVs derived from the pleural effusion of lung cancer patients was examined. It has been shown indeed that in presence of lung cancer, there is accumulation in the pleural space of liquid containing EVs. Since EVs isolated from this pleural effusion might also contain some other molecules like proteins because of the complexity of the liquid, it was important to test the platform with clinical samples to see whether it could specifically detect the vesicles or there was a high contribution from NSB.

It has been found that in biological samples the range value of small EVs, in average, goes from  $1 \cdot 10^8$  to  $3 \cdot 10^{12}$  EVs/mL [91], including also plasma samples derived from cancer patients. Considering these values, it was examined that the sensor could be suitable for clinical applications.

Given the poor reproducibility of the results carried out with the four-channels measurements and considering the valuableness and extreme limited availability of the clinical samples, for the experiments with the pleural effusion samples obtained from lung cancer patients, two-channel measurements were conducted. All of the experiments were thus performed employing two micro-capillaries: one functionalized with Cetuximab antibodies to target the EGFR protein markers on the surface of the EVs and the other one with the purpose of acting as a control capillary.

Being the EGFR mutations and its consequent increased protein expression one of the major developments that take place in lung cancer, it was chosen precisely to test this marker given its importance. The EVs derived from the pleural effusions, for each of the samples, were injected at a concentration of  $3,5 \cdot 10^9$  particles/mL.

The three available clinical samples were tested starting from the one with the highest level of EGFR (PE011) passing through the one with intermediate expression level (PE009) to end with the one that exhibited the lowest level of EGFR (PE002) as revealed by the qualitative analyzes performed by Western Blott and NTA from Karolinska Institute.

The  $\zeta^*$  potentials and the calculated  $\Delta\zeta^*$  of the two micro-capillaries interacting with PE011 sample-derived EVs are shown in *Fig.4.20*. It can be observed that the control capillary displayed a very low signal of 0,4 mV while the  $\Delta\zeta^*$  of the micro-capillary functionalized with the Cetuximab antibodies exhibited a  $\sim 28$ -fold higher signal reaching 11,3 mV. Both of the first baseline's  $\zeta^*$  potentials resulted stable and not dissimilar also with the values obtained during the Capture probes' baseline characterization.

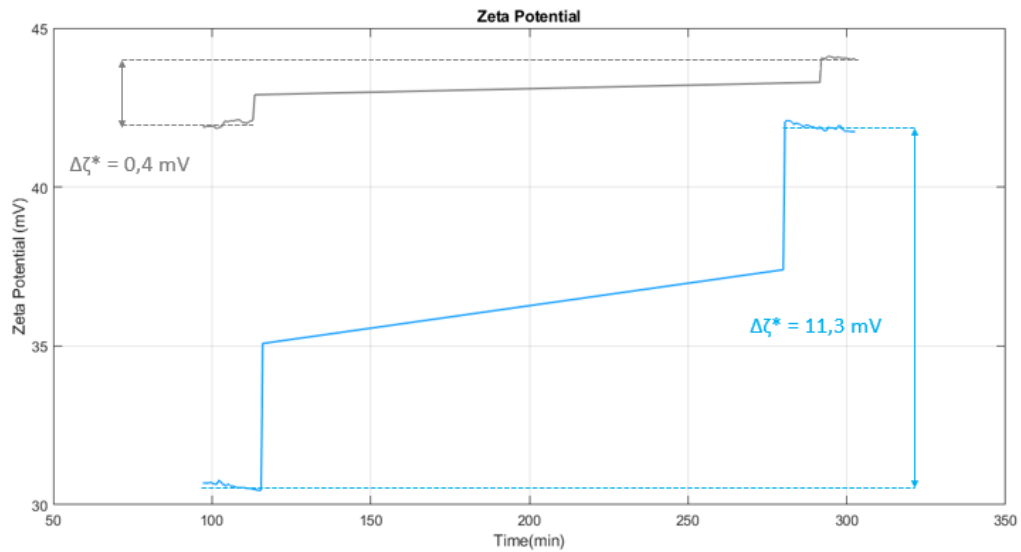


Figure 4.20: Plot showing the  $\zeta^*$  potentials and relative  $\Delta\zeta^*$  obtained during a two-channels measurement using a micro-capillary functionalized with Cetuximab antibodies and a control micro-capillary interacting with PE011 sample-derived EVs

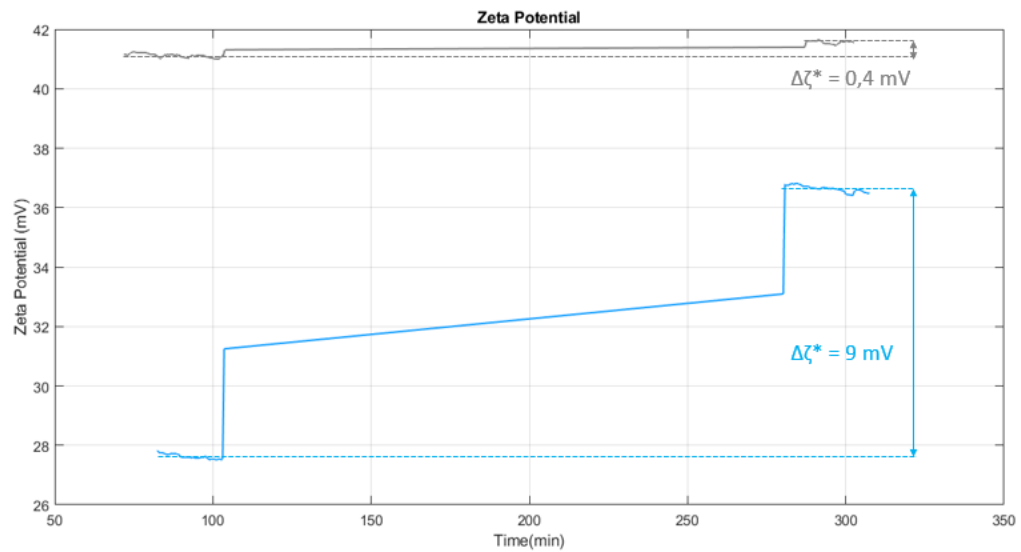


Figure 4.21: Plot showing the comparison between the  $\zeta^*$  potentials and relative  $\Delta\zeta^*$  obtained during a two-channels measurement using a micro-capillary functionalized with Cetuximab antibodies and a control micro-capillary interacting with PE009 sample-derived EVs

The same considerations on the first baseline's  $\zeta^*$  potentials can also be made for the PE009 and PE002 samples shown, respectively, in *Fig.4.21* and *Fig.4.22* in which also the control capillaries

are very low in absolute value and they exhibited relatively high  $\Delta\zeta^*$  signals.

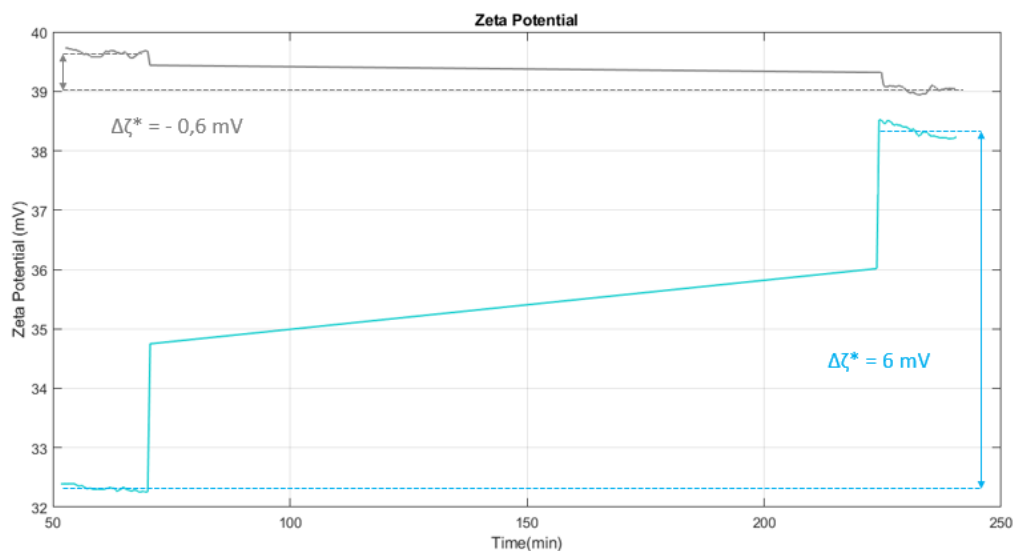


Figure 4.22: Plot showing the comparison between the  $\zeta^*$  potentials and relative  $\Delta\zeta^*$  obtained during a two-channels measurement using a micro-capillary functionalized with Cetuximab antibodies and a control micro-capillary interacting with PE002 sample-derived EVs

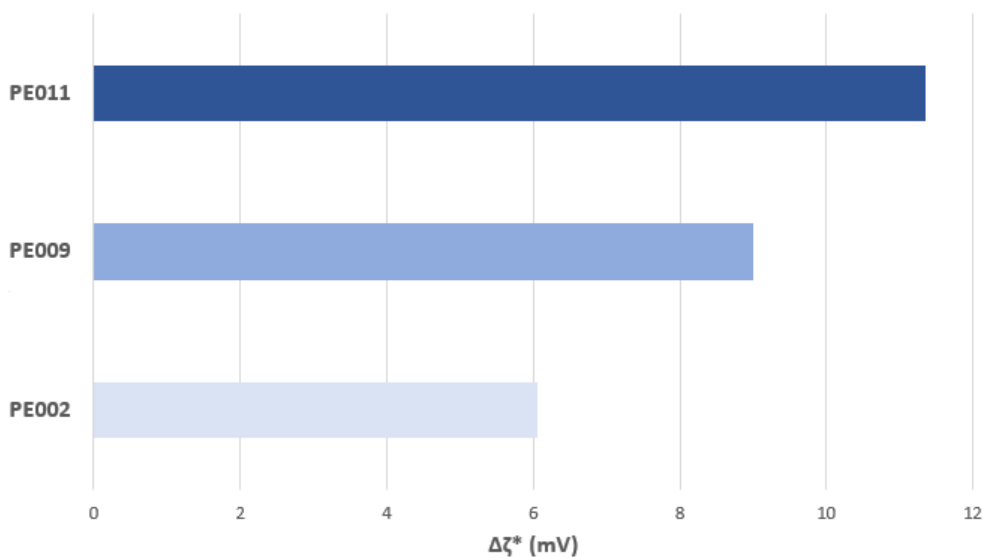


Figure 4.23: Grouped bar chart showing the  $\Delta\zeta^*$  of the Cetuximab functionalized micro-capillaries obtained from the experiments carried out with the three clinical sample-derived EVs

A grouped bar chart is shown in *Fig.4.23* to summarize the  $\Delta\zeta^*$  of the Cetuximab functionalized micro-capillaries obtained from the three experiments described in this section.

The results can be said to be very satisfactory because in accordance with what was obtained during the Western Blott analysis as they showed decreasing zeta potential values for equally decreasing levels of EGFR expression in the pleural effusion samples.

This is a very promising result although the experiments have to be repeated in order to obtain reproducible results.



## Chapter 5

# Conclusions

In this thesis work, an electrokinetic sensor for EVs detection and profiling of biomarkers expression based on affinity achieved through the recording of the streaming current produced in commercially available silica capillaries is presented. The validation of the proposed method was performed by detecting NSCLC H1975-derived EVs as well as EVs isolated in the pleural effusions of lung cancer patients targeting CD9, CD63 and EGFR surface markers.

Experiments performed on bare, non-functionalized capillaries as well as on microcapillaries functionalized with capture probes demonstrated that the  $\zeta^*$  potential recording of the first and second baseline resulted overall stable with minor signal drifting in the range of 0,2-0,3 mV during a 2-3 hours time range throughout the application of constant  $\Delta P$ .

Furthermore, repeated measurements on the capture probes functionalized micro-capillaries that lead to the calculation of their  $\zeta^*$  potential first baselines resulted in standard deviations of about 10% of the overall signals, for the majority of markers, showing, thus, a good reproducibility.

Compared to control measurements, the immobilized anti-EGFR affibodies while interacting with NSCLC H1975-derived EVs, induced a strong variation signal in the  $\zeta^*$  potential. In fact, the experiments performed in control capillaries that are obtained through the same protocol as the functionalized capillaries but without immobilized capture probes, confirmed that the recorded signal is a result of specific binding.

Moreover, by showing that in the case of 1-2 days old micro-capillaries functionalized with anti-EGFR affibodies there is a considerable increase in the  $\Delta\zeta^*$  signal compared to  $\sim$  one week old micro-capillaries functionalized with the same type of affibodies the importance of freshly functionalized microcapillaries during the carrying out of the experiments was stated.

Overall, the two-channels platform appeared to be functioning, since the flow rates remained stable for all the duration of the measurements and in most cases the signals behaved as expected.

Attempts to enhance the  $\Delta\zeta^*$  signal by performing a second incubation period after the recording of the second baseline by flowing a solution containing anti-EGFR conjugated with DNA or Cetuximab antibodies resulted fallimentary both in the two-channels and the four-channels measurements as well. Studies in this direction need further investigations.

Moreover, the results obtained from four-channels measurements lead to an overall, not-optimal reproducibility suggesting a probable batch to batch difference between the different samples. In addition, the non-equal flow distribution observed in the majority of these types of experiments was concluded leading to complications and not quite reliable results.

A sensor potential in profiling the expression of surface protein found in EVs is highly impor-

tant at the clinical application level. Within the sphere of EVs derived from tumor cells, various studies have been found indicating that certain surface markers expression levels could undergo variations during cancer treatment, giving evidence of how the tumor responds to such treatment. In the majority of case studies, the ability to perform qualitative comparisons in a certain marker expression level among different groups such as between patients at different treatment stages or between healthy controls and cancer patients, represents a sufficient condition.

Moreover, common approaches in EV profiling have consisted in the direct comparison of a sensor performance between various samples, relating a specific surface marker [91].

Thus, as presented in the Clinical samples section, the proposed sensor is successfully able to quantify the expression level of the EV surface marker EGFR in the qualitative comparison that is performed on its expression levels between different patient samples.

Lastly, it must be emphasize that the analysis carried out in this work has the function to serve for indicative purpose. In practical terms, various parameters such as the size and charge distribution of extracellular vesicles, as well as the EV surface protein profiles may highly impact the sensor sensitivity [91].

However, the experimental results presented in this thesis certainly indicate the possibility to further profile the protein expression of EVs in a semi-quantitative manner carried out by the proposed detection method.

## Chapter 6

# Future perspectives

Considering the results presented in this thesis, a better upgrade of the four-channels platform is required either by improving the flow distribution system or by integrating the platform into a chip. The last option would be preferable since it would significantly reduce the dimensions. In fact, the presented detection method would be entirely consistent with microfluidic platforms and is believed to require simple and inexpensive setup.

One of the key focuses during the design of biosensors is the mass transportation to the sensor surface, especially when considering analytes such as extracellular vesicles, which exhibit significantly larger masses than other biomarkers (e.g., RNAs, DNAs and proteins). The mass transportation rate of these larger analytes is generally lower. This can be owed to the inability of constituting an interaction with the immobilized affinity reagents simply through their vicinity to the surface. Their smaller diffusion coefficient will furthermore hinder the likelihood of this interaction. Therefore, it is expected that a large part of the EVs will establish no connection to the surface.

So in the future, a significant improvement of the presented sensing method performance can be achieved through the utilization of sample enrichment or enhanced mass transport methods.

Moreover, further experiments should be performed to improve the signal enhancement strategy, since this could allow to test two or more markers in the same micro-capillary as well as enhance the signal of a single marker. The failure of this aspect, in the present work, could be attributed to the weak charges carried by the DNA which don't appear different compared to those of the EVs. Another strategy could consist in using another buffer for the anti-EGFR conjugated with DNA incubation.



# Bibliography

- [1] Jonathan M Pitt, Guido Kroemer, Laurence Zitvogel, et al. Extracellular vesicles: masters of intercellular communication and potential clinical interventions. *The Journal of clinical investigation*, 126(4):1139–1143, 2016.
- [2] Graça Raposo and Willem Stoorvogel. Extracellular vesicles: exosomes, microvesicles, and friends. *Journal of Cell Biology*, 200(4):373–383, 2013.
- [3] Hadi Valadi, Karin Ekström, Apostolos Bossios, Margareta Sjöstrand, James J Lee, and Jan O Lötvall. Exosome-mediated transfer of mrnas and micrnas is a novel mechanism of genetic exchange between cells. *Nature cell biology*, 9(6):654–659, 2007.
- [4] Clotilde Théry, Laurence Zitvogel, and Sebastian Amigorena. Exosomes: composition, biogenesis and function. *Nature reviews immunology*, 2(8):569–579, 2002.
- [5] Johnny C Akers, David Gonda, Ryan Kim, Bob S Carter, and Clark C Chen. Biogenesis of extracellular vesicles (ev): exosomes, microvesicles, retrovirus-like vesicles, and apoptotic bodies. *Journal of neuro-oncology*, 113(1):1–11, 2013.
- [6] Paul D Robbins and Adrian E Morelli. Regulation of immune responses by extracellular vesicles. *Nature Reviews Immunology*, 14(3):195–208, 2014.
- [7] Erwin Chargaff and Randolph West. The biological significance of the thromboplastic protein of blood. *J Biol Chem*, 166(1):189–197, 1946.
- [8] Peter Wolf. The nature and significance of platelet products in human plasma. *British journal of haematology*, 13(3):269–288, 1967.
- [9] Albert J Dalton. Microvesicles and vesicles of multivesicular bodies versus “virus-like” particles. *Journal of the National Cancer Institute*, 54(5):1137–1148, 1975.
- [10] Bin-Tao Pan and Rose M Johnstone. Fate of the transferrin receptor during maturation of sheep reticulocytes in vitro: selective externalization of the receptor. *Cell*, 33(3):967–978, 1983.
- [11] C Harding, J Heuser, and Ph Stahl. Endocytosis and intracellular processing of transferrin and colloidal gold-transferrin in rat reticulocytes: demonstration of a pathway for receptor shedding. *European journal of cell biology*, 35(2):256–263, 1984.

- [12] Rose M Johnstone, Mohammed Adam, JR Hammond, L Orr, and Claire Turbide. Vesicle formation during reticulocyte maturation. association of plasma membrane activities with released vesicles (exosomes). *Journal of Biological Chemistry*, 262(19):9412–9420, 1987.
- [13] Graça Raposo, Hans W Nijman, Willem Stoorvogel, R Liejendekker, Clifford V Harding, CJ Melief, and Hans J Geuze. B lymphocytes secrete antigen-presenting vesicles. *Journal of Experimental Medicine*, 183(3):1161–1172, 1996.
- [14] Laurence Zitvogel, Armelle Regnault, Anne Lozier, Joseph Wolfers, Caroline Flament, Danielle Tenza, Paola Ricciardi-Castagnoli, Graça Raposo, and Sebastian Amigorena. Eradication of established murine tumors using a novel cell-free vaccine: dendritic cell derived exosomes. *Nature medicine*, 4(5):594–600, 1998.
- [15] Bernard Escudier, Thierry Dorval, Nathalie Chaput, Fabrice André, Marie-Pierre Caby, Sophie Novault, Caroline Flament, Christophe Leboulaire, Christophe Borg, Sebastian Amigorena, et al. Vaccination of metastatic melanoma patients with autologous dendritic cell (dc) derived-exosomes: results of the first phase I clinical trial. *Journal of translational medicine*, 3(1):10, 2005.
- [16] Michael A Morse, Jennifer Garst, Takuya Osada, Shubi Khan, Amy Hobeika, Timothy M Clay, Nancy Valente, Revati Shreenivas, Mary Ann Sutton, Alain Delcayre, et al. A phase I study of dexosome immunotherapy in patients with advanced non-small cell lung cancer. *Journal of translational medicine*, 3(1):9, 2005.
- [17] Hadi Valadi, Karin Ekström, Apostolos Bossios, Margareta Sjöstrand, James J Lee, and Jan O Lötvall. Exosome-mediated transfer of mRNAs and microRNAs is a novel mechanism of genetic exchange between cells. *Nature cell biology*, 9(6):654–659, 2007.
- [18] Lydia Alvarez-Erviti, Yiqi Seow, HaiFang Yin, Corinne Betts, Samira Lakhali, and Matthew JA Wood. Delivery of siRNA to the mouse brain by systemic injection of targeted exosomes. *Nature biotechnology*, 29(4):341–345, 2011.
- [19] María Yáñez-Mó, Pia R-M Siljander, Zoraida Andreu, Apolonija Bedina Zavec, Francesc E Borràs, Edit I Buzas, Krisztina Buzas, Enriqueta Casal, Francesco Cappelletto, Joana Carvalho, et al. Biological properties of extracellular vesicles and their physiological functions. *Journal of extracellular vesicles*, 4(1):27066, 2015.
- [20] Stephen J Gould and Graça Raposo. As we wait: coping with an imperfect nomenclature for extracellular vesicles. *Journal of extracellular vesicles*, 2(1):20389, 2013.
- [21] E Van der Pol, AN Böing, EL Gool, and R Nieuwland. Recent developments in the nomenclature, presence, isolation, detection and clinical impact of extracellular vesicles. *Journal of thrombosis and haemostasis*, 14(1):48–56, 2016.
- [22] Jan Lötvall, Andrew F Hill, Fred Hochberg, Edit I Buzás, Dolores Di Vizio, Christopher Gardiner, Yong Song Gho, Igor V Kurochkin, Suresh Mathivanan, Peter Quesenberry, et al. Minimal experimental requirements for definition of extracellular vesicles and their functions: a position statement from the international society for extracellular vesicles, 2014.

- [23] Samir EL Andaloussi, Imre Mäger, Xandra O Breakefield, and Matthew JA Wood. Extracellular vesicles: biology and emerging therapeutic opportunities. *Nature reviews Drug discovery*, 12(5):347–357, 2013.
- [24] Jose C Contreras-Naranjo, Hung-Jen Wu, and Victor M Ugaz. Microfluidics for exosome isolation and analysis: enabling liquid biopsy for personalized medicine. *Lab on a Chip*, 17(21):3558–3577, 2017.
- [25] Eduard Willms, Henrik J Johansson, Imre Mäger, Yi Lee, K Emelie M Blomberg, Mariam Sadik, Amr Alaarg, CI Edvard Smith, Janne Lehtiö, Samir EL Andaloussi, et al. Cells release subpopulations of exosomes with distinct molecular and biological properties. *Scientific reports*, 6(1):1–12, 2016.
- [26] Kristin Denzer, Monique J Kleijmeer, HF Heijnen, Willem Stoorvogel, and Hans J Geuze. Exosome: from internal vesicle of the multivesicular body to intercellular signaling device. *Journal of cell science*, 113(19):3365–3374, 2000.
- [27] Laura M Doyle and Michael Zhuo Wang. Overview of extracellular vesicles, their origin, composition, purpose, and methods for exosome isolation and analysis. *Cells*, 8(7):727, 2019.
- [28] Pierre Barbero, Lenka Bittova, and Suzanne R Pfeffer. Visualization of rab9-mediated vesicle transport from endosomes to the trans-golgi in living cells. *The Journal of cell biology*, 156(3):511–518, 2002.
- [29] Wiebke Möbius, Yoshiko Ohno-Iwashita, Elly G van Donselaar, Viola MJ Oorschot, Yukiko Shimada, Toyoshi Fujimoto, Harry FG Heijnen, Hans J Geuze, and Jan W Slot. Immunoelectron microscopic localization of cholesterol using biotinylated and non-cytolytic perfringolysin o. *Journal of Histochemistry & Cytochemistry*, 50(1):43–55, 2002.
- [30] Trairak Pisitkun, Rong-Fong Shen, and Mark A Knepper. Identification and proteomic profiling of exosomes in human urine. *Proceedings of the National Academy of Sciences*, 101(36):13368–13373, 2004.
- [31] Edouard M Bevers, Paul Comfurius, David WC Dekkers, and Robert FA Zwaal. Lipid translocation across the plasma membrane of mammalian cells. *Biochimica et Biophysica Acta (BBA)-Molecular and Cell Biology of Lipids*, 1439(3):317–330, 1999.
- [32] Robert Bucki, Christilla Bachelot-Loza, Alain Zachowski, Françoise Giraud, and Jean-Claude Sulpice. Calcium induces phospholipid redistribution and microvesicle release in human erythrocyte membranes by independent pathways. *Biochemistry*, 37(44):15383–15391, 1998.
- [33] Kenneth W Witwer, Edit I Buzás, Lynne T Bemis, Adriana Bora, Cecilia Lässer, Jan Lötval, Esther N Nolte-‘t Hoen, Melissa G Piper, Sarada Sivaraman, Johan Skog, et al. Standardization of sample collection, isolation and analysis methods in extracellular vesicle research. *Journal of extracellular vesicles*, 2(1):20360, 2013.
- [34] Clotilde Théry, Sebastian Amigorena, Graça Raposo, and Aled Clayton. Isolation and characterization of exosomes from cell culture supernatants and biological fluids. *Current protocols in cell biology*, 30(1):3–22, 2006.

- [35] Fatemeh Momen-Heravi, Leonora Balaj, Sara Alian, Pierre-Yves Mantel, Allison E Halleck, Alexander J Trachtenberg, Cesar E Soria, Shanice Oquin, Christina M Bonebreak, Elif Saracoglu, et al. Current methods for the isolation of extracellular vesicles. *Biological chemistry*, 394(10):1253–1262, 2013.
- [36] Zachary Brownlee, Kristi D Lynn, Philip E Thorpe, and Alan J Schroit. A novel “salting-out” procedure for the isolation of tumor-derived exosomes. *Journal of immunological methods*, 407:120–126, 2014.
- [37] Henry G Lamparski, Anita Metha-Damani, Jenq-Yuan Yao, Sanjay Patel, Di-Hwei Hsu, Curtis Ruegg, and Jean-Bernard Le Pecq. Production and characterization of clinical grade exosomes derived from dendritic cells. *Journal of immunological methods*, 270(2):211–226, 2002.
- [38] Anita N Böing, Edwin Van Der Pol, Anita E Grootemaat, Frank AW Coumans, Auguste Sturk, and Rienk Nieuwland. Single-step isolation of extracellular vesicles by size-exclusion chromatography. *Journal of extracellular vesicles*, 3(1):23430, 2014.
- [39] Aled Clayton, Jacquelyn Court, Hossein Navabi, Malcolm Adams, Malcolm D Mason, Jan A Hobot, Geoff R Newman, and Bharat Jasani. Analysis of antigen presenting cell derived exosomes, based on immuno-magnetic isolation and flow cytometry. *Journal of immunological methods*, 247(1-2):163–174, 2001.
- [40] Ryan T Davies, Junho Kim, Su Chul Jang, Eun-Jeong Choi, Yong Song Gho, and Jaesung Park. Microfluidic filtration system to isolate extracellular vesicles from blood. *Lab on a Chip*, 12(24):5202–5210, 2012.
- [41] Maria Serena Chiriaco, Monica Bianco, Annamaria Nigro, Elisabetta Primiceri, Francesco Ferrara, Alessandro Romano, Angelo Quattrini, Roberto Furlan, Valentina Arima, and Giuseppe Maruccio. Lab-on-chip for exosomes and microvesicles detection and characterization. *Sensors*, 18(10):3175, 2018.
- [42] Hina Kalra, Richard J Simpson, Hong Ji, Elena Aikawa, Peter Altevogt, Philip Askenase, Vincent C Bond, Francesc E Borràs, Xandra Breakefield, Vivian Budnik, et al. Vesiclepedia: a compendium for extracellular vesicles with continuous community annotation. *PLoS Biol*, 10(12):e1001450, 2012.
- [43] Reka A Haraszti, Marie-Cecile Didiot, Ellen Sapp, John Leszyk, Scott A Shaffer, Hannah E Rockwell, Fei Gao, Niven R Narain, Marian DiFiglia, Michael A Kiebish, et al. High-resolution proteomic and lipidomic analysis of exosomes and microvesicles from different cell sources. *Journal of extracellular vesicles*, 5(1):32570, 2016.
- [44] Clotilde Théry, Kenneth W Witwer, Elena Aikawa, Maria Jose Alcaraz, Johnathon D Anderson, Ramarosan Andriantsitohaina, Anna Antoniou, Tanina Arab, Fabienne Archer, Georgia K Atkin-Smith, et al. Minimal information for studies of extracellular vesicles 2018 (misev2018): a position statement of the international society for extracellular vesicles and update of the misev2014 guidelines. *Journal of extracellular vesicles*, 7(1):1535750, 2018.
- [45] Zoraida Andreu and María Yáñez-Mó. Tetraspanins in extracellular vesicle formation and function. *Frontiers in immunology*, 5:442, 2014.

- [46] Maria Francesca Baietti, Zhe Zhang, Eva Mortier, Aurélie Melchior, Gisèle Degeest, Annelies Geeraerts, Ylva Ivarsson, Fabienne Depoortere, Christien Coomans, Elke Vermeiren, et al. Syndecan–syntenin–alix regulates the biogenesis of exosomes. *Nature cell biology*, 14(7):677–685, 2012.
- [47] Chan Woo Kim, Hwan Myung Lee, Tae Hoon Lee, Chulhun Kang, Hynda K Kleinman, and Yong Song Gho. Extracellular membrane vesicles from tumor cells promote angiogenesis via sphingomyelin. *Cancer research*, 62(21):6312–6317, 2002.
- [48] Tore Skotland, Kirsten Sandvig, and Alicia Llorente. Lipids in exosomes: current knowledge and the way forward. *Progress in lipid research*, 66:30–41, 2017.
- [49] MikoŁaj P Zaborowski, Leonora Balaj, Xandra O Breakefield, and Charles P Lai. Extracellular vesicles: composition, biological relevance, and methods of study. *Bioscience*, 65(8):783–797, 2015.
- [50] Bodil Ramstedt and J Peter Slotte. Membrane properties of sphingomyelins. *FEBS letters*, 531(1):33–37, 2002.
- [51] Hina Kalra, Gregor PC Drummen, and Suresh Mathivanan. Focus on extracellular vesicles: introducing the next small big thing. *International journal of molecular sciences*, 17(2):170, 2016.
- [52] Raghu Kalluri and Valerie S LeBleu. The biology, function, and biomedical applications of exosomes. *Science*, 367(6478), 2020.
- [53] Thomas A Hartjes, Serhii Mytnyk, Guido W Jenster, Volkert van Steijn, and Martin E van Royen. Extracellular vesicle quantification and characterization: common methods and emerging approaches. *Bioengineering*, 6(1):7, 2019.
- [54] Deborah LM Rupert, Virginia Claudio, Cecilia Lässer, and Marta Bally. Methods for the physical characterization and quantification of extracellular vesicles in biological samples. *Biochimica et Biophysica Acta (BBA)-General Subjects*, 1861(1):3164–3179, 2017.
- [55] D.A. Skoog, F.J. Holler, and S.R. Crouch. *Principles of Instrumental Analysis*. International student edition. Thomson Brooks/Cole, 2007.
- [56] Min Kyo Jung and Ji Young Mun. Sample preparation and imaging of exosomes by transmission electron microscopy. *JoVE (Journal of Visualized Experiments)*, (131):e56482, 2018.
- [57] Yueting Wu, Wentao Deng, and David J Klinke II. Exosomes: improved methods to characterize their morphology, rna content, and surface protein biomarkers. *Analyst*, 140(19):6631–6642, 2015.
- [58] Petr Cizmar and Yuana Yuana. Detection and characterization of extracellular vesicles by transmission and cryo-transmission electron microscopy. In *Extracellular Vesicles*, pages 221–232. Springer, 2017.

- [59] David P Allison, Ninell P Mortensen, Claretta J Sullivan, and Mitchel J Doktycz. Atomic force microscopy of biological samples. *Wiley Interdisciplinary Reviews: Nanomedicine and Nanobiotechnology*, 2(6):618–634, 2010.
- [60] Wikipedia. Atomic force microscopy block diagram — wikipedia, the free encyclopedia. [https://en.wikipedia.org/wiki/Atomic\\_force\\_microscopy#/media/File:Atomic\\_force\\_microscope\\_block\\_diagram.svg](https://en.wikipedia.org/wiki/Atomic_force_microscopy#/media/File:Atomic_force_microscope_block_diagram.svg), 2020. [Online; Accessed 2020-04-09].
- [61] Sybren LN Maas, Jeroen De Vrij, and Marike LD Broekman. Quantification and size-profiling of extracellular vesicles using tunable resistive pulse sensing. *JoVE (Journal of Visualized Experiments)*, (92):e51623, 2014.
- [62] Valentina Palmieri, Donatella Lucchetti, Ilaria Gatto, Alessandro Maiorana, Margherita Marcantoni, Giuseppe Maulucci, Massimiliano Papi, Roberto Pola, Marco De Spirito, and Alessandro Sgambato. Dynamic light scattering for the characterization and counting of extracellular vesicles: a powerful noninvasive tool. *Journal of nanoparticle research*, 16(9):2583, 2014.
- [63] Anton Paar GmbH. The principles of dynamic light scattering. <https://wiki.anton-paar.com/en/the-principles-of-dynamic-light-scattering/>, 2020. [Online; Accessed 2020-04-17].
- [64] Vasco Filipe, Andrea Hawe, and Wim Jiskoot. Critical evaluation of nanoparticle tracking analysis (nta) by nanosight for the measurement of nanoparticles and protein aggregates. *Pharmaceutical research*, 27(5):796–810, 2010.
- [65] Su Wang, Adeel Khan, Rongrong Huang, Shiyi Ye, Kaili Di, Tao Xiong, and Zhiyang Li. Recent advances in single extracellular vesicle detection methods. *Biosensors and Bioelectronics*, 154:112056, 2020.
- [66] Rebecca A Dragovic, Christopher Gardiner, Alexandra S Brooks, Dionne S Tannetta, David JP Ferguson, Patrick Hole, Bob Carr, Christopher WG Redman, Adrian L Harris, Peter J Dobson, et al. Sizing and phenotyping of cellular vesicles using nanoparticle tracking analysis. *Nanomedicine: Nanotechnology, Biology and Medicine*, 7(6):780–788, 2011.
- [67] Azo Nano. Nanoparticle tracking analysis (nta) measurements. <https://www.azonano.com/article.aspx?ArticleID=4062>, 2020. [Online; Accessed 2020-04-19].
- [68] Abcam. Overview of the flow cytometer. <https://www.abcam.com/protocols/introduction-to-flow-cytometry>, 2020. [Online; Accessed 2020-04-22].
- [69] E Van Der Pol, MJC Van Gemert, A Sturk, R Nieuwland, and TG Van Leeuwen. Single vs. swarm detection of microparticles and exosomes by flow cytometry. *Journal of Thrombosis and Haemostasis*, 10(5):919–930, 2012.
- [70] Rafal Szatanek, Monika Baj-Krzyworzeka, Jakub Zimoch, Malgorzata Lekka, Maciej Siedlar, and Jarek Baran. The methods of choice for extracellular vesicles (evs) characterization. *International journal of molecular sciences*, 18(6):1153, 2017.

- [71] Sean Gallagher, Scott E Winston, Steven A Fuller, and John GR Hurrell. Immunoblotting and immunodetection. *Current protocols in cell biology*, 52(1):6–2, 2011.
- [72] Sybren LN Maas, Jeroen De Vrij, Els J Van Der Vlist, Biaina Geragousian, Louis Van Bloois, Enrico Mastrobattista, Raymond M Schiffelers, Marca HM Wauben, Marike LD Broekman, Esther NM Nolte, et al. Possibilities and limitations of current technologies for quantification of biological extracellular vesicles and synthetic mimics. *Journal of Controlled Release*, 200:87–96, 2015.
- [73] B Stegmayr and G Ronquist. Promotive effect on human sperm progressive motility by prostasomes. *Urological research*, 10(5):253–257, 1982.
- [74] Mathilde Chivet, Fiona Hemming, Sandrine Fraboulet, Rémy Sadoul, et al. Emerging role of neuronal exosomes in the central nervous system. *Frontiers in physiology*, 3:145, 2012.
- [75] Héctor Peinado, Maša Alečković, Simon Lavotshkin, Irina Matei, Bruno Costa-Silva, Gema Moreno-Bueno, Marta Hergueta-Redondo, Caitlin Williams, Guillermo García-Santos, Cyrus M Ghajar, et al. Melanoma exosomes educate bone marrow progenitor cells toward a pro-metastatic phenotype through met. *Nature medicine*, 18(6):883–891, 2012.
- [76] Khalid Al-Nedawi, Brian Meehan, Johann Micallef, Vladimir Lhotak, Linda May, Abhijit Guha, and Janusz Rak. Intercellular transfer of the oncogenic receptor egfrviii by microvesicles derived from tumour cells. *Nature cell biology*, 10(5):619–624, 2008.
- [77] Johan Skog, Tom Würdinger, Sjoerd Van Rijn, Dimphna H Meijer, Laura Gainche, William T Curry, Bob S Carter, Anna M Krichevsky, and Xandra O Breakefield. Glioblastoma microvesicles transport rna and proteins that promote tumour growth and provide diagnostic biomarkers. *Nature cell biology*, 10(12):1470–1476, 2008.
- [78] Khalid Al-Nedawi, Brian Meehan, Robert S Kerbel, Anthony C Allison, and Janusz Rak. Endothelial expression of autocrine vegf upon the uptake of tumor-derived microvesicles containing oncogenic egfr. *Proceedings of the National Academy of Sciences*, 106(10):3794–3799, 2009.
- [79] Evangelia Emmanouilidou, Katerina Melachroinou, Theodoros Roumeliotis, Spiros D Garbis, Maria Ntzouni, Lukas H Margaritis, Leonidas Stefanis, and Kostas Vekrellis. Cell-produced  $\alpha$ -synuclein is secreted in a calcium-dependent manner by exosomes and impacts neuronal survival. *Journal of Neuroscience*, 30(20):6838–6851, 2010.
- [80] B Sandfeld-Paulsen, N Aggerholm-Pedersen, R Baek, KR Jakobsen, P Meldgaard, BH Folkersen, TR Rasmussen, K Varming, MM Jørgensen, and BS Sorensen. Exosomal proteins as prognostic biomarkers in non-small cell lung cancer. *Molecular oncology*, 10(10):1595–1602, 2016.
- [81] Rebecca L Siegel, Kimberly D Miller, and Ahmedin Jemal. Cancer statistics, 2019. *CA: a cancer journal for clinicians*, 69(1):7–34, 2019.
- [82] LuCe report on lung cancer. <https://www.lungcancereurope.eu/wp-content/uploads/2017/10/LuCE-Report-final.pdf>., 2017. [Online; Accessed 2020-02-10].

- [83] Courtney A Granville and Phillip A Dennis. An overview of lung cancer genomics and proteomics. *American journal of respiratory cell and molecular biology*, 32(3):169–176, 2005.
- [84] Cecilia Zappa and Shaker A Mousa. Non-small cell lung cancer: current treatment and future advances. *Translational lung cancer research*, 5(3):288, 2016.
- [85] Irene Vanni, Angela Alama, Francesco Grossi, Maria Giovanna Dal Bello, and Simona Coco. Exosomes: a new horizon in lung cancer. *Drug Discovery Today*, 22(6):927–936, 2017.
- [86] Akhil Srivastava, Narsireddy Amreddy, Mohammad Razaq, Rheal Towner, Yan Daniel Zhao, Rebaz A Ahmed, Anupama Munshi, and Rajagopal Ramesh. Exosomes as theranostics for lung cancer. In *Advances in cancer research*, volume 139, pages 1–33. Elsevier, 2018.
- [87] MD Vincent, MS Kuruvilla, NB Leighl, and S Kamel-Reid. Biomarkers that currently affect clinical practice: Egfr, alk, met, kras. *Current oncology*, 19(Suppl 1):S33, 2012.
- [88] Chang Liu, Yunchen Yang, and Yun Wu. Recent advances in exosomal protein detection via liquid biopsy biosensors for cancer screening, diagnosis, and prognosis. *The AAPS Journal*, 20(2):41, 2018.
- [89] Hyungsoon Im, Huilin Shao, Yong Il Park, Vanessa M Peterson, Cesar M Castro, Ralph Weissleder, and Hakho Lee. Label-free detection and molecular profiling of exosomes with a nano-plasmonic sensor. *Nature biotechnology*, 32(5):490–495, 2014.
- [90] Apurba Dev, Josef Horak, Andreas Kaiser, Xichen Yuan, Anna Perols, Per Björk, Amelie Eriksson Karlström, Pascal Kleimann, and Jan Linnros. Electrokinetic effect for molecular recognition: A label-free approach for real-time biosensing. *Biosensors and Bioelectronics*, 82:55–63, 2016.
- [91] Sara Cavallaro, Josef Horak, Petra Hååg, Dhanu Gupta, Christiane Stiller, Siddharth S Sahu, Andre Gorgens, Hithesh K Gatty, Kristina Viktorsson, Samir El Andaloussi, et al. Label-free surface protein profiling of extracellular vesicles by an electrokinetic sensor. *ACS sensors*, 4(5):1399–1408, 2019.
- [92] Á V Delgado, F González-Caballero, RJ Hunter, LK Koopal, and J Lyklema. Measurement and interpretation of electrokinetic phenomena. *Journal of colloid and interface science*, 309(2):194–224, 2007.
- [93] Reto B Schoch, Jongyoon Han, and Philippe Renaud. Transport phenomena in nanofluidics. *Reviews of modern physics*, 80(3):839, 2008.
- [94] Robert J Hunter. *Zeta potential in colloid science: principles and applications*, volume 2. Academic press, 2013.
- [95] Thomas Luxbacher. *The Zeta Potential for Solid Surface Analysis: A Practical Guide to Streaming Potential Measurement*. Austria: Anton Paar GmbH, 2014.
- [96] Sara Ferraris, Martina Cazzola, Veronica Peretti, Barbara Stella, and Silvia Spriano. Zeta potential measurements on solid surfaces for in vitro biomaterials testing: surface charge, reactivity upon contact with fluids and protein absorption. *Frontiers in bioengineering and biotechnology*, 6:60, 2018.

- [97] Aditya Bandopadhyay and Uddipta Ghosh. Electrohydrodynamic phenomena. *Journal of the Indian Institute of Science*, 98(2):201–225, 2018.
- [98] Wikipedia. Structural formula of (3-aminopropyl)triethoxysilane (aptes)— wikipedia, the free encyclopedia. <https://en.wikipedia.org/wiki/Silanization#/media/File:APTES.svg>, 2020. [Online; Accessed 2020-05-13].
- [99] Sigma Aldrich. Glutaraldehyde solution. <https://www.sigmaaldrich.com/catalog/substance/glutaraldehydesolution1001211130811?lang=it&region=IT>, 2020. [Online; Accessed 2020-05-13].



# Appendix

## Sample preparation

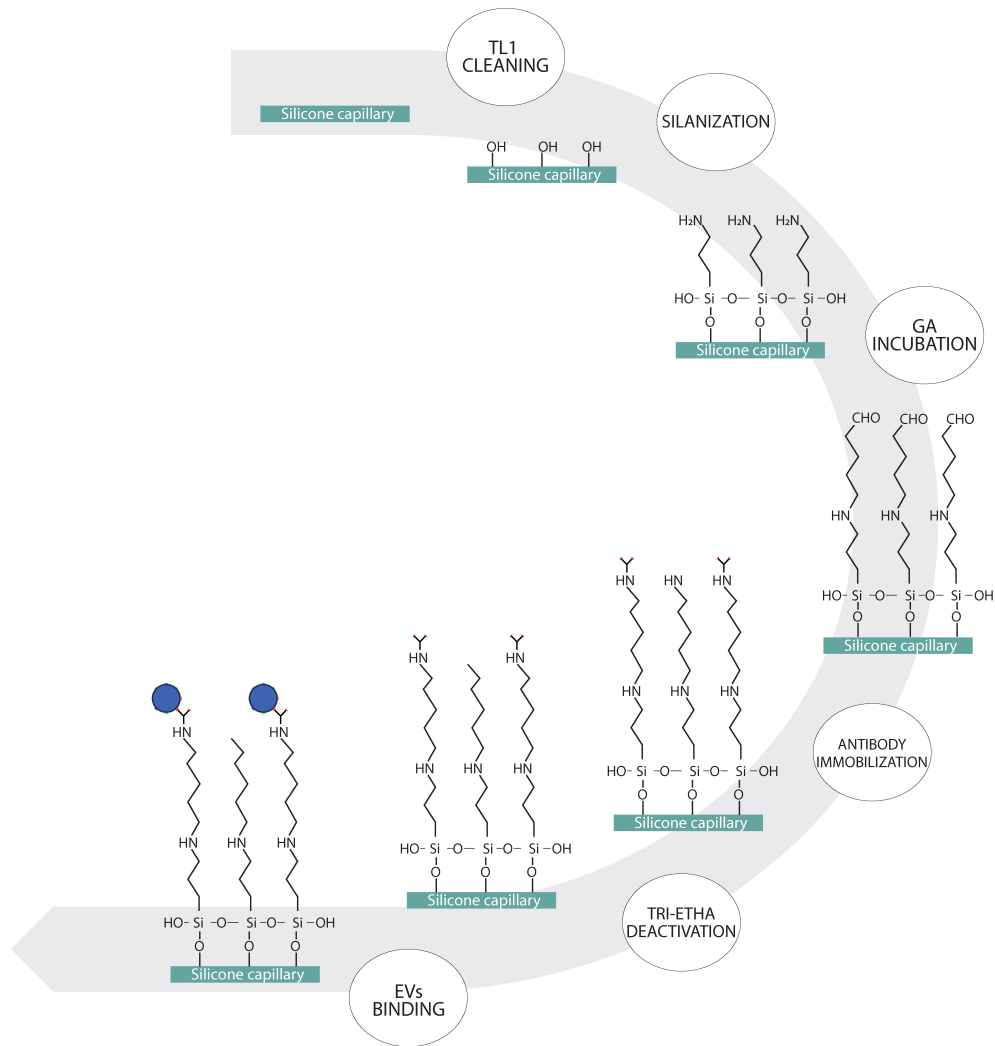


Figure 6.1: Schematic representation of EVs capture on a bio-chemically treated silicon capillary



# Acknowledgements

Prima di tutto vorrei ringraziare la mia supervisor Sara. Grazie mille per la guida, la gentilezza, le risate, e i fika pomeridiani durante i mesi più freddi in Svezia. Senza la tua conoscenza, suggerimenti e supporto sarebbe stato tutto molto più buio e difficile.

Grazie poi a Carolina, la mia compagna di avventura durante questa tesi. Caro, ti adoro e non sai quanto io sia grata di essere stata al tuo fianco durante quei mesi al KTH. La tua intelligenza, dolcezza e coraggio mi hanno illuminata ogni giorno e ho trovato in te una grande amica.

Lorenc, grazie per il supporto enorme che mi hai dato in questi ultimi tre anni! Non so dove sarei senza di te e il tuo sostegno passo dopo passo. Hai reso ogni difficoltà e insicurezza meno pesanti e di questo ti sono eternamente grata!

Un ringraziamento speciale va a mia nonna Kali! Oltre a essere la persona più speciale della mia vita è anche la ragione per cui sono capace a scrivere queste parole di ringraziamento perché mi ha permesso di uscire da uno dei momenti più difficili del mio percorso di studi e mi ha illuminata con la sua speranza e credenza, salvandomi! Nana, te dua shum!

Miriana, my soul sister! Senza la tua amicizia non sarei completa e questa tesi è stato un richiamo verso di te e oh come sono felice di essere riuscita a raggiungerti! Hai reso tutto molto più bello e divertente!

Grazie alla mia Amazona per le telefonate nei momenti più difficili! Ridere con te mi ha alleviato la mente e l'anima!

Umbs, sei l'amico migliore che una ragazza può chiedere. La tua dolcezza e affetto sono stati speciali per me.

Gio, che fine di un capitolo sarebbe senza di te che sei stata con me dall'inizio di tutto? Grazie per più di un decennio di amicizia, supporto e sopportazione!

Grazie ai miei compagni di università, Chiara e Matteo. Chiara, la mia gemella e pilastro di questi sei anni. Senza di te non sarei sopravvissuta neanche un giorno! Matteo, mostro sacro e amico vero sempre e comunque. Non potrei mai esprimere la gratitudine e ammirazione che provo verso di voi! Grazie per essere rimasti sempre al mio fianco!

Grazie ai miei amici Nene, Lollo, Marco, Tommy, Ro, Capra, Deni, Umberto, Nina, Luca, per essere stati una grandissima fonte di gioia in tutti questi anni! Senza il supporto, amicizia e spensieratezza che mi avete mostrato sarei stata molto più sola e triste nel mio studio matto e disperatissimo.

Vorrei infine, ringraziare profondamente la mia famiglia, il mio fratellino Dima, i miei cugini Eri e Miri per l'affetto, il supporto e la fiducia che hanno riposto in me!

Grazie dal cuore a tutti per essere stati un faro in questo percorso!